Earth Fissure Evaluation
Vineyard Road Flood Retarding Structure
Contract FCD 2016C010, Work Assignment No. 34
Pinal County, Arizona

Submitted to:

Flood Control District of Maricopa County
Phoenix, Arizona

Submitted by:

Wood
Environment & Infrastructure Solutions, Inc.
Phoenix, Arizona

April 1, 2020

Project No. 17-2020-4004

April 1, 2020
Project No. 17-2020-4004

Flood Control District of Maricopa County
2801 West Durango Street
Phoenix, Arizona 85009-6399

Attn: Stephen Brown, PE

Re: Earth Fissure Evaluation
Vineyard Road Flood Retarding Structure
Contract FCD 2016C010, Work Assignment No. 34
Pinal County, Arizona

Transmitted herewith is the draft of the Earth Fissure Evaluation, for the Vineyard Road Flood Retarding Structure. The scope of work for this work assignment included an evaluation of a new earth fissure approximately 2,100 feet west/southwest of the north end of Vineyard Road FRS.

Should you have any questions concerning this report, please do not hesitate to contact the undersigned.

Respectfully submitted,

Wood Environment & Infrastructure Solutions, Inc.

Reviewed by:

Kenneth C. Fergason, PG
Senior Geologist

Daniel N. Fréchette, PhD, PE
Principal Geotechnical Engineer

And

Michael L. Rucker, PE
Senior Associate Geotechnical Engineer

c: Addressee (2 copies and 2 DVDs)
Arizona Department of Water Resources (1 copy and 1 DVD)
Natural Resources Conservation Service (1 copy and 1 DVD)

G:\Geotechnical\2020 Projects\17-2020-4004 FCD_WA #34 Vineyard Earth Fissure Evaluation\02_Design\05_Reports\02_Draft\Vineyard Road FRS Fissure Evaluation_Draft.docx

4600 East Washington Street, Suite 600
Phoenix, Arizona 85034-1917
Tel: (602) 733-6000
Fax: (602) 733-6100
www.woodplc.com

TABLE OF CONTENTS

LIST OF FIGURES

LIST OF APPENDICES

1.0 INTRODUCTION

The purpose of the Vineyard Road Flood Retarding Structure (FRS) Earth Fissure Evaluation was to investigate the newly identified earth fissure that is located approximately 2,100 feet west/southwest of Station 350+00 of Vineyard Road FRS. The goals of the investigation were to identify when the surface expression of the earth fissure formed, the current extent of the earth fissure, and potential impacts of the earth fissure in the future to the existing Vineyard Road FRS, Powerline FRS and the Powerline Floodway, and to the ongoing Vineyard Road FRS Rehab design and the Powerline Channel design. This evaluation was made through the collection, review and assessment of data from the earth fissure/ground subsidence instrumentation and monitoring system installed at the Powerline and Vineyard FRSs, previous land subsidence and earth fissure investigations, aerial imagery, InSAR and additional geophysical surveys.

Wood Environment & Infrastructure Solutions, Inc. (Wood) has reviewed previous investigative findings, aerial imagery and monitoring data, evaluated InSAR data, performed seismic refraction surveys at the new fissure and along its projection, performed deep resistivity soundings to characterize subsidence potential of deep subsurface materials, evaluated nearby survey data, and developed this report summarizing Wood's findings and recommendations.

2.0 PROJECT DESCRIPTION

The newly identified earth fissure was brought to the attention of the Flood Control District of Maricopa County (District) by the Arizona Department of Water Resources (ADWR) on December 19, 2019. District personnel conducted a site visit on December 23, 2019, and concluded the feature was likely an earth fissure that required further evaluation. Wood performed a site visit of the earth fissure on January 2, 2020. Based on site observations and initial review of aerial imagery, Wood concurred with the District that the feature is likely an earth fissure. The newly identified earth fissure is located approximately 2,100 feet west/southwest of Station 350+00 of Vineyard Road FRS (**Figure 1**).

3.0 INVESTIGATIVE METHODS

The District retained Wood to perform an evaluation of the newly identified earth fissure. The project area is limited to the area in the vicinity of the newly identified earth fissure and is shown on **Figure 1**. The procedures used during the study are detailed in the document entitled Procedural Documents for Land Subsidence and Earth Fissure Appraisals (AMEC, 2011); hereafter referred to as the "Procedural Documents." The following subsections summarize the approach used to perform the evaluation.

3.1 Data Review

The findings of previous investigations were reviewed in detail, with a focus on the area around the new earth fissure, the north end of Vineyard Road FRS, the north emergency spillway of Vineyard Road FRS and the Powerline Floodway. The data reviewed was primarily from the Final Design-Level Subsidence and Earth Fissure Zoning Report (AMEC, 2014) and included FRS crest and toe survey data, InSAR, relevant deep well logs, and depth to bedrock data pertaining to the Central Arizona Project (CAP) Canal from U.S. Bureau of Reclamation (USBR) and U.S. Geological Survey deep seismic refraction and gravity data.

Additional data reviewed that was not evaluated as part of the AMEC (2014) report includes data from the Arizona Geological Survey (Gootee, 2013).

3.2 Aerial Image Review

Historical high-resolution aerial imagery that is available from past monitoring efforts was reviewed to constrain when the surficial expression of the earth fissure occurred. This data included annual high-resolution imagery with resolution of approximately 0.4 feet per pixel from 2010 to 2019. Additionally, print low-sun angle aerial imagery from 2001 and 1997 were also reviewed. The historic high-resolution aerial imagery of the newly identified earth fissure is shown on **Figure 2**. It is noted that the year shown on images typically refer to the year images were processed and that acquisition of the images may have occurred several months prior to the year shown.

3.3 InSAR Review and Analysis

InSAR products produced for ground deformation monitoring were evaluated and interpreted to detect and quantify changes in terrain elevation by comparing phase variances of satellite-based, side-looking radar data between satellite orbits of a similar trajectory. The InSAR products were previously provided by the District through its intergovernmental agreement with ADWR. Additional transects/profiles were developed in and around the area of the new earth fissure. Additional InSAR data was acquired and interpreted from the Sentinel satellite system. The Sentinel satellite system provides finer detail both in terms of frequency of data and improved spatial resolution (i.e. smaller pixel size). Eight (8) interferograms were developed for relatively short time periods from May 2018 to January 2020, for approximately one-month intervals. The one-month intervals were selected to achieve good data coherence. Results from the InSAR review and analysis are presented in **Appendix A** and discussed in Section 6.4.

3.4 Seismic Refraction Profiling

Four (4), 240-foot-long, combined seismic refraction compression wave (p-wave) and ReMi surface/shear wave (s-wave) surveys were performed to evaluate if the new earth fissure is present in the subsurface in areas beyond where there is surficial evidence. These surveys were used to identify the presence or absence of subsurface anomalies, which could indicate the potential presence and location of an earth fissure. The surveys were performed in accordance with the recommendations in the Procedural Documents (AMEC, 2011) and locations are shown on **Figure 1**. A Geometrics Geode signal enhancement seismograph and a geophone array consisting of twenty-four (24) 4.5Hz geophones at 10-foot spacings were used to complete the surveys. A sledgehammer energy source deployed at nine (9) shotpoints at 30-foot intervals along the seismic array was used to generate compression wave (p-wave) energy for seismic refraction and seismic signal anomaly analysis. Personnel jumping near the geophone array center were used to generate surface wave energy for ReMi analysis for one-dimensional vertical surface/shear wave (s-wave) profiles at each seismic line. Seismic lines were located using hand-held global positioning system (GPS) instruments with an approximate accuracy of ±3 feet. The seismic surveys were performed on January 27, 2020, by Tiana Rasmussen, PG, and Johari Pannalal, under the direction of Michael Rucker, P.E., all with Wood.

As described in the Procedural Documents (AMEC, 2011), a method of visually examining seismic traces for a sudden decrease in signal amplitude (attenuation) and/or an anomalous increase in arrival time (time offset) of the seismic signal between adjacent geophones was employed. Weak possible anomalies were interpreted at several traces of Seismic Line SL20-01 positioned at the visible end of the earth fissure. Signal continuity in both gradual attenuation of signal over distance and relatively uniform increases in time for adjacent first arrivals were observed throughout the trace results for the remaining seismic lines; no strong seismic anomalies consistent with the presence of existing earth fissures with continuous open ground fractures were identified in any of the seismic traces. The seismic refraction and ReMi data have been fully interpreted and the results are presented in **Appendix B**.

3.5 Deep Resistivity Soundings

Three (3) deep resistivity soundings were performed to characterize the subsurface in the vicinity of the new fissure to compare with conditions at the Vineyard Road FRS and Powerline FRS where previous resistivity soundings have been performed and other data exists. An L-and-R UltraminiRes resistivity meter with a four-point Wenner array configuration was used to conduct the field resistivity investigation. The surveys were performed on January 30-31, 2020, by Mr. Hossein Ganji and Mr. Pannalal, under the direction of Mr. Rucker at locations shown on **Figure 1**. Interpretations of the measurement results are presented in **Appendix C**.

Resistivity results are used to characterize alluvium containing freshwater aquifers with regard to estimating subsidence potential. Detailed resistivity measurements of the alluvial profile are available as downhole resistivity logs at only a few locations. However, surface resistivity soundings provide simplified, but much lower resolution, resistivity profiles at many additional locations. Alluvium with low resistivity (fines-dominated alluvium), typically less than 10 ohm-meters (ohm-m, also 1,000 ohm-cm), is generally considered to be very compressible. Fines-dominated alluvium will slowly to very slowly compress over time in response to changes in effective stress from declining groundwater levels; resulting subsidence may be significant but occurs over decades or more unless pumping wells tap directly into the fines-dominated materials. Alluvium with moderate resistivity (sand-dominated alluvium), typically 10 ohm-m (1,000 ohm-cm) up to about 20 to 30 ohm-m (2,000 to 3,000 ohm-cm), is generally considered to be compressible. Sand-dominated alluvium will compress at moderate rates in response to changes in effective stress from declining groundwater levels; resulting subsidence may be moderate and tends to occur over months to years. Minor subsidence may continue over decades. Alluvium with higher resistivity (gravel-dominated alluvium or conglomerate), typically about 20 or 30 to 100 ohm-m (2,000 or 3,000 to 10,000 ohm-cm), is generally considered to be less compressible, sometimes significantly less compressible. Gravel-dominated alluvium or conglomerate will compress rapidly in response to changes in effective stress from declining groundwater levels; resulting subsidence may be minor and occur rapidly. Other aspects of alluvium that influence compressibility, such as age and induration, may not be effectively characterized by resistivity alone. Materials with very high resistivity, greater than about 100 ohm-m (10,000 ohm-cm), are generally considered to be incompressible bedrock.

4.0 GEOLOGIC CONDITIONS

The following subsections of this report discuss aspects of the geological setting important to an assessment of ground subsidence and earth fissuring, such as depth to basement rock and deep alluvial

basin characteristics. The term basement rock is synonymous with bedrock throughout this report. This discussion is focused on the newly identified earth fissure and a more in-depth description of the geologic conditions is available in the Final Design-Level Subsidence and Earth Fissure Zoning Report (AMEC, 2014).

4.1 Regional Setting

The project is located within the Sonoran region of the Basin and Range physiographic province and is, in part, structurally separated from the Central Phoenix Valley by bedrock highs in the Tempe Butte area. The project area lies within the Mesa-Chandler sub-basin (often referred to as the Higley Basin), adjacent to the Superstition and Goldfield Mountains. These mountain ranges are composed of metamorphic and igneous bedrock. The Higley Basin contains basin-fill deposits of the East Salt River Valley that can be subdivided into three primary units (Laney and Hahn, 1986): lower alluvial unit (LAU), middle alluvial unit (MAU) and upper alluvial unit (UAU). As implied by gravity data, the valley margins likely contain multiple high-angle normal faults that were active in Cenozoic time (Sweeney and Hill, 2001; Laney and Hahn, 1986). These faults are now concealed under the basin alluvium and are not present at the current mountain-front exposures of bedrock.

4.2 Surficial Geology

The project area lies at the distal margin of pediments associated with the Goldfield and Superstition Mountains. The northern and central portions of the project area contain Holocene deposits typical of a basin floor. The fine-grained distal alluvial fan/alluvial plain and terrace deposits have little soil development (Pearthree and Huckleberry, 1994). The basin floor deposits are incised by channels filled with younger Holocene piedmont and intermontane deposits. The channel deposits consist of stratified sand, silt, pebbles, cobbles and boulders with little or no soil development (Pearthree and Huckleberry 1994). The surficial deposits in the area of the newly identified earth fissure consist of Holocene alluvial surfaces and modern ephemeral stream deposits. Some of the channels have rectilinear drainage patterns that have formed along two-track roads, cattle trails and earth fissures. Much of the natural drainage is disrupted by the CAP Canal and flood control structures.

4.3 Basin Geometry and Depth to Bedrock

The buried shape and depth of the bedrock-alluvium contact are likely the most dominant influences on where earth fissures form around Hawk Rock and near the Powerline FRS. The newly identified earth fissure is located about 2.1 miles southeast of Hawk Rock and is somewhat removed from the area surrounding Hawk Rock where earth fissures are typically found. The depth to bedrock is shown on **Figure 3**. Earth fissures tend to form in regions where the gradient of the bedrock-alluvium interface is quite pronounced and the thickness of the alluvium is variable. These conditions result in a differential subsidence profile, a prerequisite for earth fissure formation. Bedrock is present at the surface at Hawk Rock, which is about 4,000 feet west of the bend in the Powerline FRS embankment near Station 110+00. Historic Hawk Rock is the expression of a large, buried inselberg and ridge system (Hawk Rock bedrock complex) that partially underlies the Powerline FRS and approaches the northernmost reaches of Vineyard Road FRS. Understanding this bedrock geometry is one of the most important factors for delineating earth fissure risks within the project area.

There are six data sets that either directly or indirectly provide estimates on the depth to bedrock or the shape of the bedrock-alluvium interface in the vicinity of the project as shown on **Figure 3**: 1) Bouguer gravity data (Sweeney and Hill, 2001), 2) depth to bedrock from Laney and Hahn (1986), 3) bedrock elevations from unpublished USBR and USGS draft documents retrieved from CAP archives, 4) InSAR data, 5) geophysical measurements from previous studies, and 6) ADWR gravity data (Cook et al., 2013; Gootee, 2013). The data sets are discussed in detail in the Final Design-Level Subsidence and Earth Fissure Zoning Report (AMEC 2014).

4.4 Deep Basin Characteristics

The magnitude of ground subsidence and the location of earth fissures are controlled by the interactions of groundwater decline, the composition of compressible alluvial basin materials and the geometry of the underlying alluvial/bedrock interface. The thickness of the basin alluvial materials (the depth to bedrock) is highly variable within the project area. Alluvial thickness ranges from none at Hawk Rock (less than 1 mile west of the Powerline FRS) to a depth of 1,770 feet bgs (well SG6 in **Figure 3**) at about Dam Station 270+00 of the Vineyard Road FRS and to a depth of over 3,000 feet bgs (elevation 1,900 feet below sea level) near the southern end of the Vineyard Road FRS and the northern end of the Rittenhouse FRS. Variations in subsidence appear to reflect variations in both the depth to bedrock and the composition of the alluvial materials within the deep basins.

As discussed by Prokopovich (1983) and the USBR (1976), the basin-fill deposits of the Salt River Valley are comprised of unconsolidated to weakly indurated sediments deposited on an irregular bedrock surface. From a geotechnical perspective, the upper basin sediments likely classify as stiff soils to soft rock, with the deep Tertiary deposits classifying as soft to moderately indurated rock. The basin deposits are quite variable, ranging from fine-grained deposits of clay and silt of lacustrine or playa origins, to coarse-grained deposits of clastic materials derived from adjacent uplands. The basin deposits are described in detail in the Final Design-Level Subsidence and Earth Fissure Zoning Report (AMEC, 2014). The following bulleted list summarizes the characteristics of the three alluvial units, from oldest to youngest, largely as described by Laney and Hahn (1986).

- **Lower Alluvial Unit (LAU), Ts**. The Middle to Late Tertiary deposits of the LAU are in fault and erosional contact with the bedrock floor and buried flanks of the basin. The defining characteristic of the LAU is that it was deposited when the basin was a closed basin with internal drainage. This unit, although dominated by fine-grained sediments, is typically coarse-grained (often referred to as conglomerate) at depth and along the basin margins. The LAU is divided into Lower (Lower LAU) and Upper (Upper LAU) sections that are generally similar but differ in consolidation, homogeneity, type of evaporate deposits present, and structure. Locally along the margins of the basin, conglomerate of the Lower LAU may be within 400 feet of the surface.
    - **Lower LAU, Tsl**. The Lower LAU is more consolidated and more homogeneous in terms of clast type and stratigraphy than the Upper LAU. The Lower LAU is considered incompressible and not susceptible to significant land subsidence due to groundwater withdrawal.

  - **Upper LAU, Tsu**. The Upper LAU is weakly to strongly cemented and consists of clay, silt, mudstone, gypsiferous mudstone, sand and gravel, and conglomerate. In the project area the Upper LAU appears to be generally incompressible.

- **Middle Alluvial Unit (MAU), QTs**. This unit is often restricted to the center of alluvial basins in Central Arizona. The MAU is considered compressible and susceptible to significant ground subsidence due to groundwater withdrawal.

- **Upper Alluvial Unit (UAU), Qs**. The UAU is comprised of Late Tertiary and Quaternary clastic material derived locally from the surrounding bedrock terrain and deposited as a mantle over the older basin fill deposits. The UAU is considered compressible and susceptible to significant ground subsidence due to groundwater withdrawal. However, within the project area, the UAU is typically unsaturated due to historic withdrawals of groundwater.

Figure 4 shows a conceptual geologic profile developed along the Powerline Floodway as part of the Final Design-Level Subsidence and Earth Fissure Zoning Report (AMEC, 2014). This orientation was chosen in part due to there being data from the USBR along this alignment. The newly identified earth fissure is located approximately 1,100 feet southeast of approximate Powerline Floodway Station 30+00.

5.0 HYDROGEOLOGIC CONDITIONS

This section discusses specific conditions relative to the newly identified earth fissure, and the reader is referred to the Final Design-Level Subsidence and Earth Fissure Zoning Report (AMEC, 2014) for a detailed discussion of the hydrogeologic conditions at Vineyard Road FRS. Historically, groundwater levels in the vicinity of the project area have declined significantly due to groundwater withdrawals far exceeding natural recharge, as analyzed and discussed in previous reports (AMEC, 2014). These declines likely commenced by the 1940s as agricultural development began in earnest in the East Valley. In the vicinity of the newly identified earth fissure, it is anticipated that groundwater was about 300 feet below ground surface in 1950, and has declined about 200 feet since that time to the present. Modeling by ADWR of various scenarios of future groundwater demands and levels (Hipke, 2010) predict that possible future groundwater depths in the new fissure vicinity may range from about 500 feet (current conditions) to more than 800 feet by year 2108.

Subsidence along the Vineyard Road and Rittenhouse FRS has primarily been driven by agricultural pumping to the south and southwest. Subsidence at the north end of the Vineyard Road FRS has also been influenced by and continues to be influenced by municipal pumping to the northwest. Historic local subsidence at the northern end of Vineyard Road FRS was also impacted by Well D(1-8)9CCC, also recorded as D(1-8)17AAA, located downgradient from the CAP Canal near the combined Powerline and Vineyard Road Spillway. Records indicate this well was drilled in 1967 to provide construction water for FRS construction and may also have been used to provide construction water for CAP Canal construction. There are no data in ADWR records to document the actual pumping history of this well. However, the location of this well and the local pattern of historic subsidence around this well indicate that pumping of this well during FRS and CAP Canal construction probably resulted in the pattern of subsidence that currently exists in the vicinity of the northern end of the Vineyard Road FRS.

6.0 DISCUSSION/ANALYSIS OF FINDINGS

6.1 Geologic Reconnaissance

District personnel conducted a site visit on December 23, 2019, and concluded that the feature was likely an earth fissure that required further evaluation. Wood performed a site visit of the earth fissure as part of the annual instrumentation and monitoring project for the Powerline, Vineyard Road and Rittenhouse (PVR) FRSs on January 2, 2020. Based on site observations and initial review of aerial imagery, Wood concurs that the feature is likely an earth fissure.

The newly identified earth fissure is manifested as three separate, en échelon, ground cracks. The primary ground crack is approximately 360 feet long and trends northeast-southwest. The other ground cracks are about 95 feet and 45 feet long, respectively. The fissure is sub-parallel to a small wash, which is captured by the fissure for most of the fissure's distance (**Figure 1**) and appears to be the water source responsible for a majority of the erosion associated with the earth fissure. The surficial expression of the earth fissure has developed into an earth fissure gully as a result of the erosion that has occurred. The fissure gully is partially-filled to filled with sediment, has rounded edges, and has annual vegetation growing within the fissure gully. This suggests that the fissure collects surface runoff during rain events. Such capture of surface flow presents the opportunity for the deposition of soil in fissure openings, so that the open fractures and cracks inherent in earth fissuring can become filled. Additionally, it suggests that the fissure gully has not experienced recent ground tension associated with land subsidence in the past several years that would allow for erosion to occur without observable in-filling of the earth fissure and fissure gully. During Wood's initial field visit, water was observed ponded within the fissure gully from a rain event that occurred a few days prior to the visit, which further supports the observation that the fissure gully is partially-filled to filled and has not experienced recent ground tension from land subsidence.

Observations of the newly identified earth fissure are similar to the known earth fissure at Siphon Draw Wash Detention Basin (SDWDB) (located approximately 1.6 miles northwest of the new earth fissure). The earth fissure gullies associated with the earth fissures in the area of SDWDB show cyclical patterns through time (Wood, 2019; AMEC, 2006; AMEC, 2008). These patterns include periods where erosion of the gullies slowly widens the gullies and fills them in with sediment over many years, divided by shorter periods of a year or two where the fissure 'opens' allowing for erosion to occur down into the fissure gully, sometimes combined with lengthening of the fissures. Unlike the new earth fissure, the fissures at SDWDB have very likely formed over a distinct bedrock ridge associated with the Hawk Rock bedrock complex; continuing land subsidence, even if at a slow rate, results in increasing ground tension over that bedrock ridge in the SDWDB area. At this point it is unclear if the new earth fissure will behave with a cyclical pattern similar to the fissures at SDWDB, or if the fissure gullies will slowly fill in with time without entering into a period where the fissure 'opens' to vertical erosion and potential extension. Based on the analysis presented in this report and further discussed in sections below, Wood believes that the latter condition is more likely.

6.2 Aerial Image Review

Figure 2 shows annual high-resolution aerial images at the site of the newly identified earth fissure from 2010 to 2019. In the image from 2014, the newly identified earth fissure is present nearly to the full extent as it is in 2019. Detailed, step-by-step, annual observations are listed below.

1. 2010: No observable signs of ground cracking. The wash that intersects the earth fissure shows some local indications of erosion in the area.

2. 2011: No observable signs of ground cracking. The wash that intersects the earth fissure shows some local indications of erosion in the area, but no significant changes from 2010.

3. 2012: No observable signs of ground cracking. The wash that intersects the earth fissure shows some local indications of erosion in the area but no significant changes from 2011.

4. 2013: The wash that intersects the earth fissure shows some local indications of erosion in the area but no significant changes from 2012. Possible ground cracking appears to be present immediately south of the wash along the line of the earth fissure. If it is a ground crack, it appears that it has experienced little to no erosion.

5. 2014: The earth fissure is clearly visible as a set of two en échelon cracks. The cracks appear to have experienced relatively little erosion.

6. 2015: The earth fissure is clearly visible as a set of two en échelon cracks. The cracks appear to have experienced relatively little erosion with little to no changes from 2014 and no apparent extension of the fissure to the north or south.

7. 2016: The earth fissure is clearly visible as a set of two en échelon cracks. The cracks appear to have experienced some erosion, widening the crack expressions. The surface expression of the earth fissure is considered an earth fissure gully at this point. There is no apparent extension of the fissure to the north or south.

8. 2017: The earth fissure is clearly visible as a set of two en échelon fissure gullies. The gullies show only small amounts of additional erosion/widening occurring since 2016. There is no apparent extension of the fissure to the north or south.

9. 2018: The earth fissure is clearly visible as a set of two en échelon fissure gullies. The gullies show only small amounts of additional erosion/widening occurring since 2017. There is no apparent extension of the fissure to the north or south.

10. 2019: The earth fissure is clearly visible as a set of three en échelon fissure gullies. The gullies show small to moderate amounts of additional erosion/widening occurring since 2018 and a shorter, third fissure gully has become observable between the original two. The development of the third fissure gully is likely due to local collapse and settlement of the fissure gullies, as has been observed with other earth fissure gullies in the Hawk Rock area. There is no apparent extension of the fissure to the north or south.

These images suggest that between 2012 and 2013, some ground cracking associated with the earth fissure began to appear at the surface, and between 2013 and 2014 the surficial expression (fissure gully) of the earth fissure developed to the approximate extent that is present in 2019. Wood concludes that the surficial expression of the earth fissure was not present prior to 2013 and was unlikely to have been recognized prior to 2014. These images also indicate that the extent (i.e., length) of the surface expression of the earth fissure has remained essentially constant since 2014.

6.3 Local Deep Basin Characteristics

Deep resistivity soundings R20-01 centered at the new fissure, at R20-02 and R20-03 centered about 500 feet northwest and southeast of R20-01, respectively, provided local characterization of the compressible basin alluvium and underlying less-compressible older alluvium and bedrock in the new fissure vicinity. Sounding R20-01 at the fissure had interpreted 11.0 ohm-m compressible alluvium (LAU or less-clayey MAU) below the groundwater table (at a depth of about 500 feet) to an interpreted depth of about 658 feet. That compressible alluvium was underlain by 43 ohm-m likely older, less compressible LAU alluvium. Sounding R20-02 to the northwest had interpreted 8.2 ohm-m compressible clay-dominated alluvium (likely MAU) below the historic initial groundwater table depth of 300 feet to a depth of about 527 feet just below the current groundwater table depth of about 500 feet. That clay-dominated alluvium was underlain by about 450 ohm-m likely bedrock. Sounding R20-03 to the southeast had interpreted 12.8 ohm-m compressible alluvium (LAU or less-clayey MAU), and extended several hundred feet below the water table to an interpreted depth of about 939 feet. That compressible alluvium was underlain by about 450 ohm-m material that is likely bedrock.

Interpreted results of these current resistivity soundings are consistent with the previous deep basin characterization presented by AMEC (2014). Anticipated deep basin characterization along Profile D-D' (**Figure A-1** in **Appendix A**), including both the current resistivity soundings and previous resistivity soundings and other basin characterization, is summarized in **Figure 5**. A notable feature of the local deep basin is the presence of a localized subsidence bowl immediately to the northwest of the new fissure as can be seen in **Figure A-1**. This subsidence bowl appears to occur as a result of the presence of fine-grained alluvial deposits in the subsurface at the edge of the Hawk Rock bedrock complex, and may be similar in nature to those found at White Tanks FRS No. 3 and near the southern end of McMicken Dam (AMEC, 2013). It appears that the new fissure is positioned at the southeastern edge of this local subsidence bowl. This subsidence bowl was originally identified through InSAR and will be discussed in the following section.

6.4 InSAR and Subsidence History

Documentation of subsidence at the new earth fissure is limited to the period of historic InSAR coverage that began in 1992. The new fissure is positioned along the southeastern edge of a local subsidence bowl southeast of the Hawk Rock bedrock complex and is centered about a mile southeast of the former Hawk Rock as seen on **Figure A-1** (AMEC, 2014). InSAR Profile D-D' (**Figure 6**) is oriented perpendicular to the new fissure to document the maximum differential subsidence characteristics that would have driven the development of that fissure. It is noted that InSAR profile locations are shown on **Figures A-1** to **A-10**. Profile D-D' also encompasses part of the Hawk Rock bedrock complex (**Figure 5**) and the subsidence bowl to the northwest of the new fissure. Historic InSAR coverage from 1992 to 2000 indicated maximum

subsidence of about 0.5 feet during that period (AMEC, 2014). Further historic InSAR coverage from 2004 to 2010 indicated maximum subsidence of about 0.3 feet during that period (AMEC, 2014). More recent InSAR (**Figure A-1, Figure 6**) along Profile D-D' indicates a maximum subsidence of about 0.23 feet from 2010 to 2019. Maximum subsidence at the local subsidence bowl is summarized in Table 6-1.

There is a trend of gradual decreasing maximum subsidence rates in these InSAR time periods starting in 1992. As summarized in Table 6-1, an early average rate of about 0.06 feet/year in the 1990s declined to about 0.05 feet/year in the 2000s and declined further to about 0.025 feet/year in the 2010s. The maximum annual subsidence along Profile D-D' (**Figure 6**) at the end of the 2010s, from March 2018 to March 2019, was 0.021 feet. The presence of this local subsidence bowl feature in the historic InSAR profiles is attributable to delayed compaction of the clay-dominated alluvium still responding to significant groundwater declines that occurred from the 1940s into the 1980s. The gradual decrease in subsidence rates over time is consistent with this delayed compaction to be analogous to secondary consolidation in clays that tends to asymptotically decay over time even long after changes in effective stress (groundwater decline) have ceased.

Table 6-1: Maximum Subsidence Rates over Time at Subsidence Bowl Northeast of New Fissure

Time Period, years	Maximum Subsidence, feet	Maximum Subsidence Rate, ft/yr
1992-2000	0.5	0.06
2004-2010	0.3	0.05
2010-2019	0.23	0.025

A second zone of detectable but small subsidence is also indicated at profile distance around 20,000 feet in Profile D-D' (**Figure 6**). At a local subsidence of about 0.08 feet from 2010 to 2019, less than 0.01 feet/year, this small feature is essentially undetectable using GPS survey methods. The feature does correlate with an isolated zone of clay-dominated alluvium (8.3 ohm-m) interpreted at Sounding R-8 (AMEC, 2014) centered upstream of Vineyard Road FRS Station 263+00. The presence of this small subsidence feature in the 2010 to 2019 InSAR profile is attributable to delayed compaction of the clay-dominated alluvium interpreted in the Sounding R-8 area that is still responding to significant groundwater declines that occurred from the 1940s into the 1980s.

InSAR Profile E-E' (**Figure A-1, Figure 7**) is oriented southwest to northeast along the trend of the new fissure. It roughly parallels the Powerline Floodway channel to the southwest of the CAP Canal and Vineyard Road FRS, and extends through the spillway area north of the northwest end of Vineyard Road FRS. The 2010 to 2019 InSAR profile shows a small magnitude, about 0.07 feet maximum, but still measureable, subsidence centered around the CAP Canal and FRS. The new fissure is on the southwestern slope of this local subsidence bowl. This subsidence feature is interpreted to be related to secondary consolidation of clayey alluvium impacted by historic groundwater pumping at the construction well D(1-8)9CCC, also recorded as D(1-8)17AAA, previous discussed in Section 5.0. Various implications of that well to the subsidence history of the northern end of Vineyard Road FRS are evaluated and discussed in the AMEC (2014) report. In brief, that well was installed into a zone of localized clay-dominated alluvium. The use of that well for construction water for the FRSs and CAP Canal resulted in accelerated subsidence in that alluvium at the northern end of Vineyard Road FRS through the 1980s. In subsequent years, this same area had slower subsidence relative to the surrounding basin as the surrounding basin subsidence 'caught

up' with that local specific well-induced subsidence. By the 2010s, as the surrounding basin alluvium 'caught up' with the well-induced subsidence pattern, the small secondary consolidation-type subsidence continuing at the northern end of Vineyard Road FRS is measurable in the InSAR profile.

Finally, InSAR Profile F-F' (**Figure A-1, Figure 8**) indicates that the maximum strain becomes smaller along the trend of the new fissure between the new earth fissure and the Vineyard Road FRS. This can be seen in **Figure A-1** where the yellow color band in the InSAR pattern is at its' thinnest near the new fissure, and becomes thicker, indicating a more gradual differential subsidence rate, as it moves to the northeast and north. Perhaps more significantly, the zone of maximum strain is turning northward as it follows the edge of the local subsidence bowl northwest of the new fissure. This change in maximum strain direction is moving away from the northwest corner of Vineyard Road FRS and towards the southeast corner of the Powerline Dam FRS (red to yellow interface in **Figure A-1**). Rehabilitation plans being implemented include decommissioning and abandoning Powerline Dam FRS following its' replacement with the future Powerline Diversion Channel currently under design. Thus, the possibility of a gradual increase in ground tension towards the Powerline Dam FRS is not a concern.

Current Sentinel InSAR data was processed to evaluate its potential value for providing finer detail with smaller pixel size and increased frequency of data acquisition compared to Radarsat data currently utilized by ADWR. Eight (8) interferograms covering short time periods (typically about a month) were developed from available data between May 2018 and January 2020. Given the smaller pixel sizes in the Sentinel data, the short time periods of about a month were needed to achieve effective data coherence (95% coherence or better across the InSAR image pairs). It was determined that the resulting interferograms with minimal filtering were noisy, rendered the results less useful for general subsidence assessment than the more highly filtered and 'less granular' results provided by ADWR, For purposes of this project, further filtering and averaging of the Sentinel results was not performed.

6.5 Seismic Refraction Profiling

The purpose of the seismic refraction profiling was to identify and locate subsurface anomalies that would indicate the presence, location and extent of earth fissuring in the shallow subsurface. Previous experience has demonstrated the effectiveness of the method to trace incipient earth fissuring where visible and identifiable surficial evidence of that earth fissuring had not yet developed. The seismic refraction and ReMi data have been fully interpreted; results of the interpretations are presented in **Appendix B**. Weak possible anomalies were interpreted at several traces of Seismic Line SL20-01 positioned at the visible end of the earth fissure. Signal continuity in both gradual attenuation of signal over distance and relatively uniform increases in time for adjacent first arrivals were observed throughout the trace results for the remaining Seismic Lines SL20-02 through SL20-04; interpretations of the seismic signals at these seismic lines resulted in a determination of no incipient earth fissuring beyond the end of the visible earth fissure trace.

No strong seismic anomalies consistent with the presence of existing earth fissures with continuous open ground fractures were identified in any of the seismic traces, including no strong anomalies at Seismic Line SL20-01. Upon visual inspection of the new earth fissure, it was apparent that the fissure gully collects surface runoff during rain events. If earth fissure crack and fracture apertures are too thin to allow high-velocity, erosive water flow into the subsurface, such capture of surface flow presents the opportunity for

the deposition of soil in fissure openings. Under such conditions, where there is insufficient active tension to increase fissure crack and fracture apertures to widths capable of supporting high velocity, erosive water flow, the open fractures and cracks inherent in earth fissuring can become filled. Filled fractures, cracks and other openings can pass seismic signals across the now-filled fissure openings so that signal attenuation and time delays become minimized and result in the detection and interpretation of weak seismic anomalies. Thus, it is anticipated that the fracturing, cracking and other openings that would have been initially present in the new earth fissure are in a state of having been filled at Seismic Line SL20-01, and that such open aperture cracks and fracture features are not present at Seismic Lines SL20-02 through SL20-04 located closer to the Vineyard Road FRS.

7.0 CONCLUSIONS & RECOMMENDATIONS

The newly identified earth fissure located approximately 2,100 feet west/southwest of Vineyard Road FRS appears to have developed into an earth fissure with surface expression between 2012 and 2014, and the length of the earth fissure has largely remained unchanged since 2014. The earth fissure appears to have developed at this location due to the site-specific geologic combination at its location of relatively shallow bedrock in the area, the presence of low-resistivity, fine-grained deep alluvium to northwest of its location, and the presence of higher-resistivity, highly permeable deep alluvial materials underlying the fissure and present to the immediate southeast. These geologic conditions, combined with regional groundwater withdrawal and pumping at Well D(1-8)9CCC for construction of Powerline and Vineyard Road FRSs, create the unique characteristics that lead to concentrated differential subsidence, tensional ground strain, and the development of the earth fissure.

Analysis of data acquired for this evaluation, data reviewed and acquired for previous investigations, and instrumentation and monitoring data show that conditions at the Vineyard Road FRS differ from those at the newly identified earth fissure. The ground strain present at the newly identified earth fissure appears to dissipate toward the FRS, and InSAR and survey data indicate that at the north end of Vineyard Road FRS, historic and ongoing subsidence has created an area where ground compression is likely. This condition appears to have been caused by pumping at well D(1-8)9CCC that created localized land subsidence patterns that concentrated ground strains in the area of the new earth fissure and away from the Vineyard Road FRS. Additionally, the seismic refraction data indicates that the newly identified earth fissure is not present in the subsurface beyond its surficial extent.

The culmination of this analysis is that Wood believes that conditions at the Vineyard Road FRS do not appear to be conducive to the development of earth fissures and that the presence of the new earth fissure is unlikely to impact the FRS, or the ongoing Vineyard Road FRS Rehab and the Powerline Channel designs.

7.1 Vineyard Road FRS Earth Fissure Risk Zone Delineation

Figure 9 shows the earth fissure risk zone delineation developed for the Final Design-Level Subsidence and Earth Fissure Zoning Report (AMEC, 2014). The newly identified earth fissure is located outside of District right-of-way and beyond the area shown on the existing earth fissure zones. Considering the conclusion that conditions at the Vineyard Road FRS do not appear to be conducive to the development of earth fissures and that the presence of the new earth fissure is unlikely to impact the FRS, Wood

recommends no changes be made to the earth fissure risk zone delineation along Vineyard Road FRS. The risk zone delineation shown on Figure 9 has been updated to reflect low-moderate earth fissure risk zone in the area between the newly identified earth fissure and Powerline FRS that is located within District right-of-way. This update slightly increases the previous low-moderate earth fissure risk zone for Powerline FRS in the vicinity of Station 50+00 and places the Powerline Floodway within a low-moderate risk zone from about Station 0+50 to 30+00. It is noted that the Powerline Floodway is a lined, below-grade channel in this area.

7.2 Instrumentation & Monitoring

Wood recommends that monitoring of the newly identified earth fissure be incorporated into the annual instrumentation and monitoring activities for Vineyard Road FRS. Areas between the new earth fissure and Vineyard Road FRS and the Powerline Floodway should be included. Additional activities should include annual inspections of the earth fissure, annual review of aerial imagery as part of the cursory review of aerial imagery activities, and inclusion in the photo-geologic lineament analysis that occurs every three years. It is also recommended that InSAR Profiles D-D′ and F-F′ be incorporated into the annual InSAR analysis and reporting. No additional ground instrumentation is recommended at this time for monitoring the newly identified earth fissure.

8.0 REFERENCES

AMEC Earth & Environmental Inc. (AMEC). 2006. Preliminary Earth Fissure Risk Zone Investigation Report, Hawk Rock Study Area, Maricopa and Pinal Counties, Contract FCD 2006C005 Work Assignment 2, AMEC Job No. 6-117-001053. September 25.

AMEC, 2008. Siphon Draw Drainage Improvement Project, Geologic Hazard Assessment and Geotechnical Characterization Report, Maricopa County, Contract FCD 2007C012, AMEC Job No. 7-117-001080. September 3.

AMEC, 2011. Procedural Documents for Land Subsidence and Earth Fissure Appraisals. Prepared for the Flood Control District of Maricopa County. Contract FCD2008C016, Work Assignment No. 13. May.

AMEC, 2013. Subsidence and Earth Fissure Risk Zoning Report, McMicken Dam Final Design-Level Geohazard Investigation. Phoenix, Arizona. Contract FCD 2011C005, Work Assignment No. 4. AMEC Job No. 17-2011-4052. February 28.

AMEC, 2014. *Final Design-Level Subsidence and Earth Fissure Risk Zoning Report, Powerline, Vineyard Road and Rittenhouse Flood Retarding Structures Design Project; Pinal County, Arizona*. Contract No. FCD 2011C005, Work Assignment No. 12, AMEC Job No. 17-2013-4045, December 9.

Cook, J.P., B.D. Conway, and P.A. Ivanich. 2013. Land subsidence and earth fissure risk analysis for the Hawk Rock area of Fannin McFarland Reaches 1 through 3 of the Central Arizona Project Canal, Maricopa and Pinal Counties, Arizona. A report to the Maintenance and Engineering Department, Central Arizona Project, June.

Gootee, B.F. 2013, An Evaluation of Carbon Dioxide Sequestration Potential in the Higley Basin, South-Central Arizona. Arizona Geological Survey Open File Report, OFR-13-10, 14 p., 6 map plates and 2 appendices.

Hipke, W. 2010. 100-Year Predictive Scenarios Used for the Determination of Physical Availability in the Phoenix Active Management Area: A Salt River Valley Groundwater Flow Model Application. Arizona Department of Water Resources Modeling Report No. 22. Hydrology Division, Phoenix Arizona. July.

Laney, R.L. and M.E. Hahn. 1986. Hydrogeology of the Eastern Part of the Salt River Valley Area: Maricopa and Pinal Counties, Arizona. U.S. Geological Survey Water Resources Investigations Report 86-4147. 4 sheets.

Pearthree, P.A. and G. Huckleberry. 1994. Surficial Geologic Map of the Mesa 30' x 60' Quadrangle, Arizona. Arizona Geological Survey Open File Report, OFR-94-24, 1 map sheet, map scale 1:100,000.

Prokopovich, Nikola P. 1983. Reconnaissance Estimates of Subsidence Along Salt Gila Aqueduct, Arizona. Bulletin of the Association of Engineering Geologists 22(3): 297 315.

Sweeney, R.E., and P.L. Hill. 2001. Arizona Aeromagnetic and Gravity Maps and Data. U.S. Geological Survey Open-File Report 01-0081.

U.S. Bureau of Reclamation (USBR). 1976. Geology and Ground Water Resources Report of Maricopa and Pinal Counties, Arizona. Phoenix, Arizona: USBR, Phoenix Projects Office.

Wood Environment & Infrastructure Solutions, Inc. (Wood). 2019. *2018-2019 Earth Fissure Monitoring Report, Siphon Draw Wash Drainage Improvements Project*, Prepared for the Flood Control District of Maricopa County. Contract No. FCD 2016C010, Work Assignment No. 21, Wood Job No. 17-2018-4065.

FIGURES

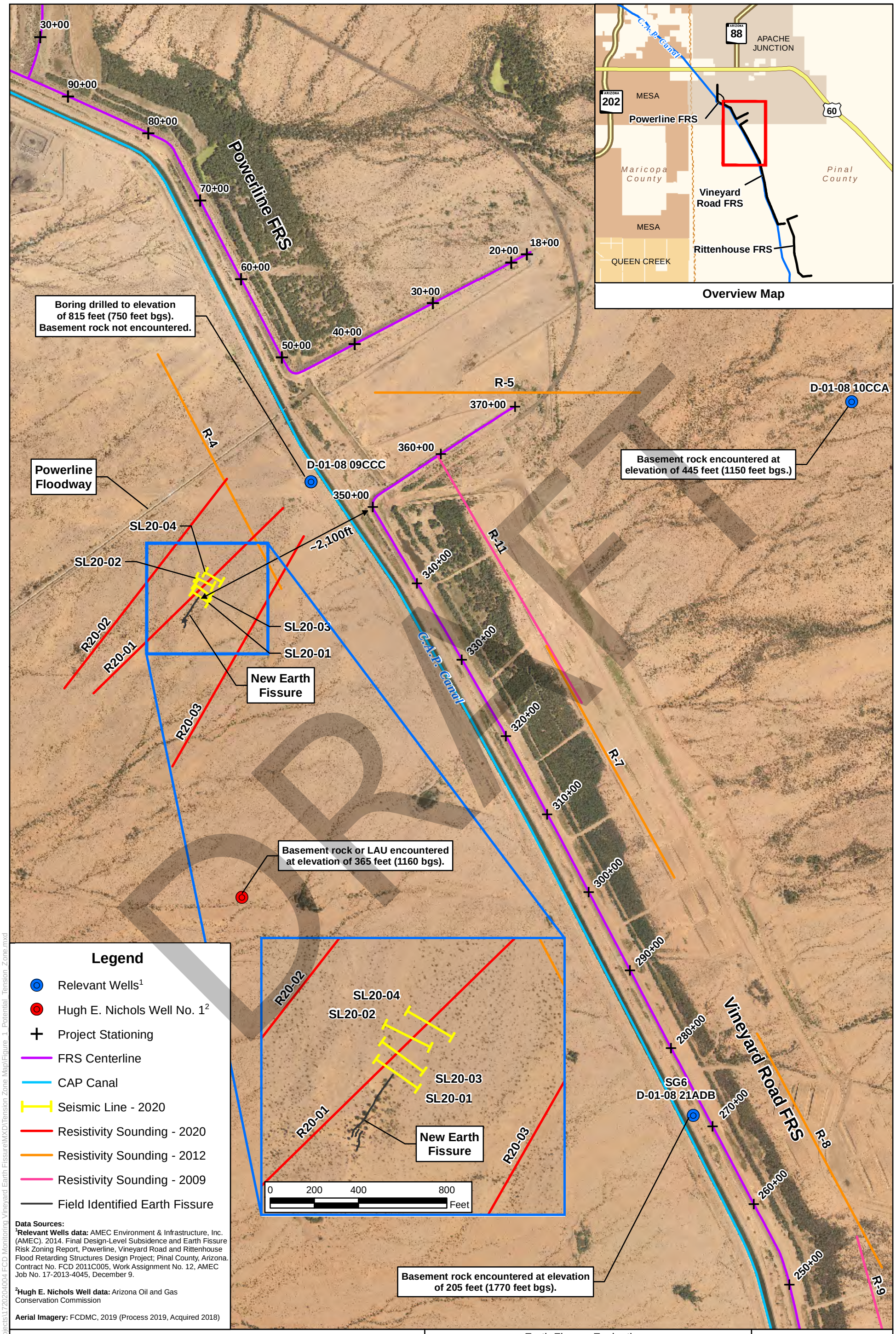

Legend

- Relevant Wells[1]
- Hugh E. Nichols Well No. 1[2]
- Project Stationing
- FRS Centerline
- CAP Canal
- Seismic Line - 2020
- Resistivity Sounding - 2020
- Resistivity Sounding - 2012
- Resistivity Sounding - 2009
- Field Identified Earth Fissure

Data Sources:

[1]**Relevant Wells data:** AMEC Environment & Infrastructure, Inc. (AMEC). 2014. Final Design-Level Subsidence and Earth Fissure Risk Zoning Report, Powerline, Vineyard Road and Rittenhouse Flood Retarding Structures Design Project; Pinal County, Arizona. Contract No. FCD 2011C005, Work Assignment No. 12, AMEC Job No. 17-2013-4045, December 9.

[2]**Hugh E. Nichols Well data:** Arizona Oil and Gas Conservation Commission

Aerial Imagery: FCDMC, 2019 (Process 2019, Acquired 2018)

0 500 1,000 2,000
Feet

Job No.	17-2020-4004
PM:	DNF
Date:	3/12/2020
Scale:	1" = 1000'

N

Earth Fissure Evaluation
Vineyard Road Flood Retarding Structure
Contract FCD 2016C010, Work Assignment No. 34
Pinal County, Arizona

Site Plan and Vicinity Map

FIGURE
1

wood.

Path: X:\Projects\2020 Projects\172020004 FCD Monitoring Vineyard Earth Fissure\MXD\Tension Zone Map\Figure_1_Potential_Tension_Zone.mxd

2019

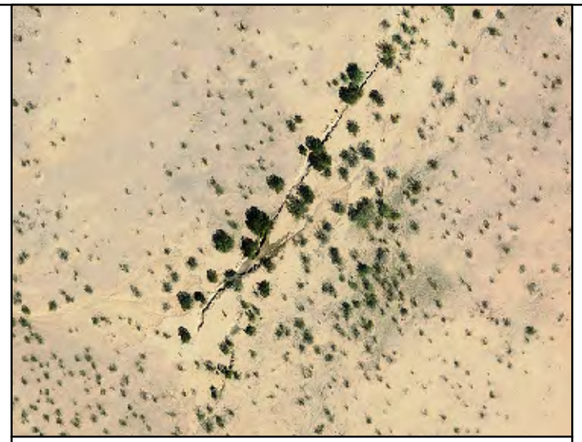

2018

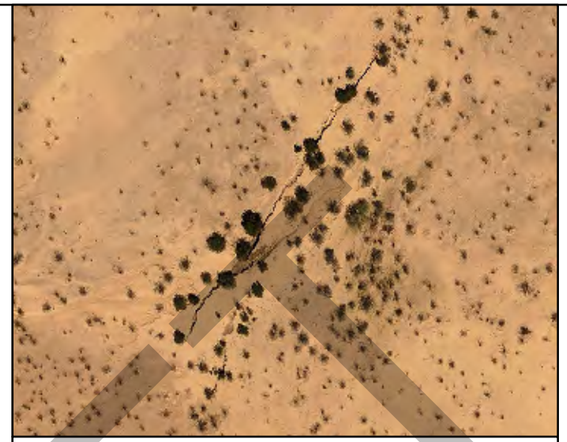

2017

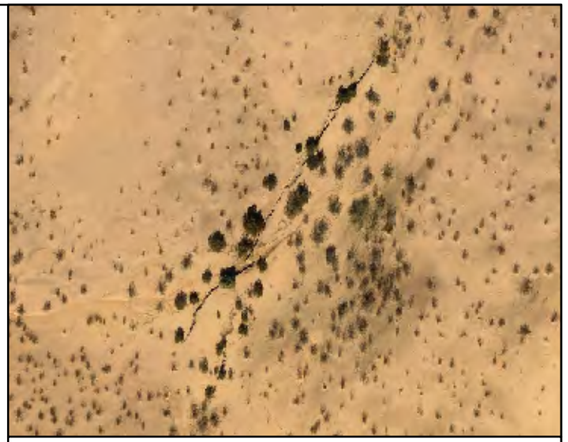

2016

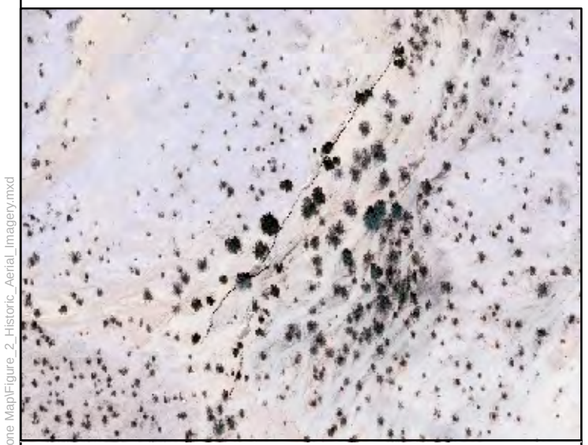

2015

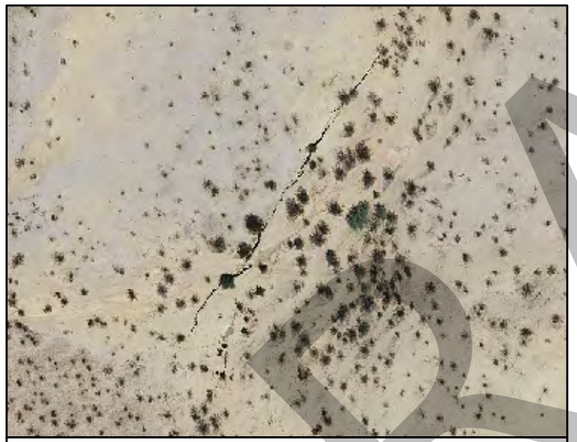

2014

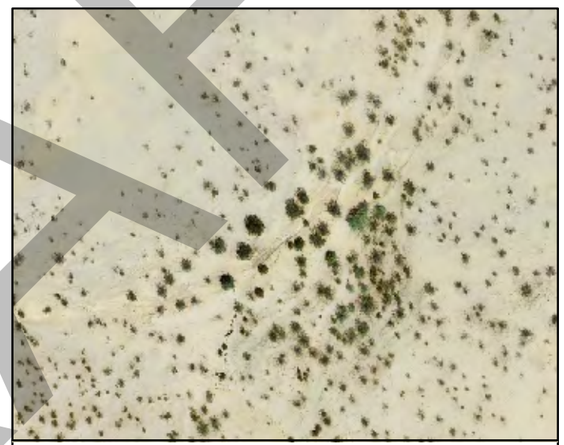

2013

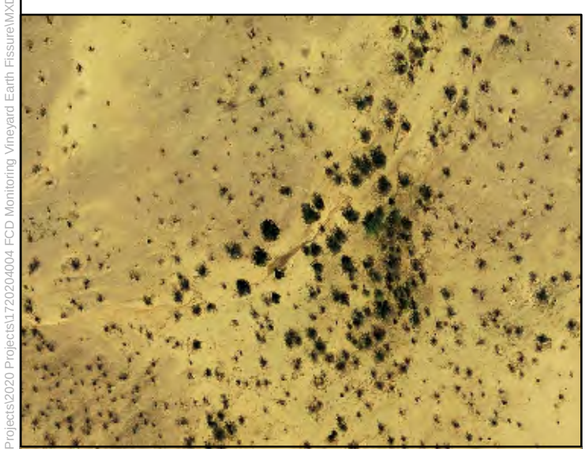

2012

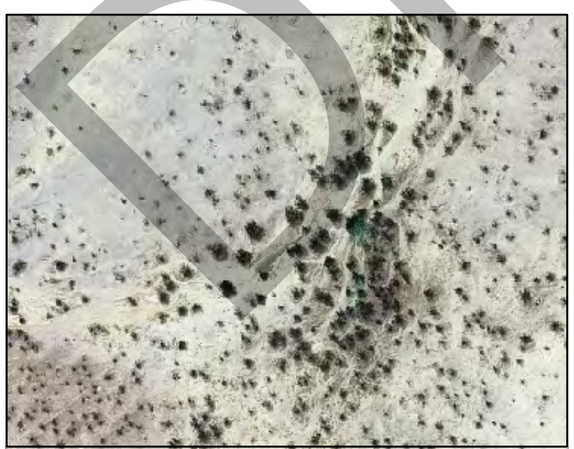

2011

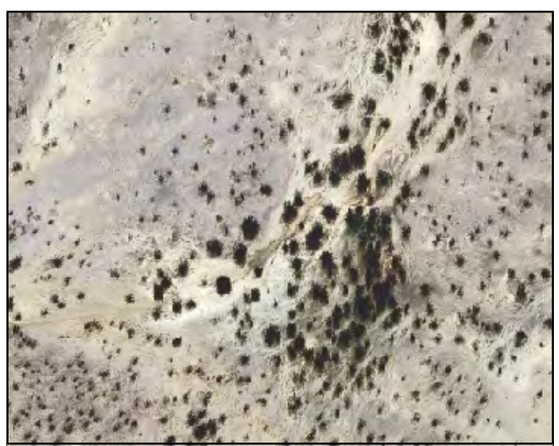

2010

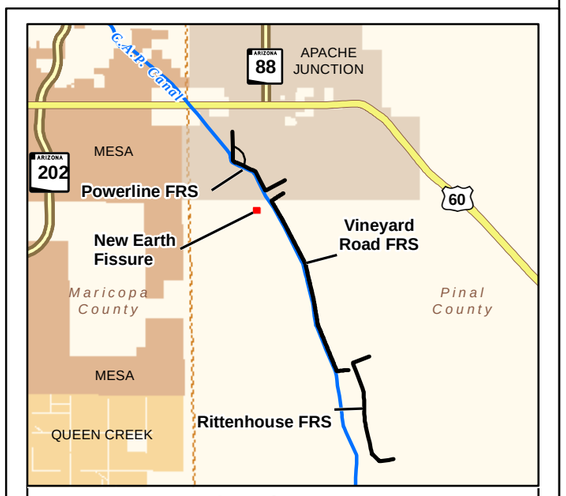

Overview Map

Years shown on images refer to the year the images were processed.
Acquisition of the images may have occurred in the prior year.

0 50 100 150 300 Feet

N

Earth Fissure Evaluation
Vineyard Road Flood Retarding Structure
Contract FCD 2016C010, Work Assignment No. 34
Pinal County, Arizona

Figure **2**

Historic Aerial Imagery

Job No.	17-2020-4004
PM:	DNF
Date:	3/12/2020
Scale:	1"= 150 feet

wood.

Path: X:\Projects\2020 Projects\172020004 FCD Monitoring Vineyard Earth Fissure\MXD\Tension Zone Map\Figure_2_Historic_Aerial_Imagery.mxd

Powerline North Diversion Channel
Powerline Fissure
Powerline IDSM
Powerline FRS
Powerline Floodway
New Earth Fissure
Vineyard Road FRS Spillway
Vineyard Road FRS
Rittenhouse FRS
CAP Canal
60
10+00
20+00
30+00
50+00
100+00
150+00
200+00
290+00
300+00
310+00
320+00
330+00
340+00
350+00
360+00
370+00
D-01-08 09CCC
D-01-08 10CCA
SG6
D-01-08 21ADB
Boring drilled to elevation of 815 feet (750 feet bgs). Basement rock not encountered.
Basement rock encountered at elevation of 445 feet (1150 feet bgs.)
Basement rock or LAU encountered at elevation of 365 feet (1160 feet bgs.)
Basement rock encountered at elevation of 205 feet (1770 feet bgs.)

Legend

- FRS Stationing
- Conceptual Powerline Floodway Geologic Profile Endpoint[5]
- Relevant Wells[5]
- Hugh E. Nichols Well No. 1[6]
- CAP Canal
- Flood Control Structure Centerline
- Vineyard Road FRS Spillway
- Estimated Depth to Basement Rock (ft)[1]
- Bouguer Gravity Contours (milligals)[2]
- Interpreted Basement Rock Elevation (ft)[3]

Earth Fissures[4]

- Continuous Earth Fissures
- Discontinuous Earth Fissures
- Confirmed, unsurveyed earth fissures
- Unconfirmed Earth Fissures

Data Sources:

[1]**Depth to Basement Rock digitized from:** Laney, R. L. and Hahn, M.E., Hydrogeology of the Eastern Part of the Salt River Valley Area, Maricopa and Pinal Counties, Arizona, 1986, US Geological Survey Water Resources Investigations Report 86-4147.

[2]**Gravity data from:** Arizona Complete Bouguer Gravity Anomaly Map, U.S. Department of the Interior, U.S. Geological Survey, OFR--01-0081.

[3]**Basement Rock Elevation Interpreted from:** USGS Bureau of Reclaimation, unpublished (AMEC 2002).

[4]**Earth Fissure data:** Arizona Geological Survey, 2019, Locations of Mapped Earth Fissure Traces in Arizona, 06.03.2019. Arizona Geological Survey Digital Information (DI-39 v. 06.03.2019), Tucson, Arizona.

[5]**Profile and Relevant Well data:** AMEC Environment & Infrastructure, Inc. (AMEC). 2014. Final Design-Level Subsidence and Earth Fissure Risk Zoning Report, Powerline, Vineyard Road and Rittenhouse Flood Retarding Structures Design Project; Pinal County, Arizona. Contract No. FCD 2011C005 Work Assignment No. 12, AMEC Job No. 17-2013-4045, December 9.

[6]**Hugh E. Nichols Well data:** Arizona Oil and Gas Conservation Commission.

Aerial Imagery: FCDMC, 2019 (Process 2019, Acquired 2018).

0 2,000 4,000 8,000 Feet

N

Job No.	17-2020-4004
PM:	DNF
Date:	3/11/2020
Scale:	1" = 4000'

The map shown here has been created with all due and reasonable care and is strictly for use with Wood Environment & Infrastructure Solutions, Inc. Project Number 17-2020-4004. This map has not been certified by a licensed land surveyor, and any third party use of this map comes without warranties of any kind. Wood Environment & Infrastructure Solutions, Inc. assumes no liability, direct or indirect, whatsoever for any such third party or unintended use.

Earth Fissure Evaluation
Vineyard Road Flood Retarding Structure
Contract FCD 2016C010, Work Assignment No. 34
Pinal County, Arizona

Gravity Data and Depth to Bedrock

FIGURE 3

wood.

Path: X:\Projects\2020 Projects\17-2020-4004 FCD Monitoring Vineyard Earth Fissure\MXD\Tension Zone Map\Figure_3_Gravity_map.mxd

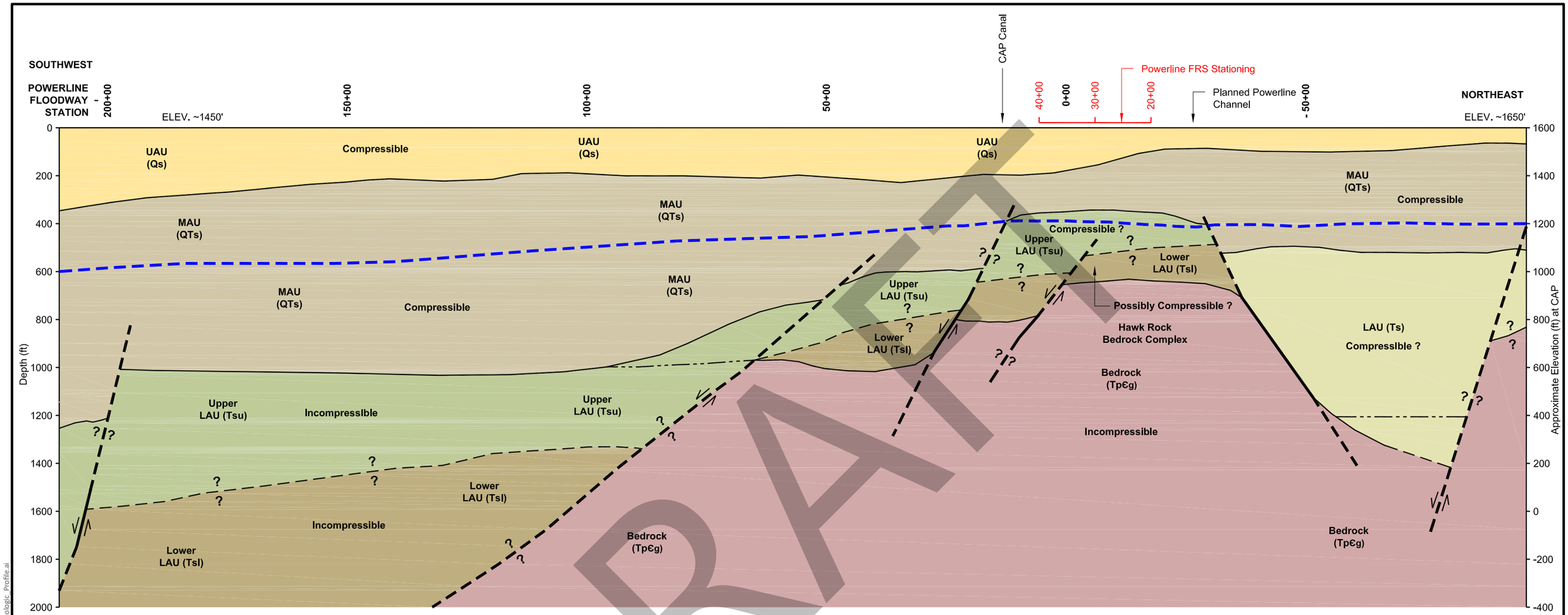

Geologic Descriptions

Upper Alluvial Unit (UAU - Qs) Intercalated alluvial fan and fluvial deposits of predominately clastic material deposited as a mantle over the older basin fill deposits. The UAU may be as old as 3.3 million years; however, most of the unit is likely less than 1 million years in age. Compressible.

Middle Alluvial Unit (MAU - QTs) Weakly consolidated playa, alluvial fan, and fluvial deposits of silt, siltstone, and silty sand and gravel. Moderately to well-cemented siltstone occurs locally. Near the margin of the basin the MAU contains more silt and clay than the LAU. The age of the MAU is constrained between 8 and 3.3 million ybp. Compressible.

Lower Alluvial Unit (LAU - Ts) Undifferentiated LAU likely consisting of moderately to well-cemented mudstone gypsiferous and anhydritic mudstone, anhydrite, sand and gravel, conglomerate and basalt. Compressible where similar to Upper LAU as described below.

Upper Lower Alluvial Unit (Upper LAU - Tsu) Weakly to well-cemented clay, silt, mudstone, gypsiferous mudstone, sand and gravel, and conglomerate. Age is between 8 and 10 million years. Variably compressible. In the study area it appears to be compressible to the northeast of the Powerline FRS and incompressible south of the Powerline FRS.

Lower Lower Alluvial Unit (Lower LAU - Tsl) Well-cemented mudstone, gypsiferous and anhydritic mudstone, anhydrite, conglomerate and basalt. In areas near the basin margins the unit is greater than 10 million ybp. Incompressible.

Bedrock (TpЄg). Crystalline rocks including granite, schist, gneiss, quartzite and metavolcanics. Tertiary to Precambrian in age. Incompressible.

Legend

- Approximate Geologic Contact
- Fault, Arrows Show Direction of Movement
- Inferred Fault, Queried Where Less Certain
- Approximate Current Water Table
- Assumed Limit of Compressible LAU (Ts)

Data Source:

AMEC Environment & Infrastructure, Inc. (AMEC). 2014. Final Design-Level Subsidence and Earth Fissure Risk Zoning Report, Powerline, Vineyard Road and Rittenhouse Flood Retarding Structures Design Project; Pinal County, Arizona. Contract No. FCD 2011C005, Work Assignment No. 12, AMEC Job No. 17-2013-4045, December 9.

JOB NO.	17-2020-4004
DESIGN:	DNF
DRAWN:	GWH
DATE:	03/04/2020
SCALE:	AS SHOWN

Earth Fissure Evaluation
Vinyard Road Flood Retarding Structure
Contract FCD 2016C010, Work Assignment No. 34
Pinal County, Arizona

GEOLOGIC PROFILE OF THE POWERLINE FLOODWAY

FIGURE 4

wood.

X:\Projects\2019 Projects\172019405\4 PVR & Siphon Draw\MXD\Tension Zone Map\Figure_4_Powerline_Floodway_GeologIc_Profile.ai

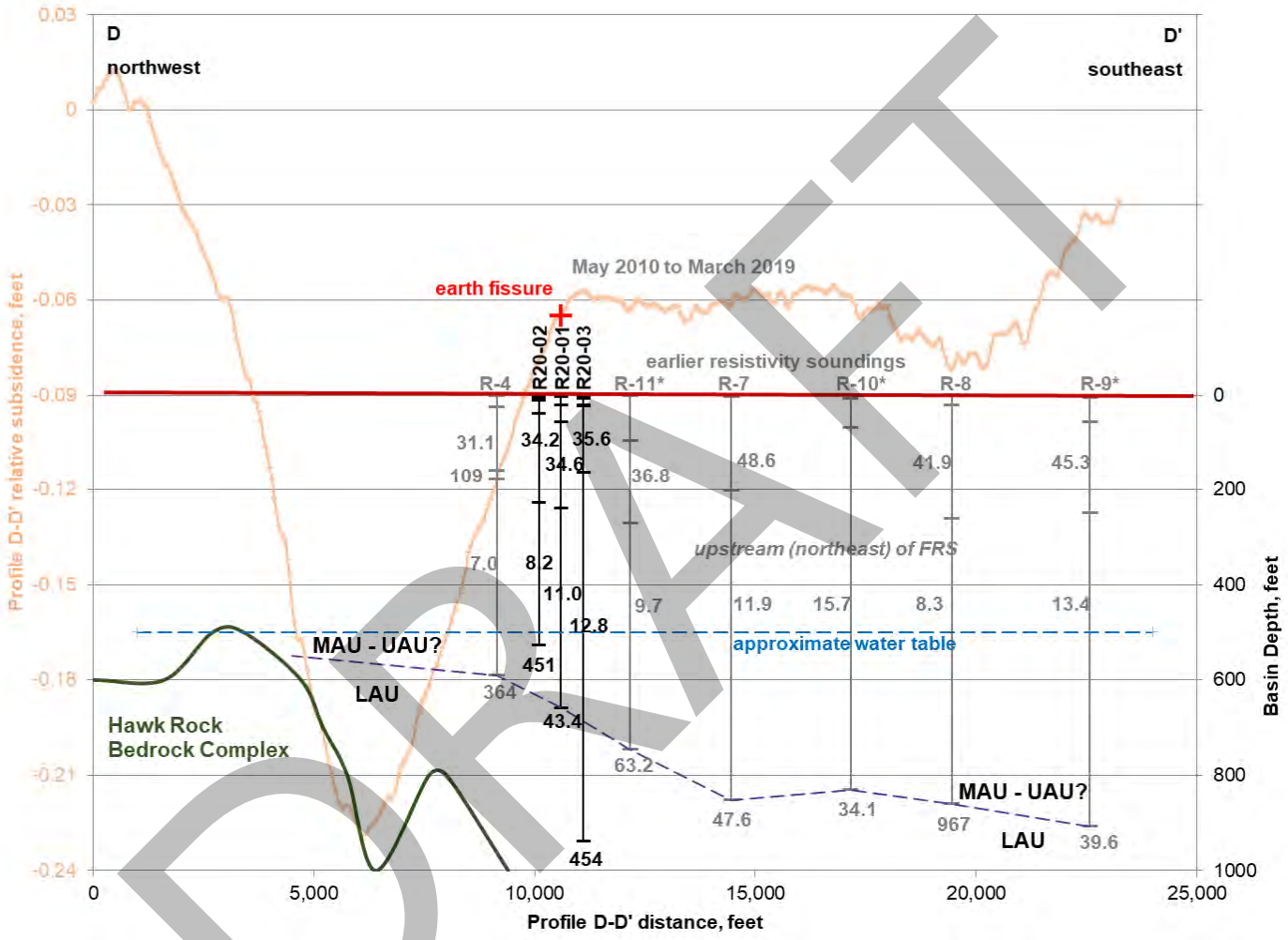

Vineyard Earth Fissure Evaluation Vineyard Road Flood Retarding Structure Contract FCD 2016C010, Work Assignment No. 34 Pinal County, Arizona	**Deep Resistivity Profile** **Profile D-D'**	FIGURE **5**	Job No. 1720204004 PM DNF Date 3/12/2020 Scale : n/a

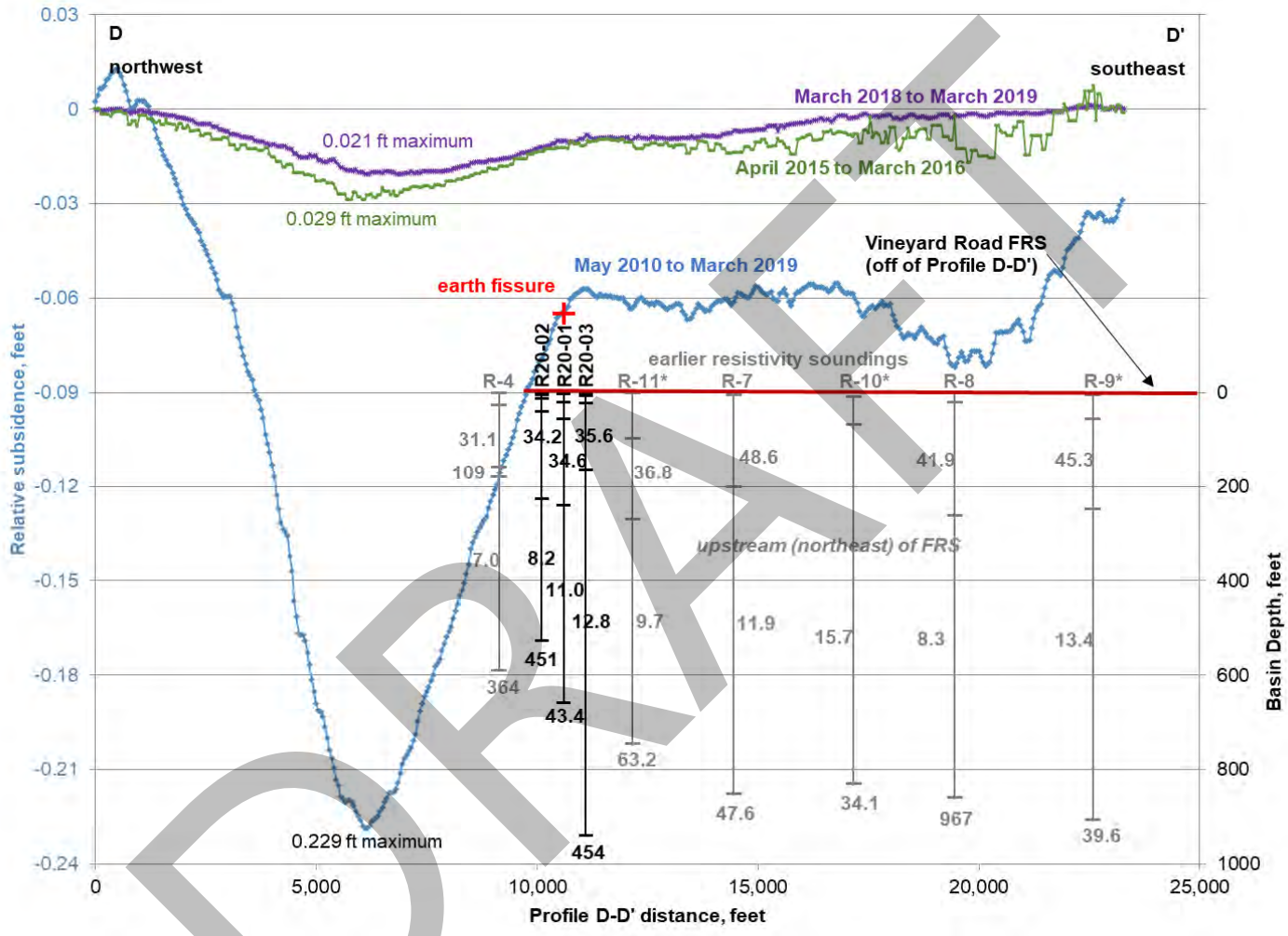

Vineyard Earth Fissure Evaluation Vineyard Road Flood Retarding Structure Contract FCD 2016C010, Work Assignment No. 34 Pinal County, Arizona	**InSAR Profile** **Profile D-D'**	FIGURE **6**	Job No. 1720204004 PM DNF Date 3/12/2020 Scale : n/a

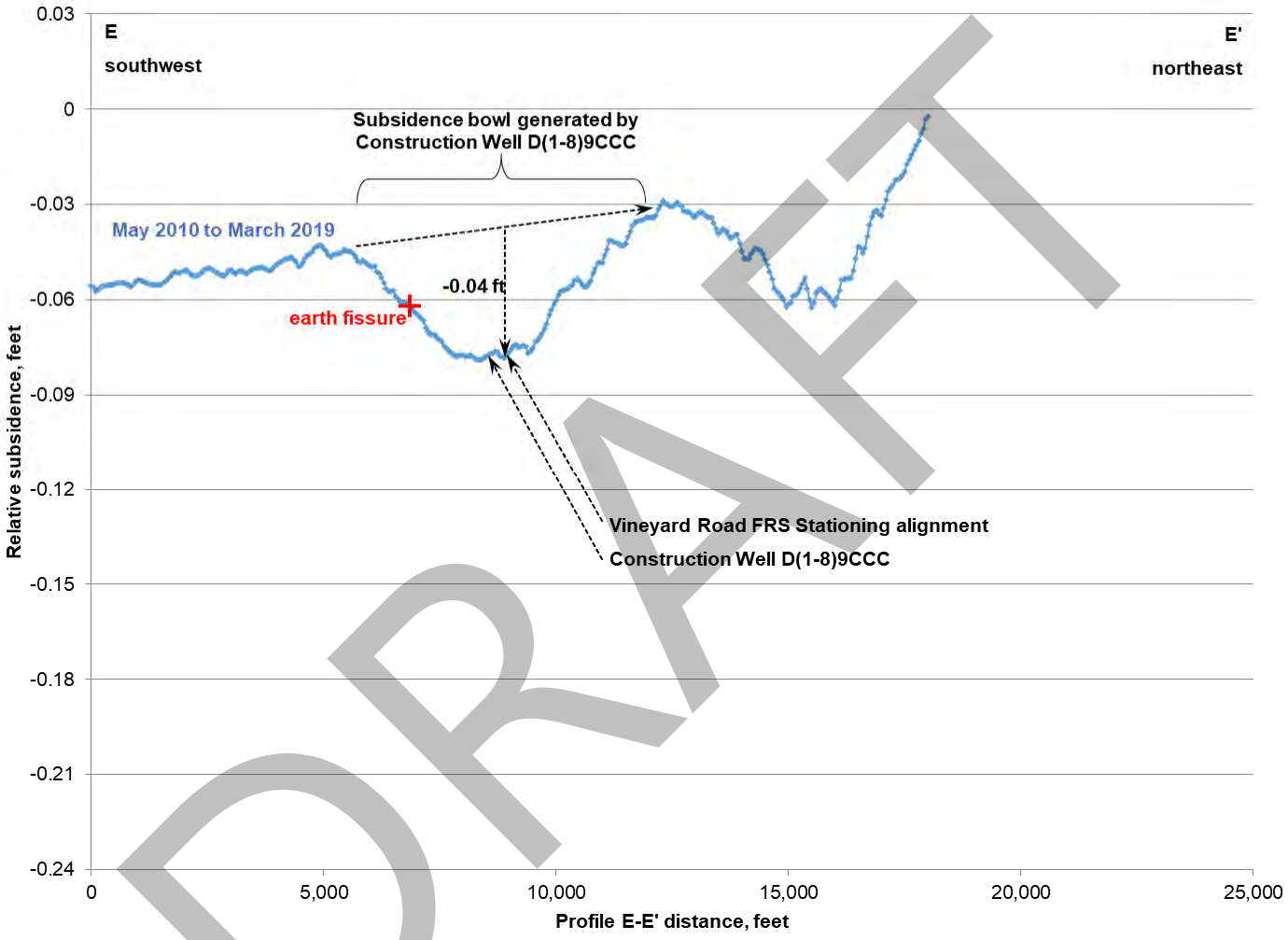

Vineyard Earth Fissure Evaluation Vineyard Road Flood Retarding Structure Contract FCD 2016C010, Work Assignment No. 34 Pinal County, Arizona	**InSAR Profile** **Profile E-E'**	FIGURE **7**	Job No. 1720204004 PM DNF Date 3/12/2020 Scale : n/a

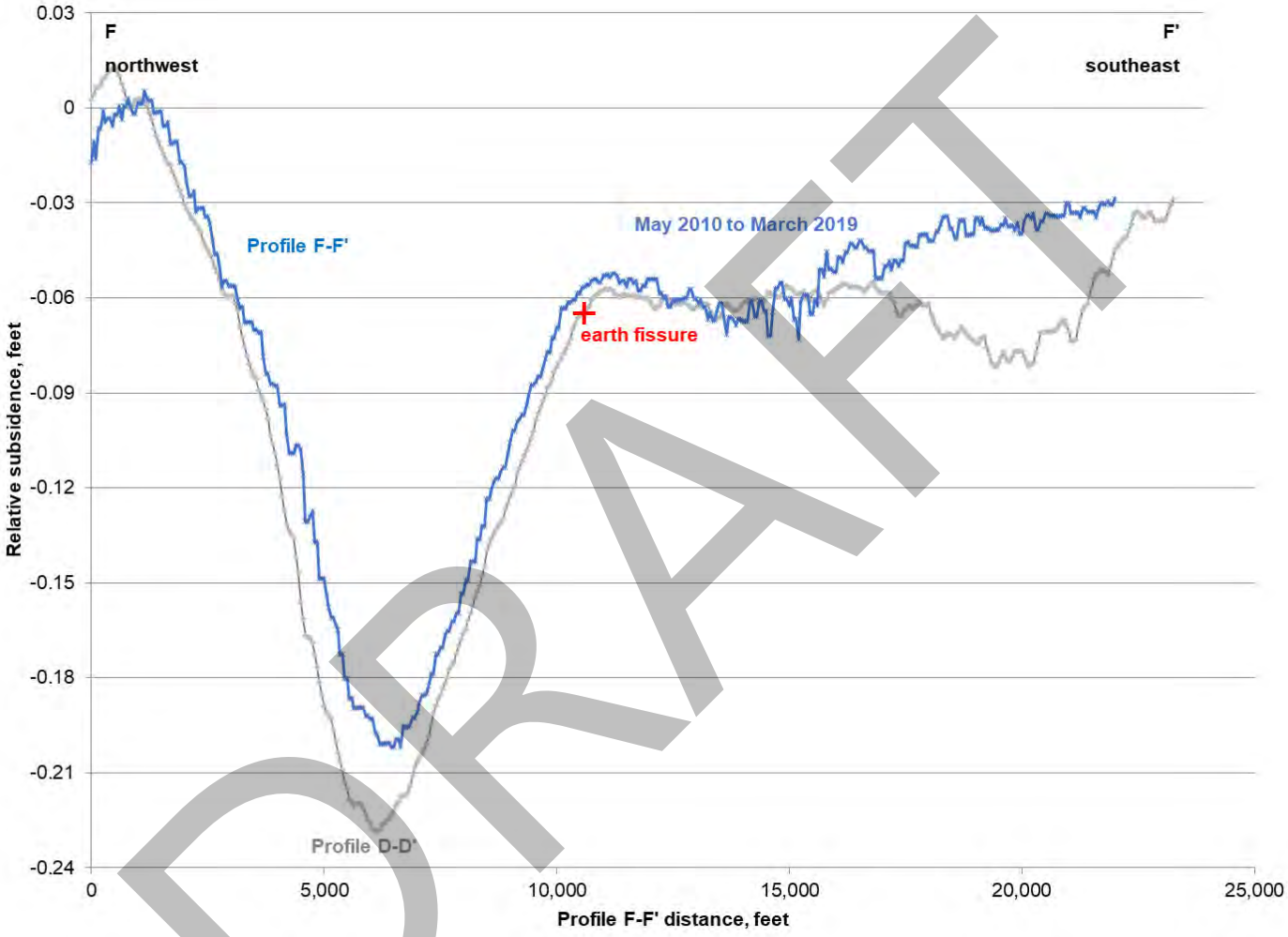

Vineyard Earth Fissure Evaluation Vineyard Road Flood Retarding Structure Contract FCD 2016C010, Work Assignment No. 34 Pinal County, Arizona	**InSAR Profile** **Profile F-F'**	FIGURE **8**	Job No. 1720204004 PM DNF Date 3/12/2020 Scale : n/a

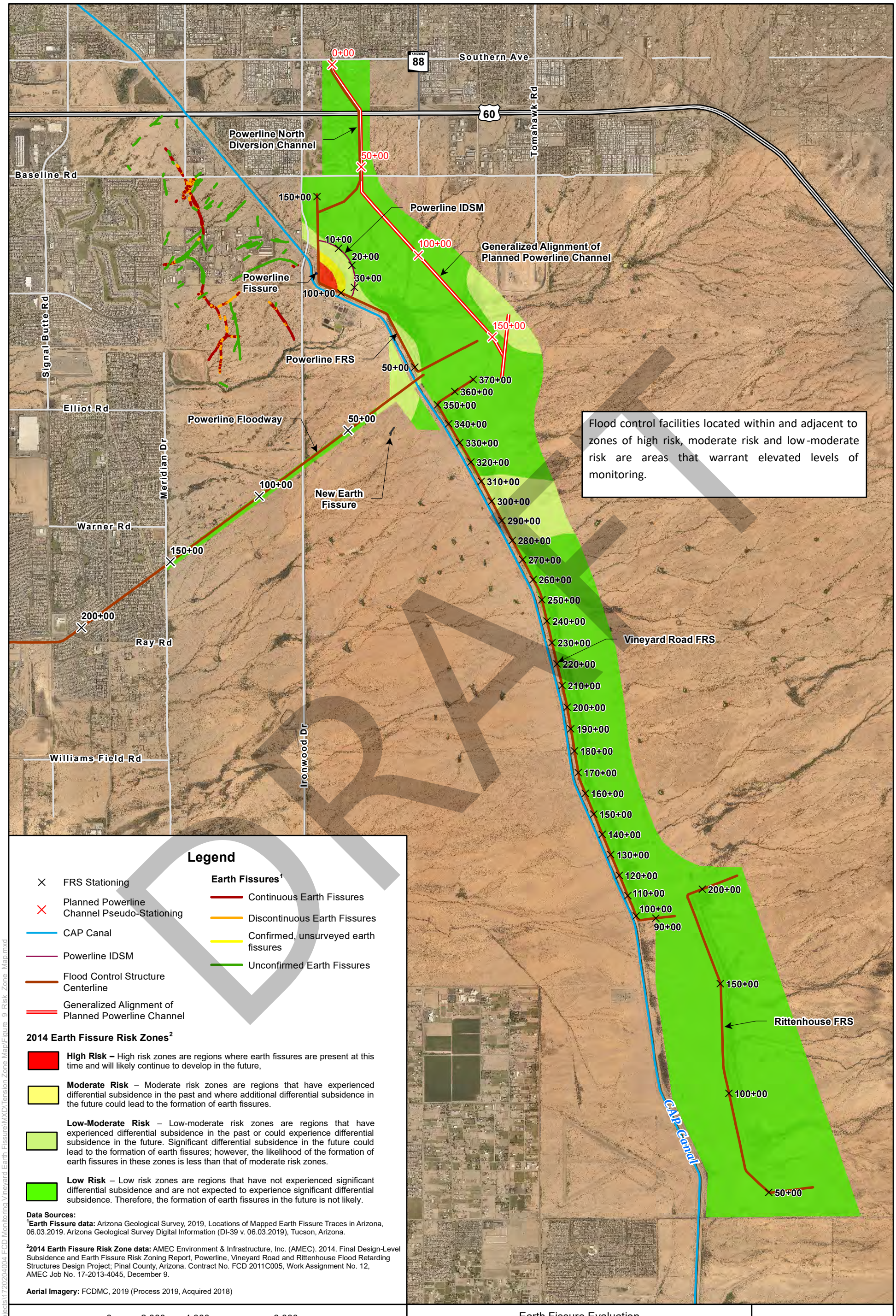

Legend

- FRS Stationing
- Planned Powerline Channel Pseudo-Stationing
- CAP Canal
- Powerline IDSM
- Flood Control Structure Centerline
- Generalized Alignment of Planned Powerline Channel

Earth Fissures[1]

- Continuous Earth Fissures
- Discontinuous Earth Fissures
- Confirmed, unsurveyed earth fissures
- Unconfirmed Earth Fissures

2014 Earth Fissure Risk Zones[2]

High Risk – High risk zones are regions where earth fissures are present at this time and will likely continue to develop in the future,

Moderate Risk – Moderate risk zones are regions that have experienced differential subsidence in the past and where additional differential subsidence in the future could lead to the formation of earth fissures.

Low-Moderate Risk – Low-moderate risk zones are regions that have experienced differential subsidence in the past or could experience differential subsidence in the future. Significant differential subsidence in the future could lead to the formation of earth fissures; however, the likelihood of the formation of earth fissures in these zones is less than that of moderate risk zones.

Low Risk – Low risk zones are regions that have not experienced significant differential subsidence and are not expected to experience significant differential subsidence. Therefore, the formation of earth fissures in the future is not likely.

Data Sources:

[1]**Earth Fissure data:** Arizona Geological Survey, 2019, Locations of Mapped Earth Fissure Traces in Arizona, 06.03.2019. Arizona Geological Survey Digital Information (DI-39 v. 06.03.2019), Tucson, Arizona.

[2]**2014 Earth Fissure Risk Zone data:** AMEC Environment & Infrastructure, Inc. (AMEC). 2014. Final Design-Level Subsidence and Earth Fissure Risk Zoning Report, Powerline, Vineyard Road and Rittenhouse Flood Retarding Structures Design Project; Pinal County, Arizona. Contract No. FCD 2011C005, Work Assignment No. 12, AMEC Job No. 17-2013-4045, December 9.

Aerial Imagery: FCDMC, 2019 (Process 2019, Acquired 2018)

0 2,000 4,000 8,000 Feet

Job No.	17-2020-4004
PM:	DNF
Date:	3/31/2020
Scale:	1" = 4000'

N

Earth Fissure Evaluation
Vineyard Road Flood Retarding Structure
Contract FCD 2016C010, Work Assignment No. 34
Pinal County, Arizona

Earth Fissure Risk Zone Classifications

FIGURE **9**

wood.

Path: X:\Projects\2020 Projects\172020004 FCD Monitoring Vineyard Earth Fissure\MXD\Tension Zone Map\Figure_9_Risk_Zone_Map.mxd

APPENDIX A

INSAR

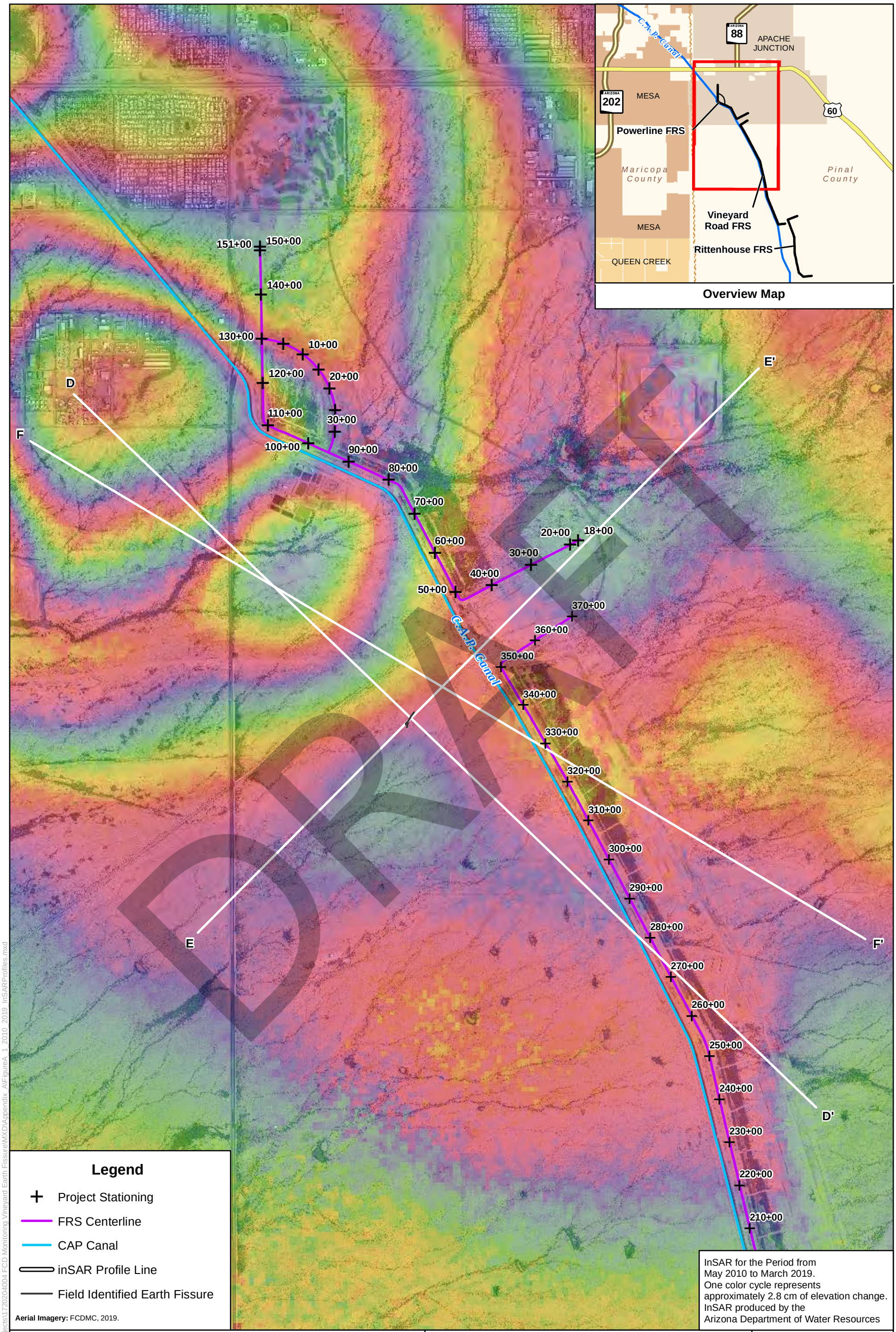
C.A.P. Canal
ARIZONA 88
APACHE JUNCTION
ARIZONA 202
MESA
60
Powerline FRS
Maricopa County
Pinal County
Vineyard Road FRS
MESA
Rittenhouse FRS
QUEEN CREEK
Overview Map
151+00
150+00
140+00
130+00
10+00
120+00
20+00
110+00
30+00
100+00
90+00
80+00
70+00
60+00
50+00
40+00
30+00
20+00
18+00
370+00
360+00
350+00
340+00
330+00
320+00
310+00
300+00
290+00
280+00
270+00
260+00
250+00
240+00
230+00
220+00
210+00
C.A.P. Canal
D
D'
E
E'
F
F'
DRAFT
Legend
Project Stationing
FRS Centerline
CAP Canal
inSAR Profile Line
Field Identified Earth Fissure
Aerial Imagery: FCDMC, 2019.
InSAR for the Period from
May 2010 to March 2019.
One color cycle represents
approximately 2.8 cm of elevation change.
InSAR produced by the
Arizona Department of Water Resources
0
1,000
2,000
4,000
Feet
N
Job No. 17-2020-4004
PM: DNF
Date: 3/5/2020
Scale: 1" = 2000'
The map shown here has been created with all due and reasonable care and is strictly for use with Wood Environment & Infrastructure Solutions, Inc. Project Number 17-2020-4004. This map has not been certified by a licensed land surveyor, and any third party use of this map comes without warranties of any kind. Wood Environment & Infrastructure Solutions, Inc. assumes no liability, direct or indirect, whatsoever for any such third party or unintended use.
Earth Fissure Evaluation
Vineyard Road Flood Retarding Structure
Contract FCD 2016C010, Work Assignment No. 34
Pinal County, Arizona
Synthetic Aperature Radar Interferogram
May 2010 to March 2019
FIGURE
A-1
wood.
Path: X:\Projects\2020 Projects\172020004 FCD Monitoring Vineyard Earth Fissure\MXD\Appendix_A\FigureA_1_2010_2019_InSARProfiles.mxd

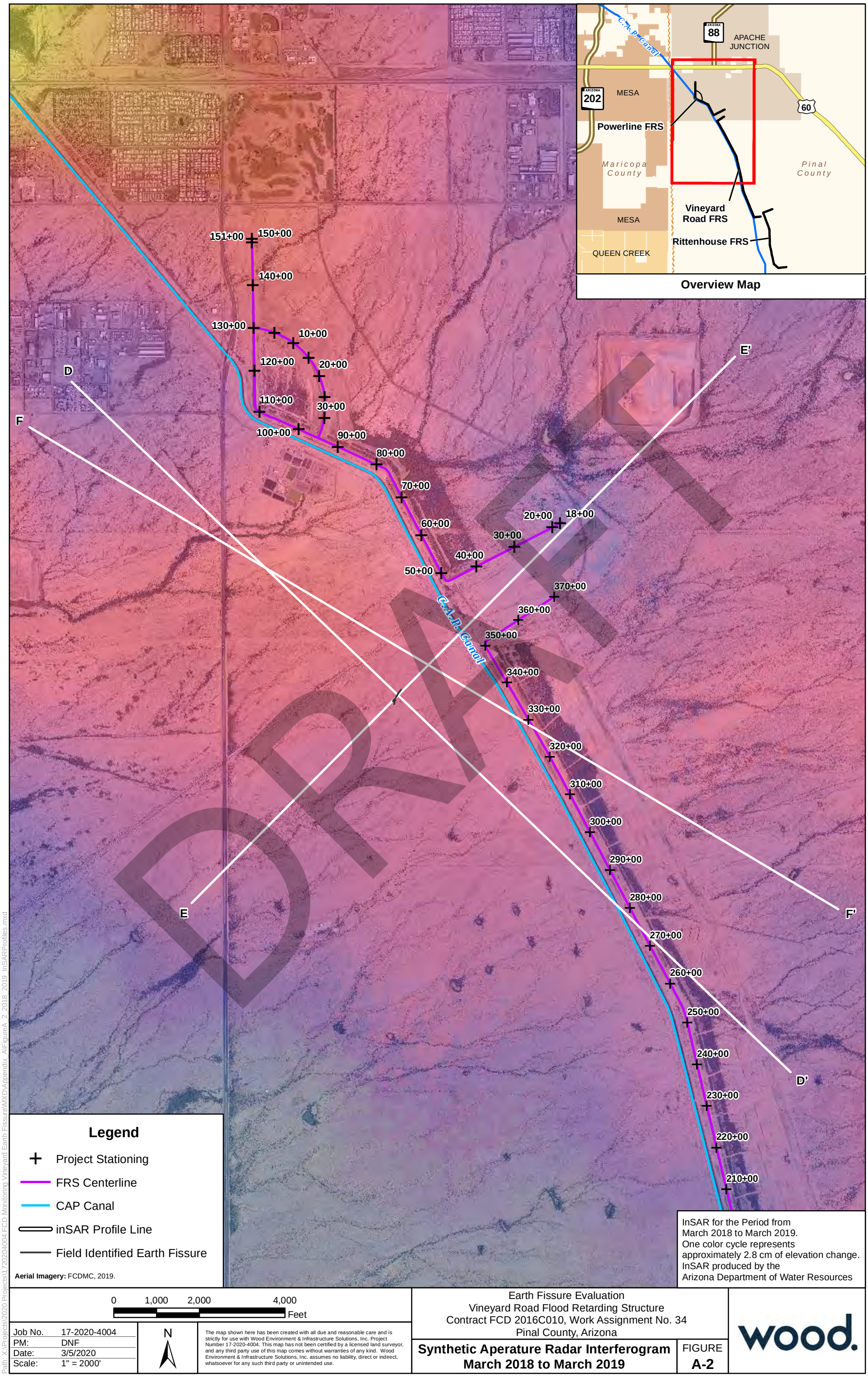

Job No.	17-2020-4004
PM:	DNF
Date:	3/5/2020
Scale:	1" = 2000'

The map shown here has been created with all due and reasonable care and is strictly for use with Wood Environment & Infrastructure Solutions, Inc. Project Number 17-2020-4004. This map has not been certified by a licensed land surveyor, and any third party use of this map comes without warranties of any kind. Wood Environment & Infrastructure Solutions, Inc. assumes no liability, direct or indirect, whatsoever for any such third party or unintended use.

Earth Fissure Evaluation
Vineyard Road Flood Retarding Structure
Contract FCD 2016C010, Work Assignment No. 34
Pinal County, Arizona

Synthetic Aperature Radar Interferogram March 2018 to March 2019

FIGURE **A-2**

wood.

Path: X:\Projects\2020 Projects\172020004 FCD Monitoring Vineyard Earth FissureMXD\Appendix_A\FigureA_2_2018_2019_InSARProfiles.mxd

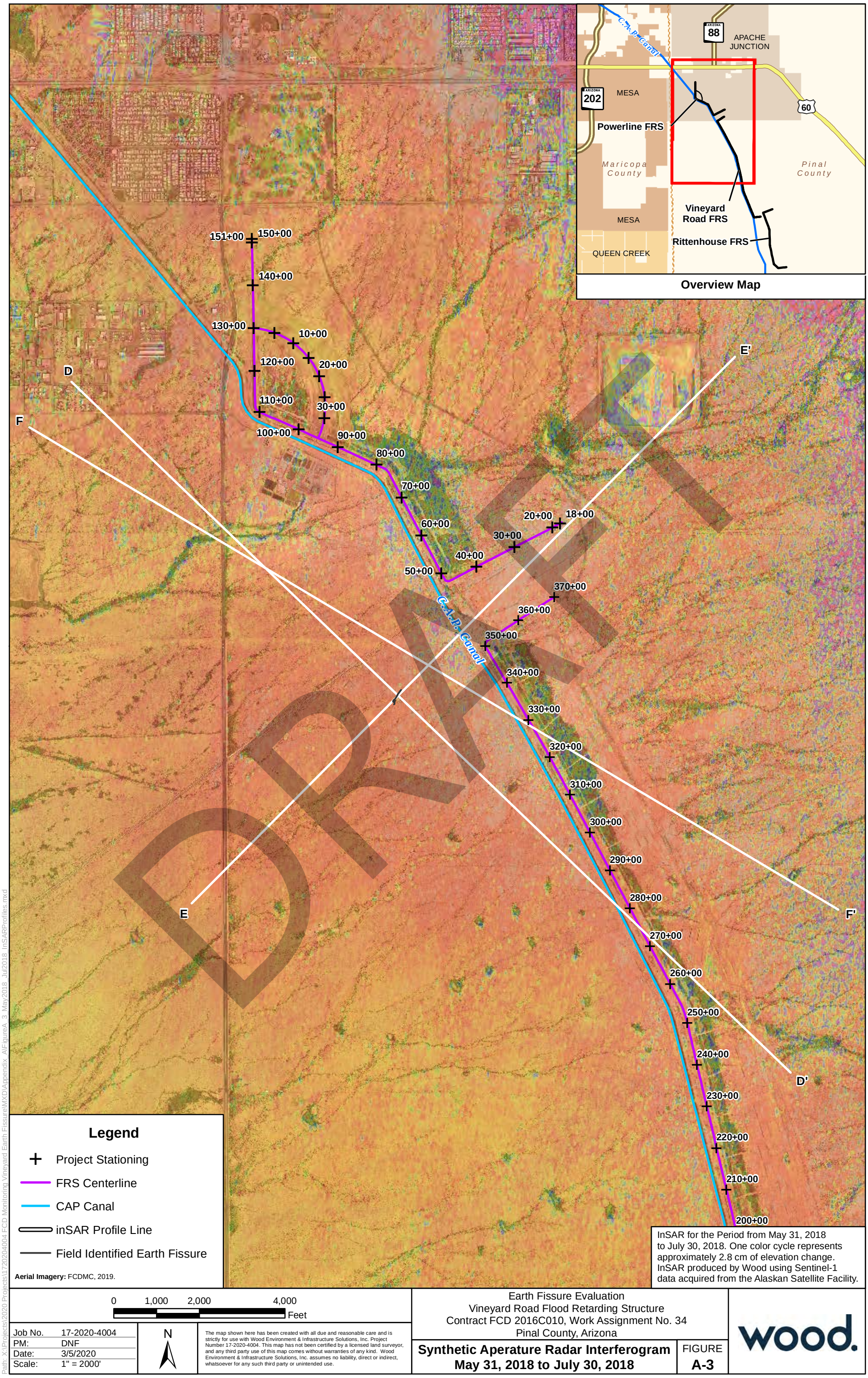

Job No.	17-2020-4004
PM:	DNF
Date:	3/5/2020
Scale:	1" = 2000'

The map shown here has been created with all due and reasonable care and is strictly for use with Wood Environment & Infrastructure Solutions, Inc. Project Number 17-2020-4004. This map has not been certified by a licensed land surveyor, and any third party use of this map comes without warranties of any kind. Wood Environment & Infrastructure Solutions, Inc. assumes no liability, direct or indirect, whatsoever for any such third party or unintended use.

Earth Fissure Evaluation
Vineyard Road Flood Retarding Structure
Contract FCD 2016C010, Work Assignment No. 34
Pinal County, Arizona

Synthetic Aperature Radar Interferogram
May 31, 2018 to July 30, 2018

FIGURE
A-3

wood.

Path: X:\Projects\2020 Projects\172020004 FCD Monitoring Vineyard Earth Fissure\MXD\Appendix A\FigureA_3 May2018_Jul2018 InSARprofiles.mxd

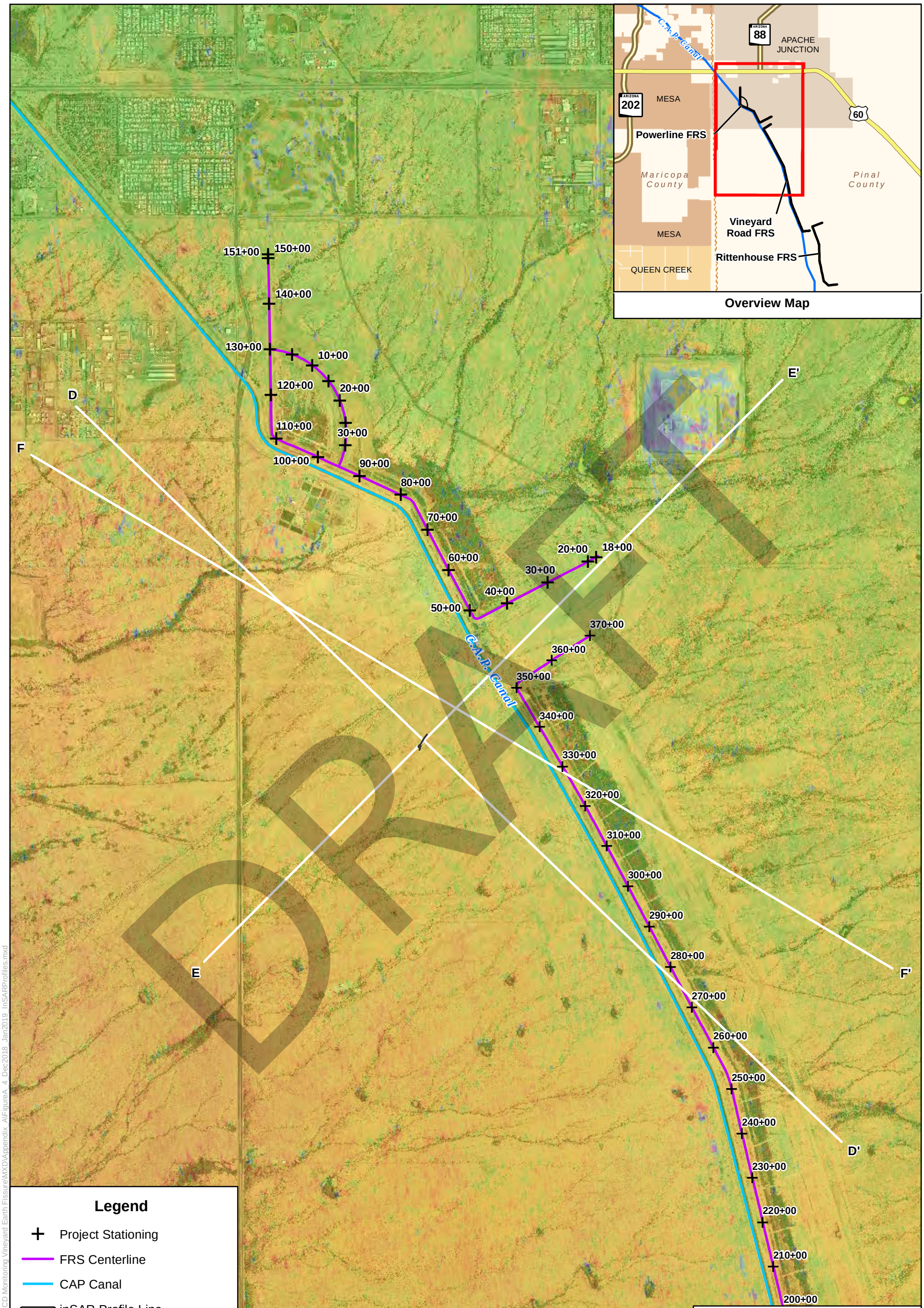

Legend

- Project Stationing
- FRS Centerline
- CAP Canal
- inSAR Profile Line
- Field Identified Earth Fissure

Aerial Imagery: FCDMC, 2019.

InSAR for the Period from December 15, 2018 to January 8, 2019. One color cycle represents approximately 2.8 cm of elevation change. InSAR produced by Wood using Sentinel-1 data acquired from the Alaskan Satellite Facility.

0 1,000 2,000 4,000 Feet

Job No.	17-2020-4004
PM:	DNF
Date:	3/5/2020
Scale:	1" = 2000'

N

Earth Fissure Evaluation
Vineyard Road Flood Retarding Structure
Contract FCD 2016C010, Work Assignment No. 34
Pinal County, Arizona

Synthetic Aperature Radar Interferogram
December 15, 2018 to January 8, 2019

FIGURE
A-4

wood.

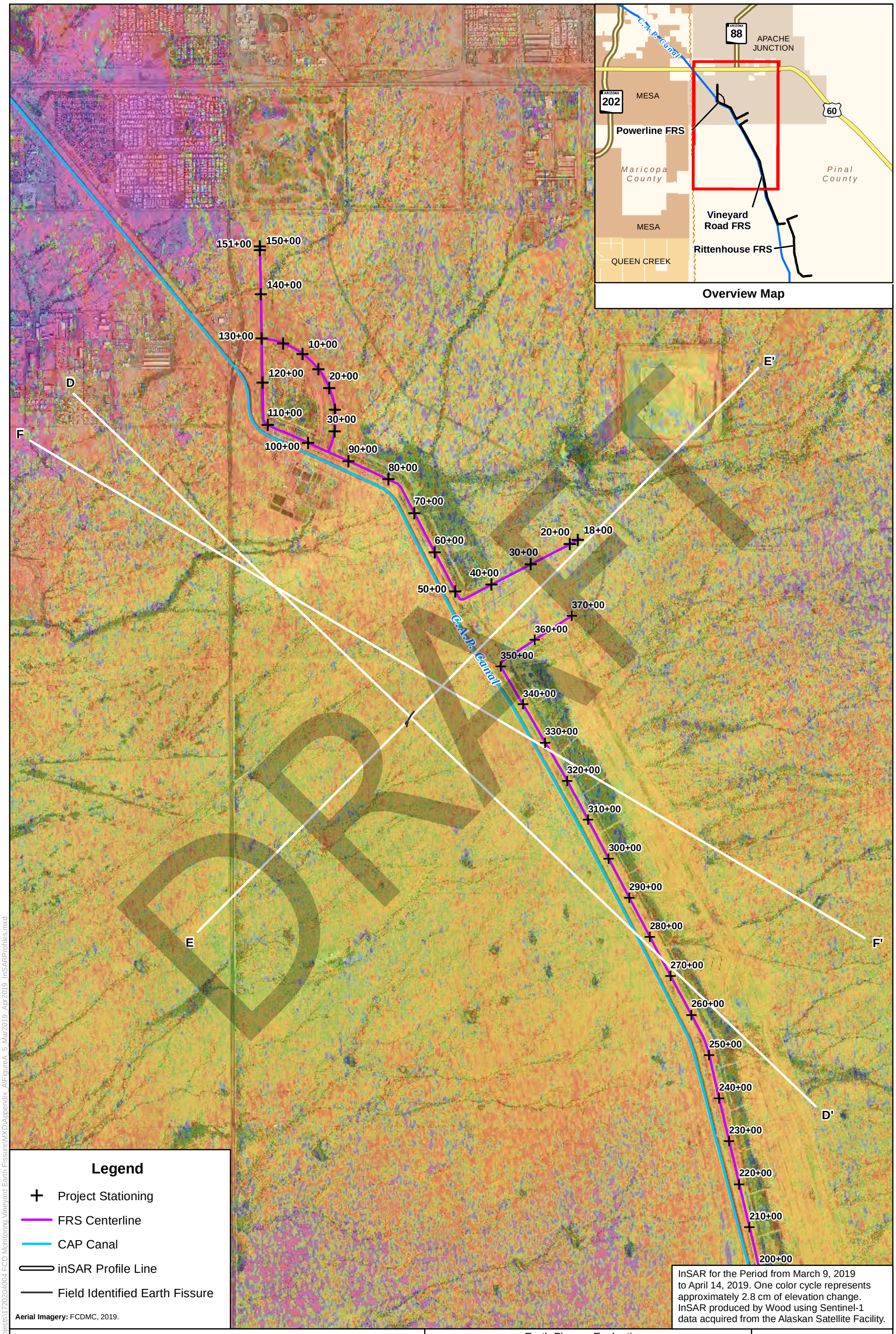
C.A.P. Canal
ARIZONA 88
APACHE JUNCTION
ARIZONA 202
MESA
60
Powerline FRS
Maricopa County
Pinal County
Vineyard Road FRS
MESA
Rittenhouse FRS
QUEEN CREEK
Overview Map
151+00
150+00
140+00
130+00
10+00
120+00
20+00
110+00
30+00
100+00
90+00
80+00
70+00
60+00
50+00
40+00
30+00
20+00
18+00
370+00
360+00
350+00
340+00
330+00
320+00
310+00
300+00
290+00
280+00
270+00
260+00
250+00
240+00
230+00
220+00
210+00
200+00
C.A.P. Canal
D
D'
E
E'
F
F'
DRAFT
Legend
Project Stationing
FRS Centerline
CAP Canal
inSAR Profile Line
Field Identified Earth Fissure
Aerial Imagery: FCDMC, 2019.
InSAR for the Period from March 9, 2019 to April 14, 2019. One color cycle represents approximately 2.8 cm of elevation change. InSAR produced by Wood using Sentinel-1 data acquired from the Alaskan Satellite Facility.
0 1,000 2,000 4,000
Feet
N
Job No. 17-2020-4004
PM: DNF
Date: 3/5/2020
Scale: 1" = 2000'
The map shown here has been created with all due and reasonable care and is strictly for use with Wood Environment & Infrastructure Solutions, Inc. Project Number 17-2020-4004. This map has not been certified by a licensed land surveyor, and any third party use of this map comes without warranties of any kind. Wood Environment & Infrastructure Solutions, Inc. assumes no liability, direct or indirect, whatsoever for any such third party or unintended use.
Earth Fissure Evaluation
Vineyard Road Flood Retarding Structure
Contract FCD 2016C010, Work Assignment No. 34
Pinal County, Arizona
Synthetic Aperature Radar Interferogram
March 9, 2019 to April 14, 2019
FIGURE
A-5
wood.
Path: X:\Projects\2020 Projects\172020004 FCD Monitoring Vineyard Earth Fissure\MXD\Appendix_A\FigureA_5_Mar2019_Apr2019_InSARProfiles.mxd

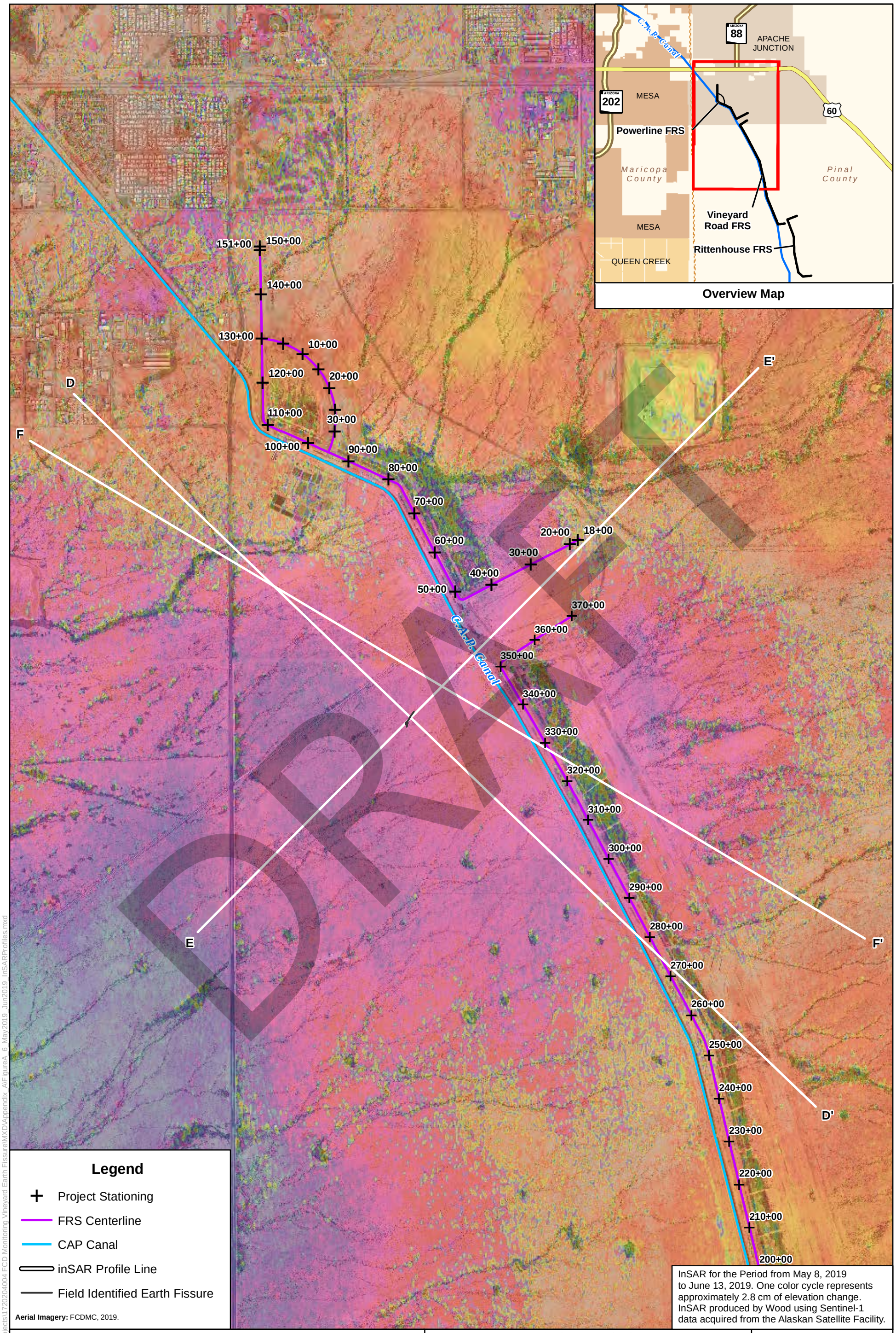

Job No.	17-2020-4004
PM:	DNF
Date:	3/5/2020
Scale:	1" = 2000'

Earth Fissure Evaluation
Vineyard Road Flood Retarding Structure
Contract FCD 2016C010, Work Assignment No. 34
Pinal County, Arizona

Synthetic Aperature Radar Interferogram May 8, 2019 to June 13, 2019

FIGURE **A-6**

wood.

Path: X:\Projects\2020 Projects\172020004004 FCD Monitoring Vineyard Earth Fissure\MXD\Appendix_A\FigureA_6_May2019_Jun2019_InSARProfiles.mxd

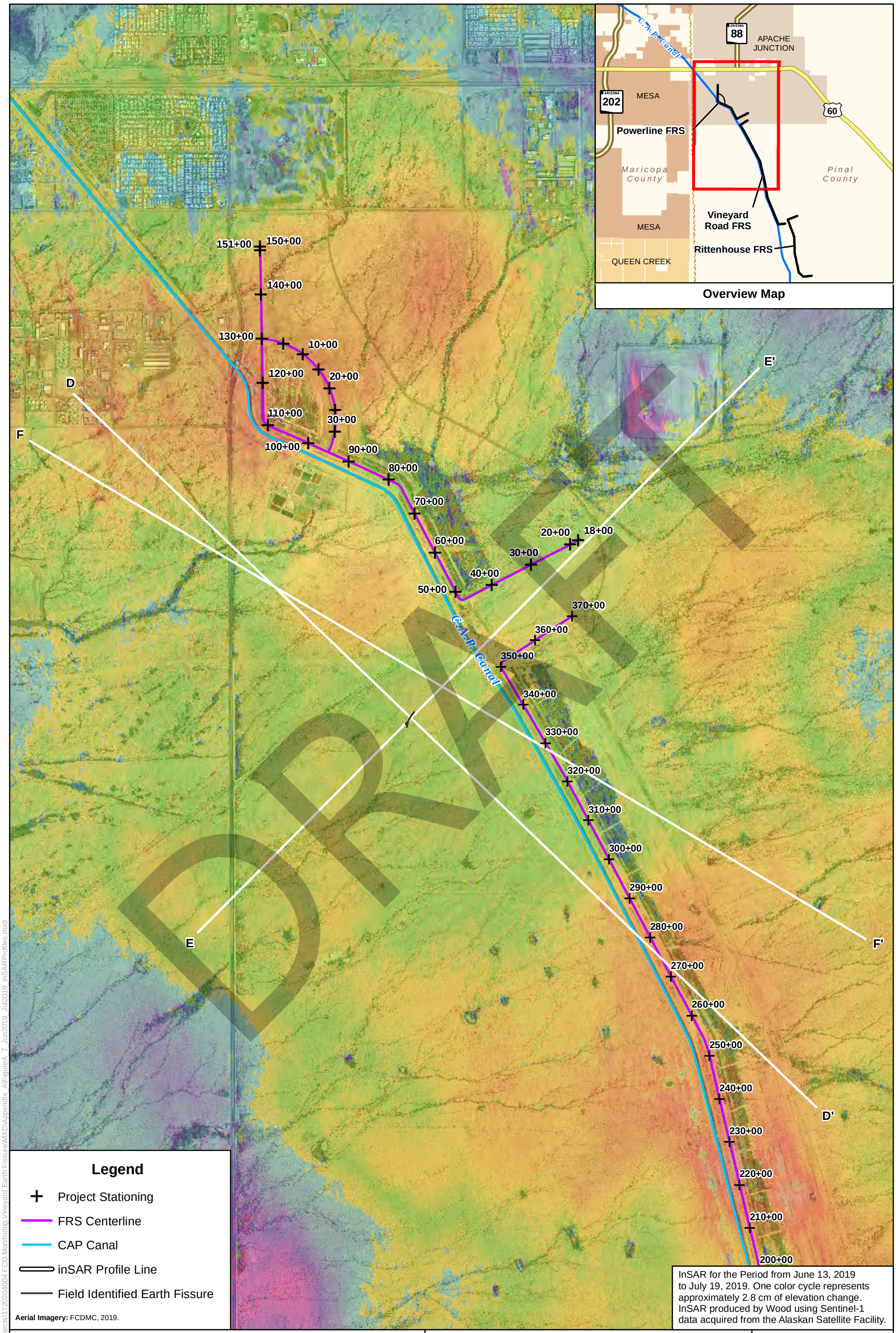

Job No.	17-2020-4004
PM:	DNF
Date:	3/5/2020
Scale:	1" = 2000'

The map shown here has been created with all due and reasonable care and is strictly for use with Wood Environment & Infrastructure Solutions, Inc. Project Number 17-2020-4004. This map has not been certified by a licensed land surveyor, and any third party use of this map comes without warranties of any kind. Wood Environment & Infrastructure Solutions, Inc. assumes no liability, direct or indirect, whatsoever for any such third party or unintended use.

Earth Fissure Evaluation
Vineyard Road Flood Retarding Structure
Contract FCD 2016C010, Work Assignment No. 34
Pinal County, Arizona

Synthetic Aperature Radar Interferogram
June 13, 2019 to July 19, 2019

FIGURE
A-7

wood.

Path: X:\Projects\2020 Projects\172020004 FCD Monitoring Vineyard Earth Fissure\MXD\Appendix_A\FigureA_7_Jun2019_Jul2019_InSARProfiles.mxd

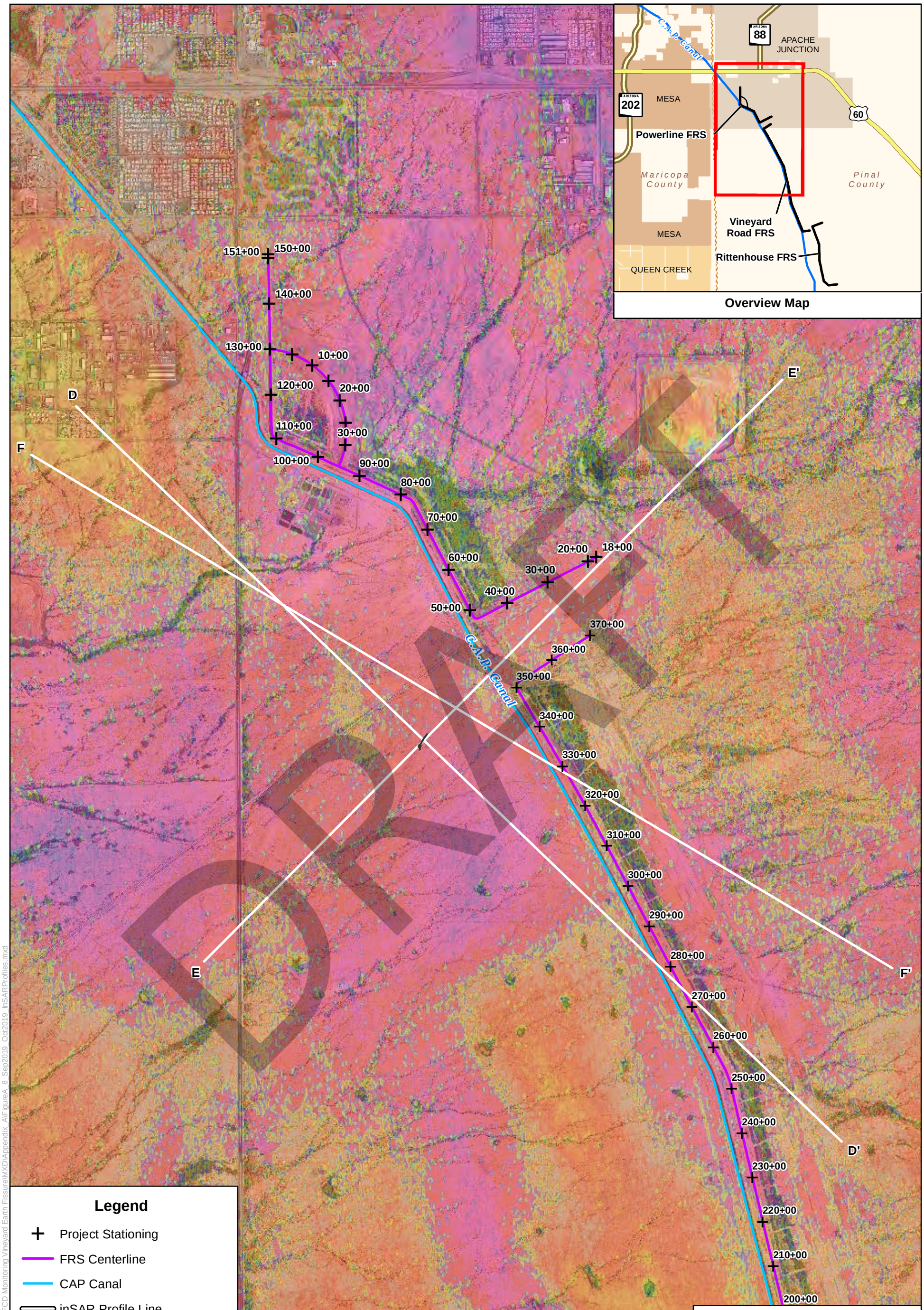

Job No.	17-2020-4004
PM:	DNF
Date:	3/5/2020
Scale:	1" = 2000'

The map shown here has been created with all due and reasonable care and is strictly for use with Wood Environment & Infrastructure Solutions, Inc. Project Number 17-2020-4004. This map has not been certified by a licensed land surveyor, and any third party use of this map comes without warranties of any kind. Wood Environment & Infrastructure Solutions, Inc. assumes no liability, direct or indirect, whatsoever for any such third party or unintended use.

Earth Fissure Evaluation
Vineyard Road Flood Retarding Structure
Contract FCD 2016C010, Work Assignment No. 34
Pinal County, Arizona

Synthetic Aperature Radar Interferogram
September 29, 2019 to October 23, 2019

FIGURE
A-8

wood.

Path: X:\Projects\2020 Projects\172020004 FCD Monitoring Vineyard Earth Fissure\MXD\Appendix A\FigureA_8_Sep2019_Oct2019_InSARProfiles.mxd

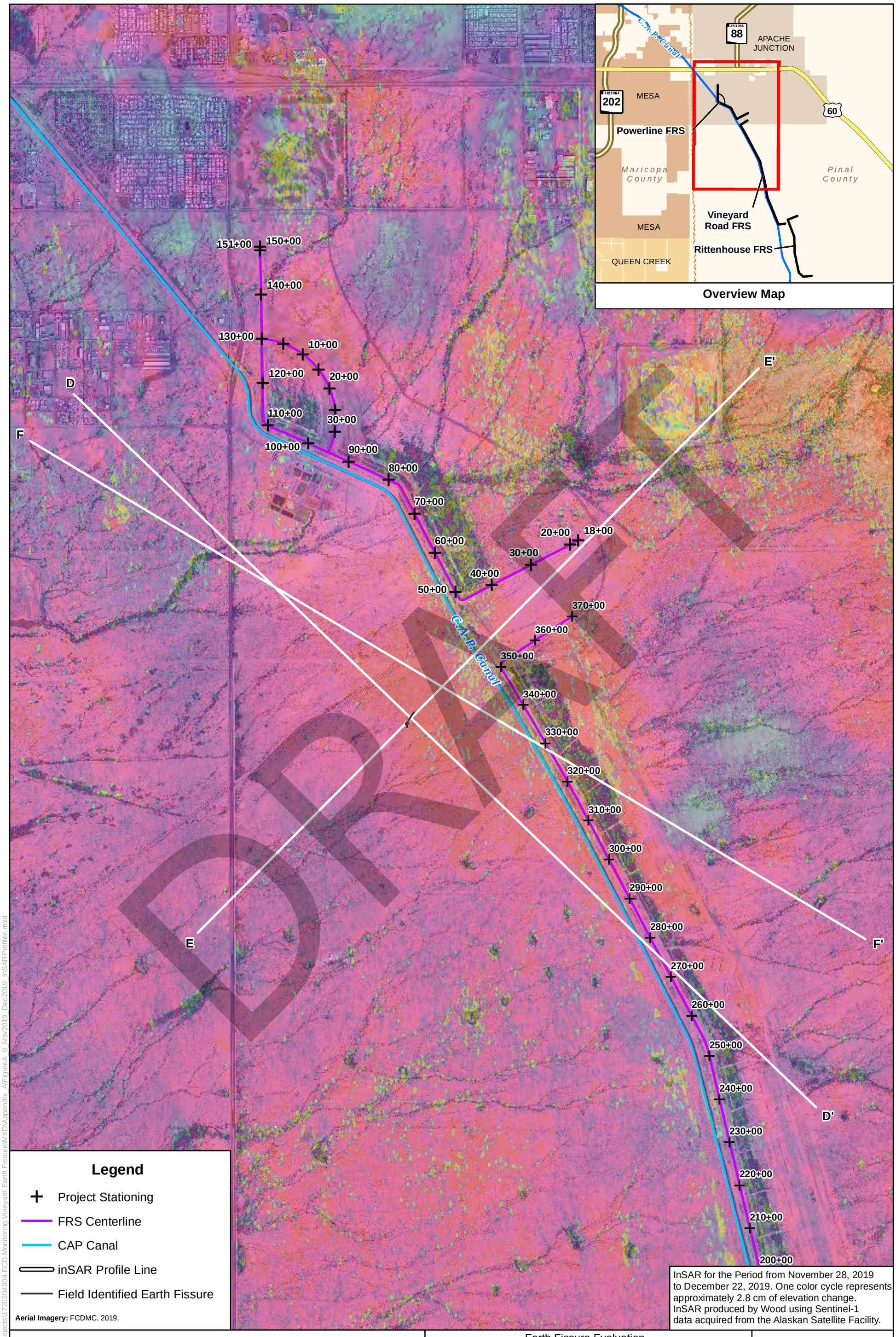

Legend

- Project Stationing
- FRS Centerline
- CAP Canal
- inSAR Profile Line
- Field Identified Earth Fissure

Aerial Imagery: FCDMC, 2019.

InSAR for the Period from November 28, 2019 to December 22, 2019. One color cycle represents approximately 2.8 cm of elevation change. InSAR produced by Wood using Sentinel-1 data acquired from the Alaskan Satellite Facility.

0 1,000 2,000 4,000 Feet

Job No.	17-2020-4004
PM:	DNF
Date:	3/5/2020
Scale:	1" = 2000'

N

Earth Fissure Evaluation
Vineyard Road Flood Retarding Structure
Contract FCD 2016C010, Work Assignment No. 34
Pinal County, Arizona

Synthetic Aperature Radar Interferogram November 28, 2019 to December 22, 2019

FIGURE **A-9**

wood.

Path: X:\Projects\2020 Projects\172020404 FCD Monitoring Vineyard Earth Fissure\MXD\Appendix_A\FigureA_9_Nov2019_Dec2019_InSARProfiles.mxd

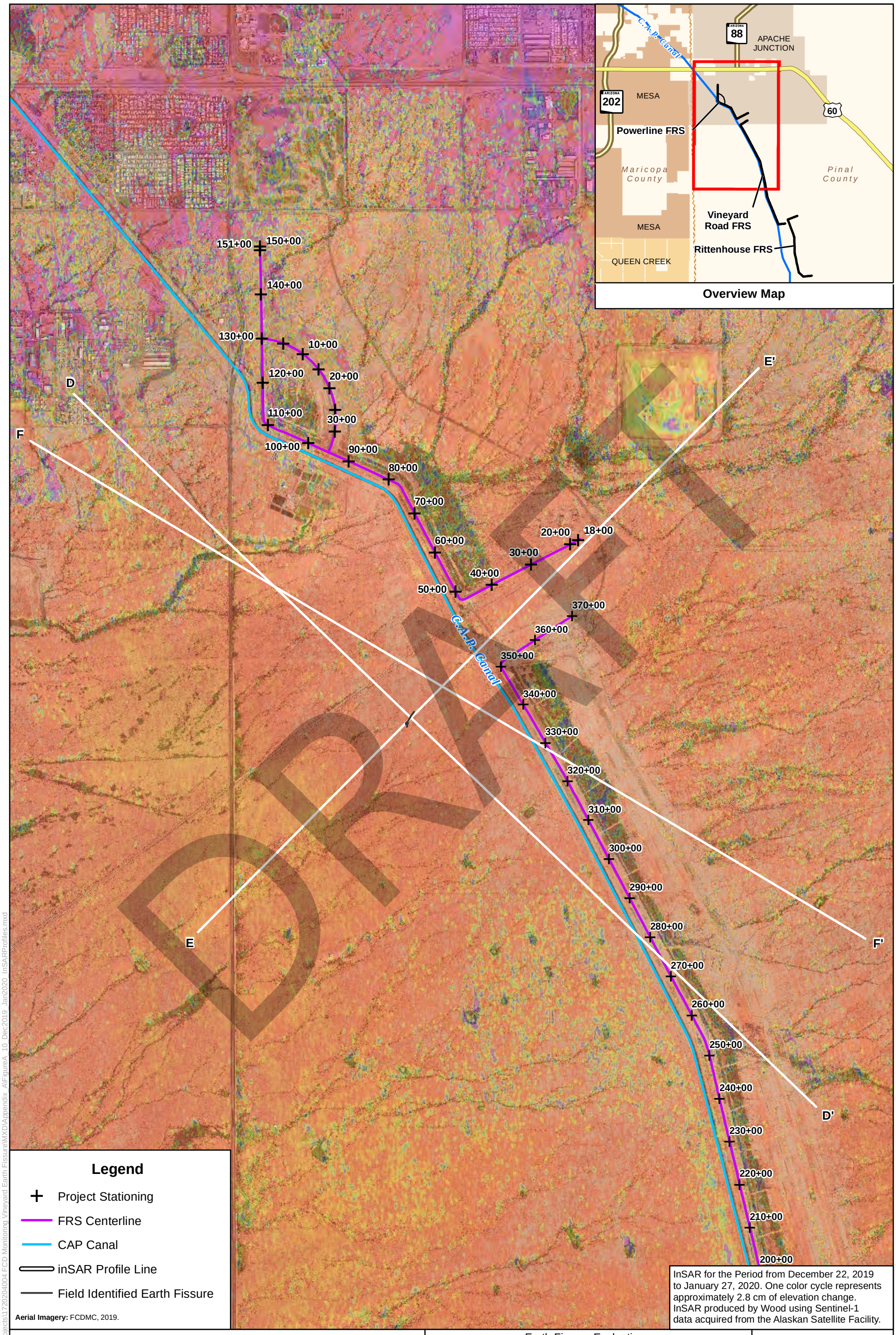

Legend

- Project Stationing
- FRS Centerline
- CAP Canal
- inSAR Profile Line
- Field Identified Earth Fissure

Aerial Imagery: FCDMC, 2019.

InSAR for the Period from December 22, 2019 to January 27, 2020. One color cycle represents approximately 2.8 cm of elevation change. InSAR produced by Wood using Sentinel-1 data acquired from the Alaskan Satellite Facility.

0 1,000 2,000 4,000 Feet

Job No.	17-2020-4004
PM:	DNF
Date:	3/5/2020
Scale:	1" = 2000'

N

Earth Fissure Evaluation
Vineyard Road Flood Retarding Structure
Contract FCD 2016C010, Work Assignment No. 34
Pinal County, Arizona

Synthetic Aperature Radar Interferogram
December 22, 2019 to January 27, 2020

FIGURE
A-10

wood.

Path: X:\Projects\2020 Projects\172020004 FCD Monitoring Vineyard Earth Fissure\MXD\Appendix_A\FigureA_10_Dec2019_Jan2020_InSARProfiles.mxd

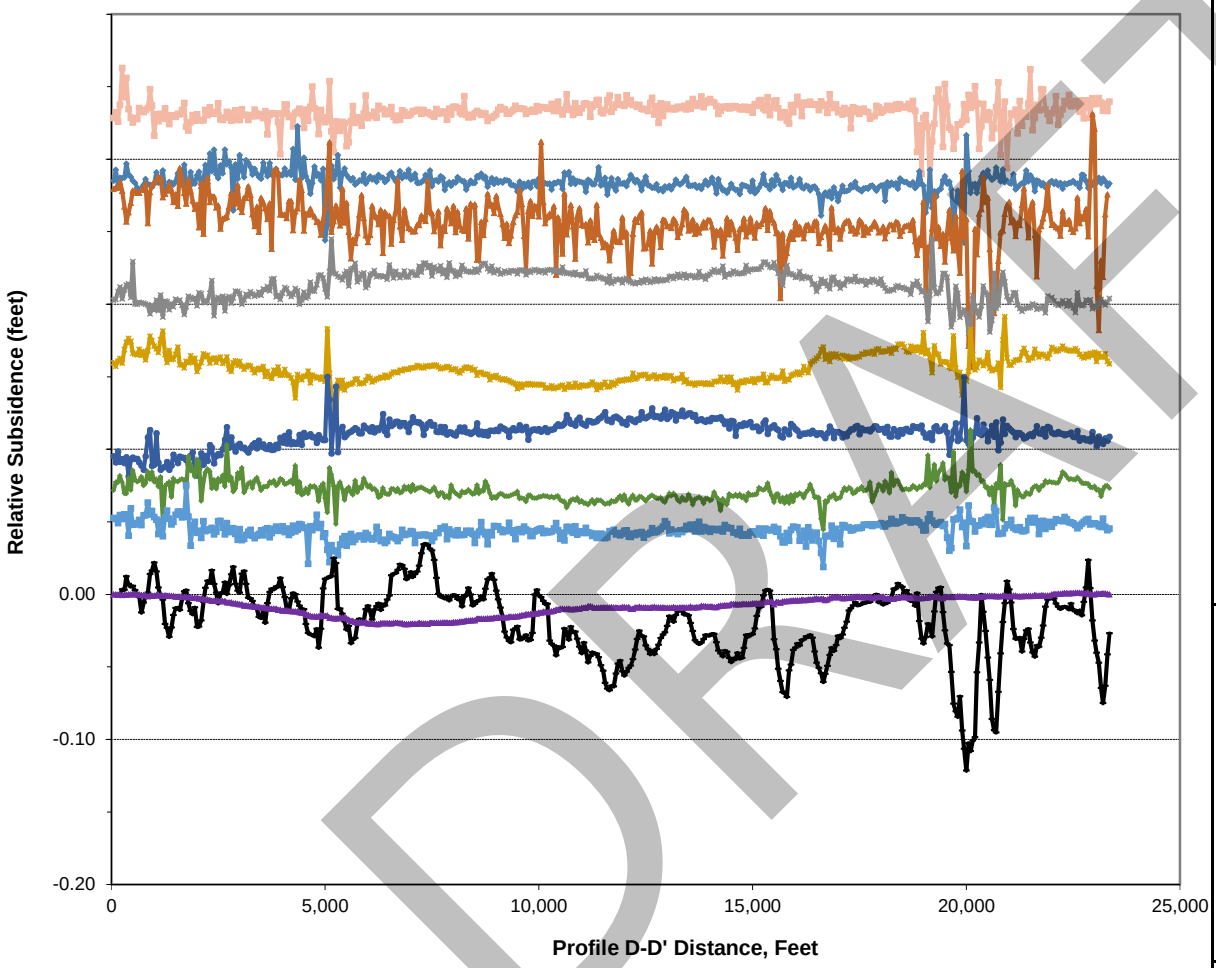

Wood Environment & Infrastructure Solutions, Inc. notes that our interpretation of the InSAR data is not absolute; our interpretations are focused on subsidence trends demonstrated through relative differences in elevation. A higher level of precision greater than common levels of InSAR absolute precision (±1 cm [0.39 inches]) should not be assumed.

Legend

- Sentinel InSAR 05/31/18 to 07/30/18
- Sentinel InSAR 12/15/18 to 01/08/19
- Sentinel InSAR 03/09/19 to 04/14/19
- Sentinel InSAR 05/08/19 to 06/13/19
- Sentinel InSAR 06/13/19 to 07/19/19
- Sentinel InSAR 09/29/19 to 10/23/19
- Sentinel InSAR 11/28/19 to 12/22/19
- Sentinel InSAR 12/22/19 to 01/27/20
- Sum 12/15/18 to 12/22/19[1]
- ADWR March 03/2018 to 03/2019

Notes:
[1] Only five months of data.

Vineyard Earth Fissure Evaluation
Vineyard Road Flood Retarding Structure
Contract FCD 2016C010, Work Assignment No. 34
Pinal County, Arizona

Sentinel InSAR
Profile D-D' Data

FIGURE
A-11

Job No. 1720204004
PM DNF
Date 3/11/2020
Scale : n/a

APPENDIX B

SEISMIC REFRACTION PROFILING

REFRACTION SEISMIC EQUIPMENT AND PROCEDURES

Refraction seismic surveys are performed in general conformance with the guidelines presented in ASTM D5777-95 Standard Guide for Using the Seismic Refraction Method for Subsurface Investigation for refraction surveys using compression waves (p-waves). ASTM D5777 does not address shear wave (s-wave) surveys; standard practice is followed for refraction surveys using s-waves. In some investigations, such as seeking and tracing earth fissures or other significant discontinuities (Rucker and Keaton, 1998), non-standard procedures and analyses, such as signal amplitude analysis, are used as part of the investigation process.

Seismic Equipment - Refraction seismic surveys are performed using a Geometrics Geode 24-channel signal enhancement seismograph. This instrument has the capability to simultaneously record 12 or 24 channels of geophone data. Signal enhancement capability permits the use of a sledgehammer as the seismic energy source. A timing sensor is attached to the hammer, and for p-waves, a metal plate is set securely on the ground surface and struck. Generating horizontally polarized s-waves typically involves jumping on the ground or dropping a 10-pound sledgehammer at the end of the line for a 12-channel system or in the center for a 24-channel system.

Because of the signal enhancement capability, signals from several or many strikes can be added together to increase the total signal available relative to noise to obtain the seismic record. Although explosives can also be used as a p-wave seismic energy source, a sledgehammer does not require licenses or permits, or involve special limitations, regulations and liabilities. Explosive energy sources may be needed for long geophone arrays. Geophone cables with 12 geophone takeouts at 10-foot, 25-foot or 20-meter spacings are presently used. Vertical geophones are used to obtain p-wave data and horizontal geophones are used to obtain s-wave data. The seismograph system is extremely portable. In areas where vehicular access is not possible, the equipment can be mobilized by various means, including backpacking, packhorse, helicopter and canoe.

Field Procedures - The field operations are directed by our experienced engineer or geologist, who operates the equipment, prepares the records and examines the data in the field. Refraction seismic lines are generally laid out using the standard spacings on the geophone cables. A maximum depth of investigation of about 75 to 100 feet may be possible using a 300-foot array. For shorter lines with improved near-surface resolution, 10-foot spacings between geophones with a 120-foot array have a maximum depth of investigation of about 30 to 40 feet, and with a 240-foot array have a maximum depth of investigation of about 60 to 80 feet. Other geophone spacings can also be used. To improve the resolution of near-surface interfaces, energy source positions generally are set at 12.5 feet from the ends of a 25-foot spacing geophone array or at 5 feet from the ends of a 10-foot geophone spacing array. Several shots locations are utilized along the length of an array. When three shots are obtained, there is a foreshot and a backshot at the array ends and a midshot at the array center. The midshot is usually placed midway between the two centermost geophones. When five shots are obtained, the additional shotpoints are located midway between the foreshot-midshot and the midshot-backshot. For 240-foot 24-channel arrays, shotpoints are arrayed at 30-foot intervals along the array. These multiple shot points permit interpretation of near-surface interfaces at various locations along the array as well as near the endpoints for variable subsurface profiles, and permits more refined overall interpretations of shallow and mid-depth subsurface velocities and interfaces. In cases when both enhanced depth of investigation and improved shallow resolution are needed, multiple geophone arrays are completed end to end and combined into longer composite geophone arrays with greater depths of investigation. Additional energy shotpoints are then, at a minimum, performed at the midpoint and far endpoint of each adjacent geophone array to provide seismic energy travel path coverage over the extended array.

Surface wave data is also typically collected for each seismic line setup and interpreted for vertical shear wave profiles using the Refraction Microtremor method. This procedure is described separately. To facilitate the collection of low frequency surface wave data, 4.5 Hz geophones are typically used for surface seismic work.

REFRACTION SEISMIC EQUIPMENT AND PROCEDURES (Cont.)

P-wave data are recorded for general exploration work. S-wave data are also recorded when dynamic subsurface material properties are desired. An s-wave arrival is verified by obtained two sets of horizontal data that are 180 degrees out of phase. The phase reversal is obtained by either reversing the horizontal geophone orientation or reversing the hammer impact direction. Hard copy printouts of all field data are made and inspected as the information is collected. Field notes, including line number and orientation, topographic variations and other notes as appropriate are made in a field logbook. Locations and other notes are made on site maps and in notebooks as appropriate. Initial first arrival picks are made in the field and array endpoint arrival times are checked for immediate data adequacy verification as part of the quality control process.

Interpretation - Although preliminary or quality control initial refraction seismic data interpretations may sometimes be performed in the field, full interpretations are completed in the office. At the present time, two interpretation methods are being used; the intercept time method (ITM) and an optimization software routine based on finite difference optimization software. ITM breaks an interpretation into several distinct layers. It is simple, can be performed with a calculator, and can provide excellent interpretations of near surface layer depths and velocities. Optimization provides a continuously variable velocity interpretation through a discrete grid. Interpretations using optimization also indicate zones where interpretation has occurred, thus providing quality control on the depths to which the interpretation can be relied upon. However, the discrete grid used by optimization results in a low resolution near surface interpretation. The combination of both ITM and, when appropriate, optimization methods provides two separate interpretations with complimentary strengths and cross-checking capability. These interpretation methods are applied as appropriate to a particular project.

Refraction seismic data interpretation using the intercept time method is detailed by Mooney (1973). A personal computer spreadsheet is used to perform the necessary calculations to obtain depths and layer velocities, and print out time-distance plots and depth interpretations. This method is used for interpretations of up to three layers. It is considered that more than three layers cannot be effectively interpreted using twelve geophone data points. Interpretations are then completed manually to produce a final interpreted geologic profile and layer depths.

Refraction seismic data interpretation using optimization is performed using the SeisOpt2D (presently Version 4.0) software package by Optim, L.L.C., 1999-2016, of Reno, Nevada. Energy source and geophone receiver locations and elevations, and first arrival times are entered into the software package, and first arrival travel times are optimized through a process of repeated (typically 10,000 to 100,000) iterations. Multiple seismic lines combined end to end into a longer composite line can be effectively interpreted using this software. Model grid dimensions and element sizes are selected, with larger grids containing smaller elements providing greater potential resolution. However, very large grids containing small elements may become unstable, and several runs may need to be made to obtain stable, robust interpretations. Once a robust interpretation has been obtained, the resulting seismic velocity profile is printed out with varying colors indicating the interpreted velocities.

References:

Mooney, H.M., 1973, Engineering Seismology Using Refraction Methods, Bison Instruments, Inc., Minneapolis, Minnesota.

Rucker, M.L. and Keaton, J.R., 1998, Tracing an Earth Fissure Using Seismic-Refraction Methods with Physical Verification, in Land Subsidence Case Studies and Current Research: Proceedings of the Dr. Joseph F. Poland Symposium on Land Subsidence, Edited by Borchers, J.W., Special Publication No. 8, Association of Engineering Geologists, Star Publishing Company, Belmont, California, p. 207-216.

REFRACTION MICROTREMOR (ReMi) SHEAR WAVE EQUIPMENT AND PROCEDURES

Refraction microtemor or ReMi surveys are performed in general accordance with the method described by Louie (2001) to develop vertical one-dimensional shear wave (s-wave) velocity profiles. The same equipment used for ReMi is also used for refraction seismic. When appropriate, both p-wave and s-wave data can be collected with the same physical seismic line setup.

ReMi Seismic Equipment - ReMi surveys are performed using a Geometrics Geode 24-channel signal enhancement seismograph. These instruments have the capability to digitally record and store up to 12 or 24 channels of geophone data in SEG2 format. Up to 16,384 samples can be acquired for each geophone channel at sample intervals as long as 0.25, 0.5, 1 and 2 milliseconds. Sampling events to collect ReMi field data may typically last 6, 12 or 24 seconds. Geophone cables with 12 geophone takeouts at 10-foot or 20-meter spacings are presently used. Vertical geophones with resonant frequencies of 28 Hz and 4.5 Hz are used to obtain surface wave data for s-wave vertical profile analysis. High frequency geophones are used for shorter arrays with shallower depths of investigation, and low frequency geophones are used for longer arrays with greater depths of investigation. Broad band ambient site noise may be used as a surface wave energy source. Controlled surface wave energy sources include jogging alongside shorter geophone arrays and driving a field vehicle alongside longer geophone arrays. The seismograph system is extremely portable. In areas where vehicular access is not possible, the equipment can be mobilized by various means, including backpacking, packhorse, helicopter and canoe.

ReMi Field Procedures - The field operations are directed by our experienced engineer or geologist, who operates the equipment, prepares the records and examines the data in the field. ReMi seismic lines are generally laid out using the standard spacings on the geophone cables. A depth of investigation of about 100 meters or more may be possible using a 240 meter array. For shorter lines with improved near-surface resolution, 10-foot array spacings between geophones have a shallower depth of investigation. Other geophone spacings can also be used.

Data collection consists of the system sampling the ambient or generated surface waves (a sampling event) at the geophone array for several to many seconds. Typical sampling times and intervals for a sampling event may be 6 seconds at 0.5 milliseconds, 12 seconds at 1 millisecond and 24 seconds at 2 milliseconds for array lengths of 60 feet, 120 to 240 feet, and 240 meters, respectively. Several sampling events are collected at each ReMi setup. For shorter arrays where ReMi with surface wave energy generated by jogging is conducted in concert with seismic refraction data collection, four sampling events may typically be recorded. For longer arrays where urban ambient noise or a field vehicle generates the surface wave energy, six to ten sampling events may be recorded. Field notes, including line number and orientation, topographic variations, locations and other notes as appropriate are made in a logbook. Sample data files are saved and stored on a field laptop computer connected to the Geode seismograph and preliminary interpretations made for immediate data adequacy verification as part of the quality control process.

Interpretation - Although preliminary or quality control initial ReMi seismic data interpretations may sometimes be performed in the field, full interpretations are completed in the office. Data files, typically about 580kb each in size, are stored in the laptop computer memory. Interpretation is performed using the SeisOpt ReMi Version 6.0 (2010) software package by Optim, L.L.C., of Reno, Nevada. The software consists of two modules. The ReMiVsSpect module is used to convert the SEG2 files into a spectral energy shear wave frequency versus shear wave velocity presentation for a ReMi seismic setup. The interpreter then selects a dispersion curve consisting of the lower bound of the spectral energy shear wave velocity versus frequency trend, and that dispersion curve is saved to disk. Tracing the lower bound (slowest) of the shear wave velocity at each frequency selects the ambient energy propagating parallel to the geophone array, since energy propagating incident to the array will appear to have a faster propagating velocity. The second module, ReMiDisper, is then invoked. The interpreter models a dispersion curve with multiple layers and s-wave velocities to match the selected dispersion curve from the field data. An interpreted vertical s-wave profile is obtained through this process. It must be understood that this type of interpretation may not result in a unique solution.

Louie, J.L., 2001, Faster, Better: Shear-wave velocity to 100 meters depth from refraction microtremor arrays, Bulletin of the Seismological Society of America, Vol. 91, 347-364.

Line 36
Sta 346+00

Interpretation of Refraction Seismic Data

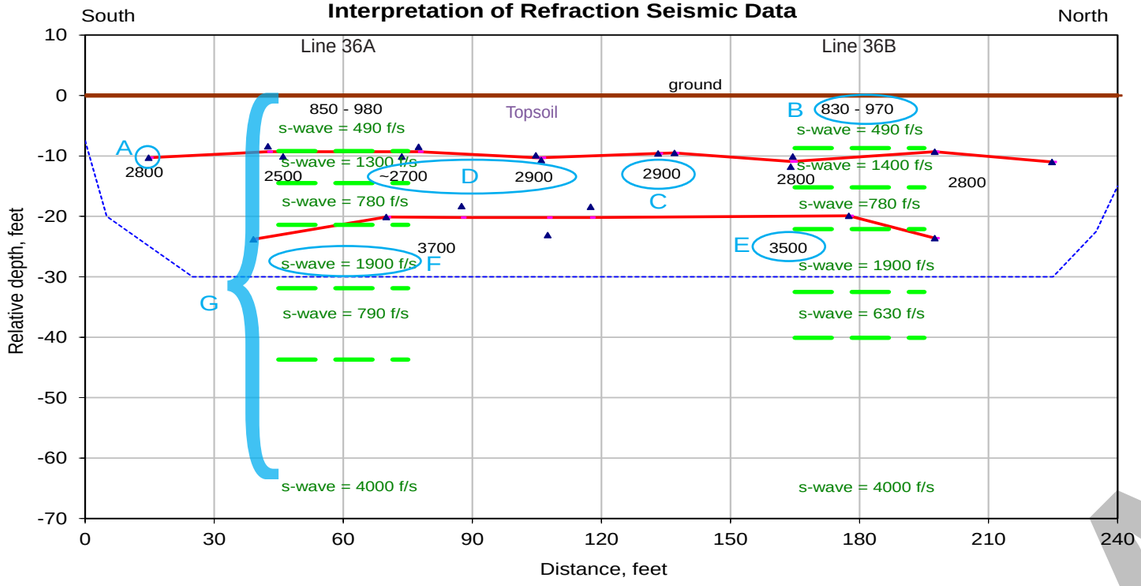

Key

- **A** Interpreted depth from time-distance plot
- **B** Harmonic mean of p-wave velocities (f/s) in opposite directions; '~' where velocities differ by more than 10%
- **C** Interpreted p-wave velocities (f/s)
- **D** Differing p-wave velocities (f/s) to show the lateral variability in the interpretation
- **E** Harmonic mean of p-wave velocities (f/s) in opposite directions; '~' where velocities differ by more than 10%;
- **F** Interpreted s-wave velocity (f/s)
- **G** Interpreted s-wave profile of channels 1 - 12

Legend

▲	Interpreted depth (ft) from time-distance plot
—	Interpreted p-wave velocity (f/s) interface
- -	Interpreted s-wave velocity (f/s) interface
- -	Calculated depth (ft) of investigation of p-wave data utilizing SEISOPT2D software
—	Ground surface (interpreted depths assumed to be below zero)
(value)	Interpreted value is likely high
~	Greater than 10 percent difference between foreshot and backshot values
XXXX	P-wave interpretation value
XXXX	S-wave interpretation value
XXXX	Notes or call-outs regarding interpretation

Examples of Complex Interpretations

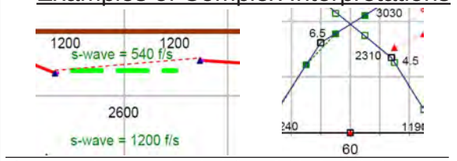

A p-wave interpretation is inferred (dashed line) on the interpretation plot because data at shot location is missing or of poor quality on the time-distance plot.

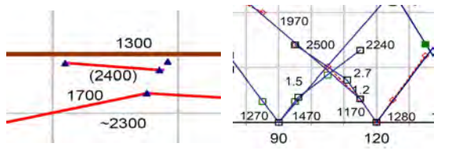

A p-wave velocity interpretation is shown in parantheses on the interpretation plot (left) because a shallow high velocity layer is seen on the time-distance plot (right), however the interpretation of other layers is still seen.

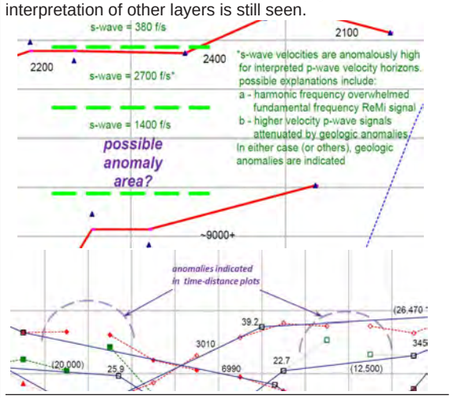

An anomaly in the p-wave velocity interpretation is shown in purple on the interpretation plot (top) and the anomolous data is also shown in purple on the time-distance plot (bottom).

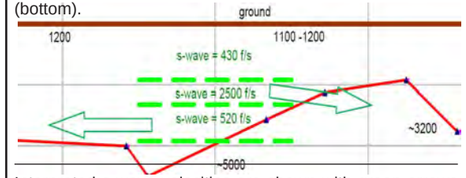

Interpreted s-wave velocities are shown with green arrows indicating the portion of the 2-dimensional interpretation that the 1-dimensional ReMi horizon corresponds with.

Line 36
Sta 346+00

Time-Distance Plots with Interpreted Velocities (ft/sec) & Depths (ft)

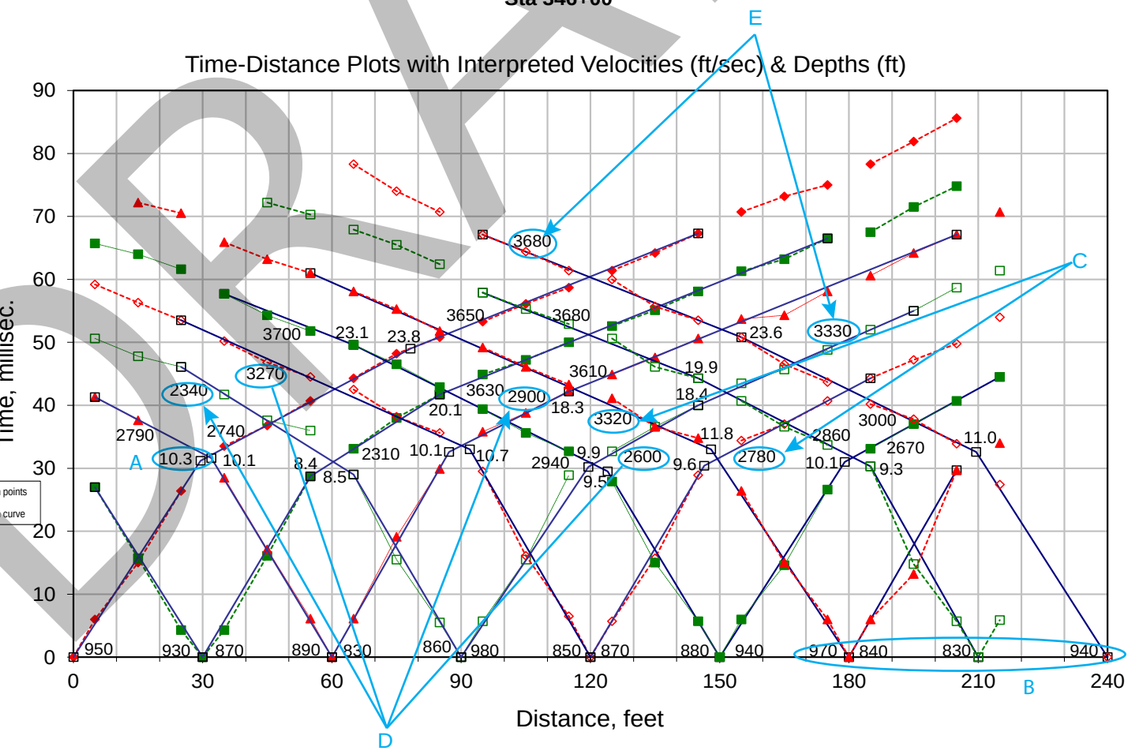

ReMi Interpretation utilizing channels 1 through 12

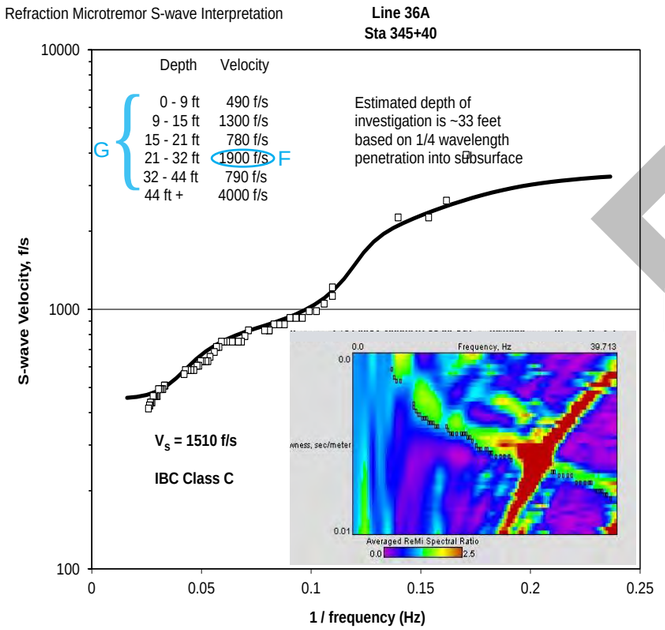

Standard
Seimic Refraction
Interpretation Figure

FIGURE **C-1**	Created by: TKR Reviewd by: MLR Date: 12/21/2018	wood.

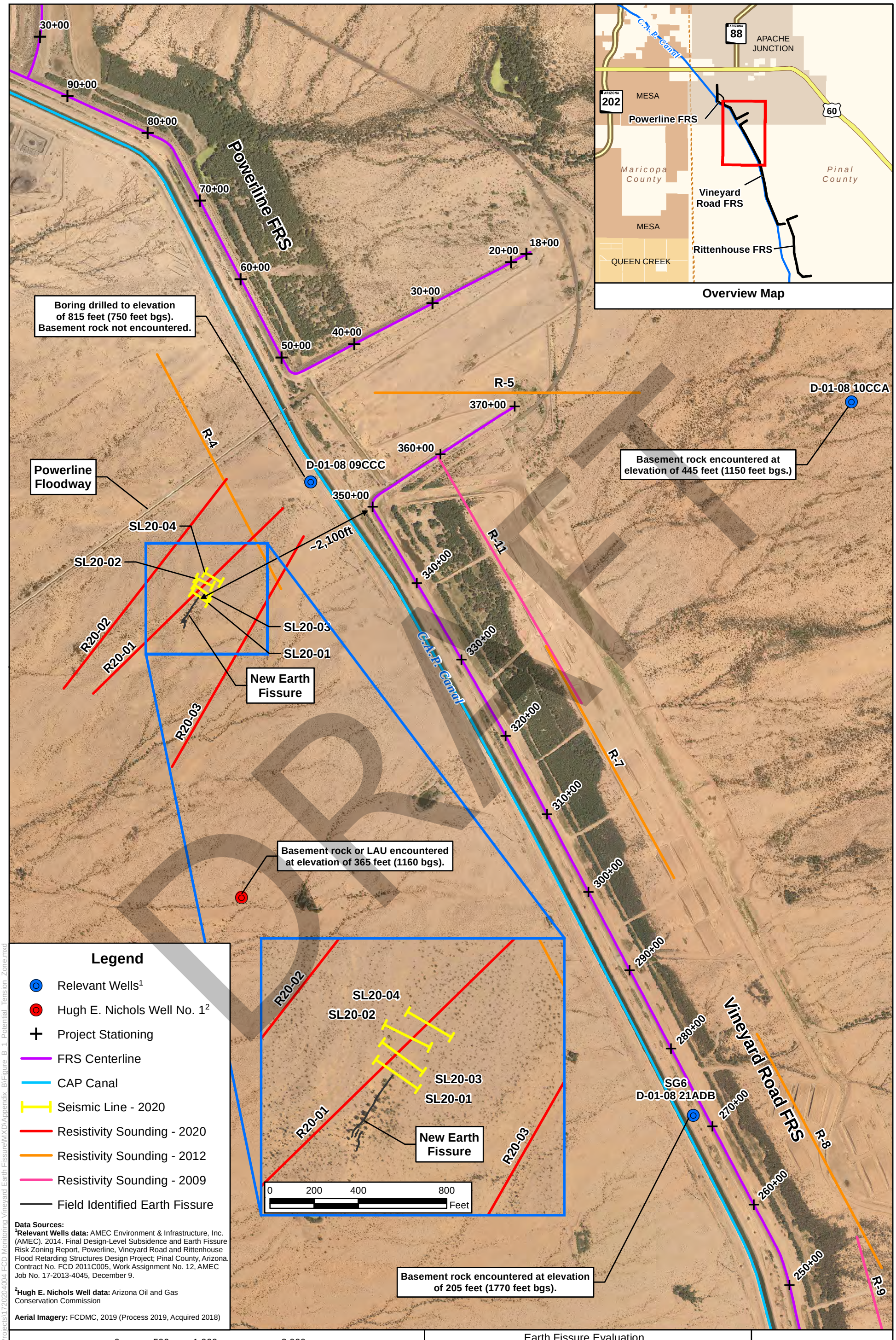

Legend

- Relevant Wells[1]
- Hugh E. Nichols Well No. 1[2]
- Project Stationing
- FRS Centerline
- CAP Canal
- Seismic Line - 2020
- Resistivity Sounding - 2020
- Resistivity Sounding - 2012
- Resistivity Sounding - 2009
- Field Identified Earth Fissure

Data Sources:

[1]**Relevant Wells data:** AMEC Environment & Infrastructure, Inc. (AMEC). 2014. Final Design-Level Subsidence and Earth Fissure Risk Zoning Report, Powerline, Vineyard Road and Rittenhouse Flood Retarding Structures Design Project; Pinal County, Arizona. Contract No. FCD 2011C005, Work Assignment No. 12, AMEC Job No. 17-2013-4045, December 9.

[2]**Hugh E. Nichols Well data:** Arizona Oil and Gas Conservation Commission

Aerial Imagery: FCDMC, 2019 (Process 2019, Acquired 2018)

0 500 1,000 2,000 Feet

Job No.	17-2020-4004
PM:	DNF
Date:	3/31/2020
Scale:	1" = 1000'

N

Earth Fissure Evaluation
Vineyard Road Flood Retarding Structure
Contract FCD 2016C010, Work Assignment No. 34
Pinal County, Arizona

Site Plan and Vicinity Map

FIGURE **B-1**

wood.

Path: X:\Projects\2020 Projects\172020004 FCD Monitoring Vineyard Earth Fissure\MXD\Appendix_B\Figure_B_1_Potential_Tension_Zone.mxd

Seismic Refraction and Refraction
Microtremor Interpretation

Line 01
(SL20-01)

Wood Job No. 17-2020-4004

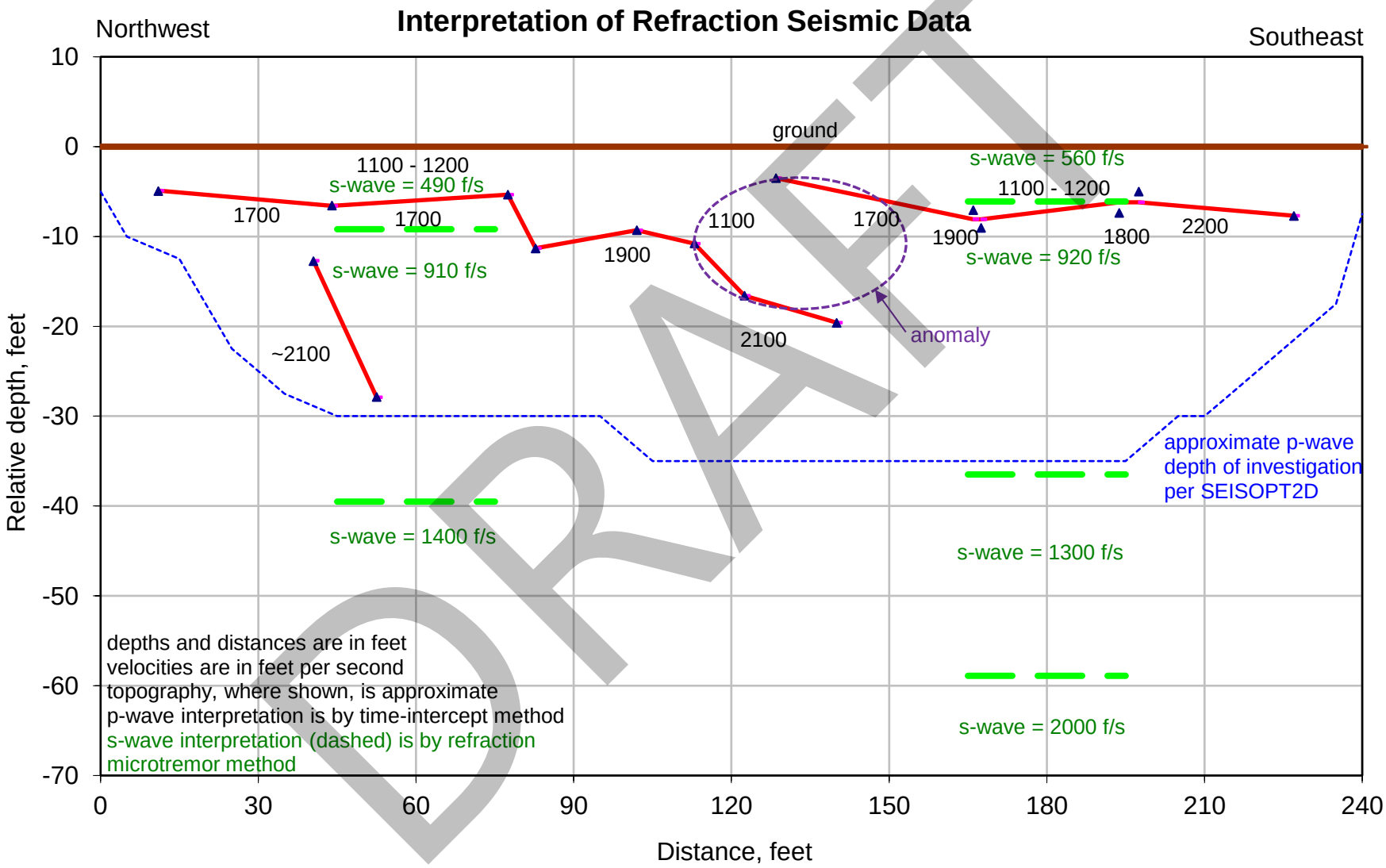

Seismic Refraction Interpretation
Time-Distance Plots

Line 01
(SL20-01)

Wood Job No. 17-2020-4004

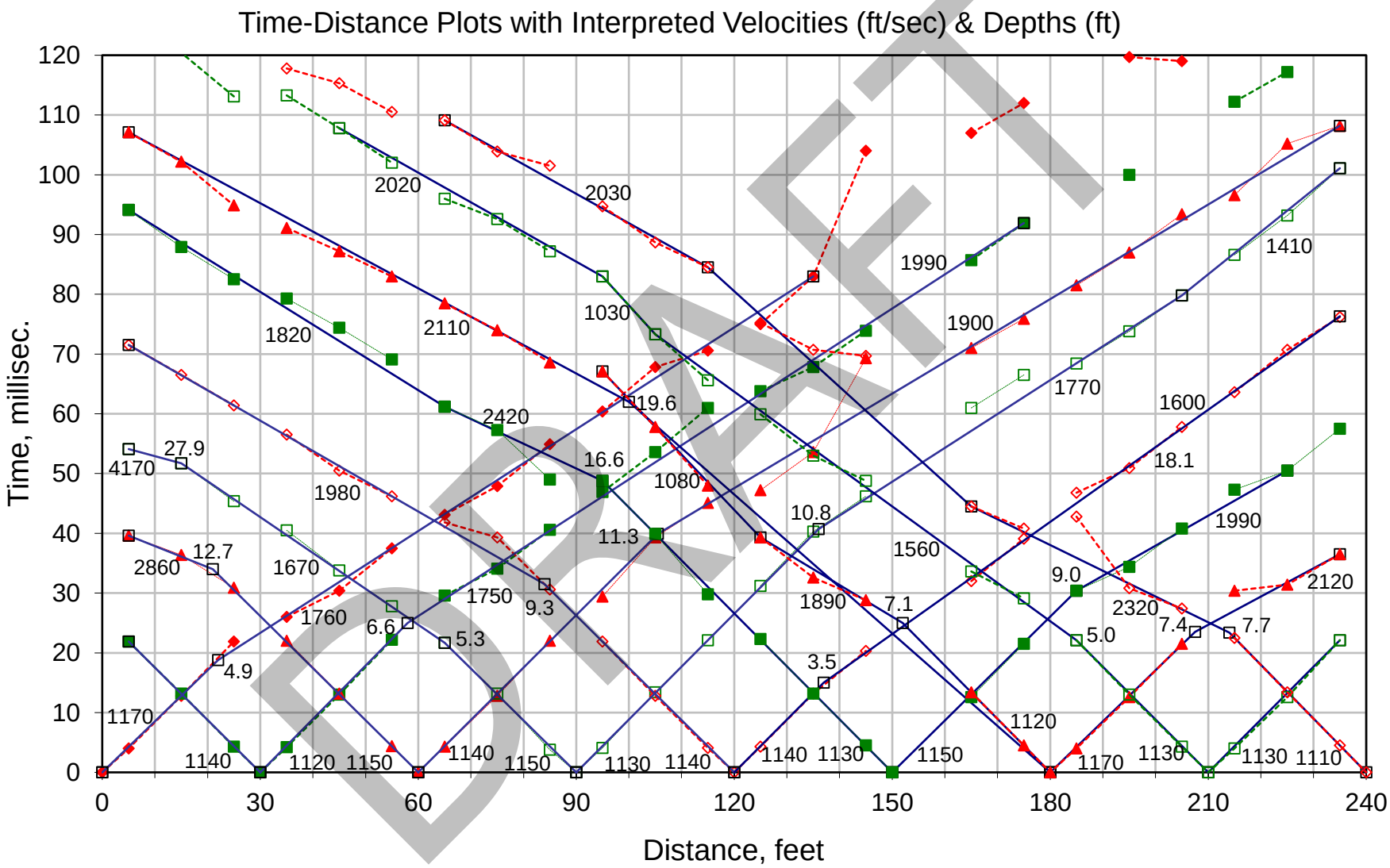

Refraction Microtremor S-wave Interpretation

Line 01A
(S20-01A)

Wood Job No. 17-2020-4004

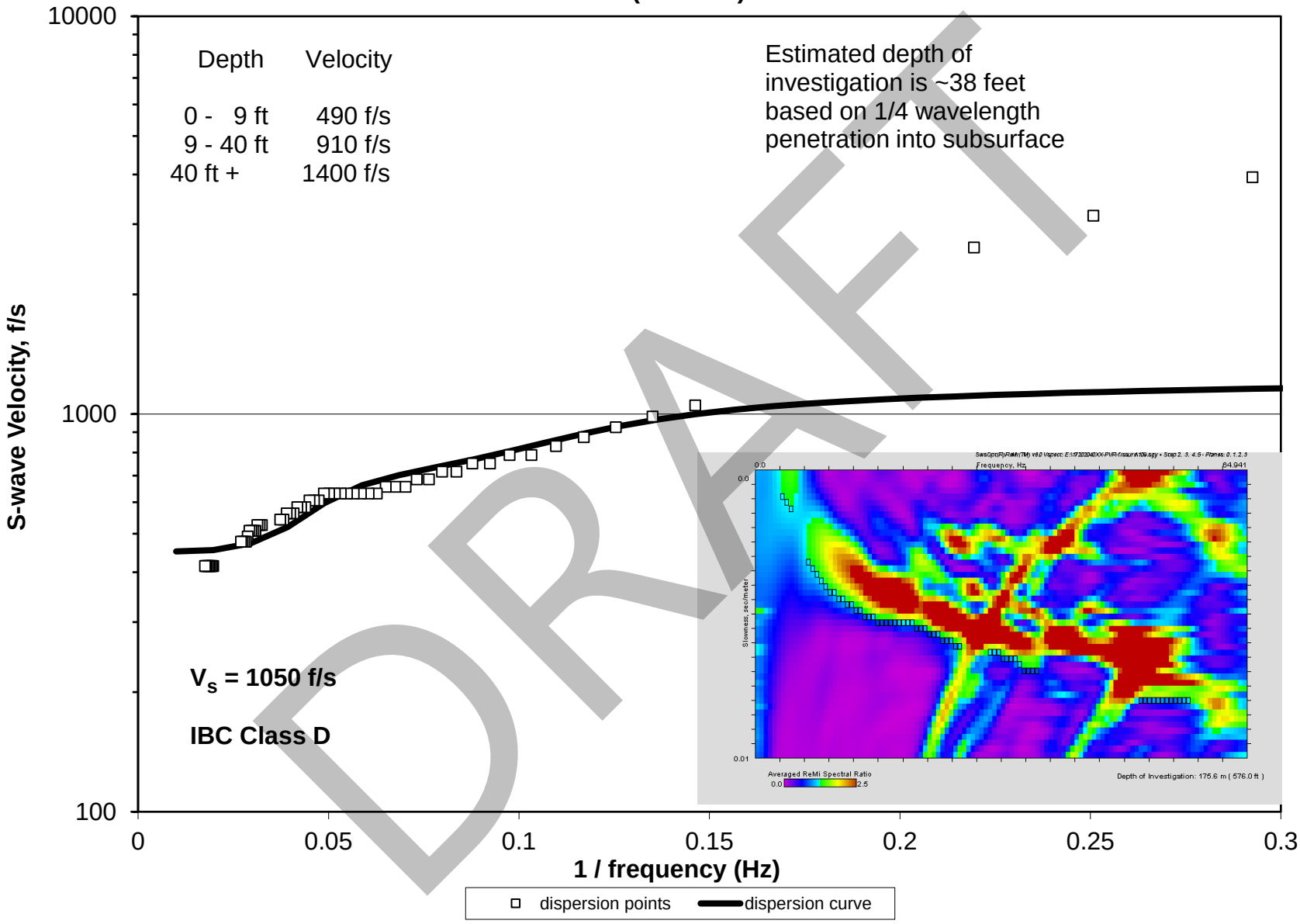

Refraction Microtremor S-wave Interpretation

Line 01B
(SL20-01B)

Wood Job No. 17-2020-4004

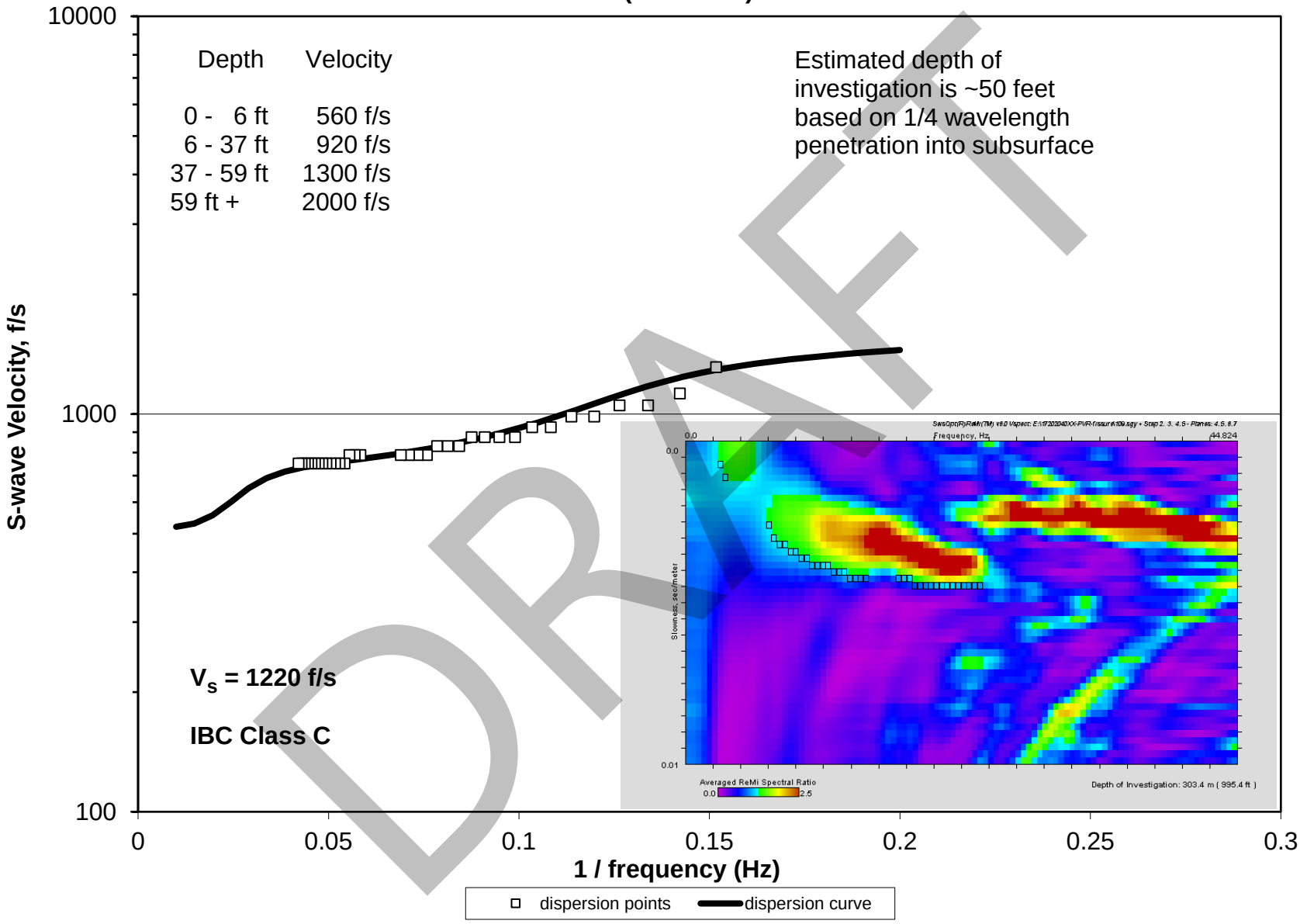

Seismic Refraction and Refraction
Microtremor Interpretation

Line 02
(SL20-02)

Wood Job No. 17-2020-4004

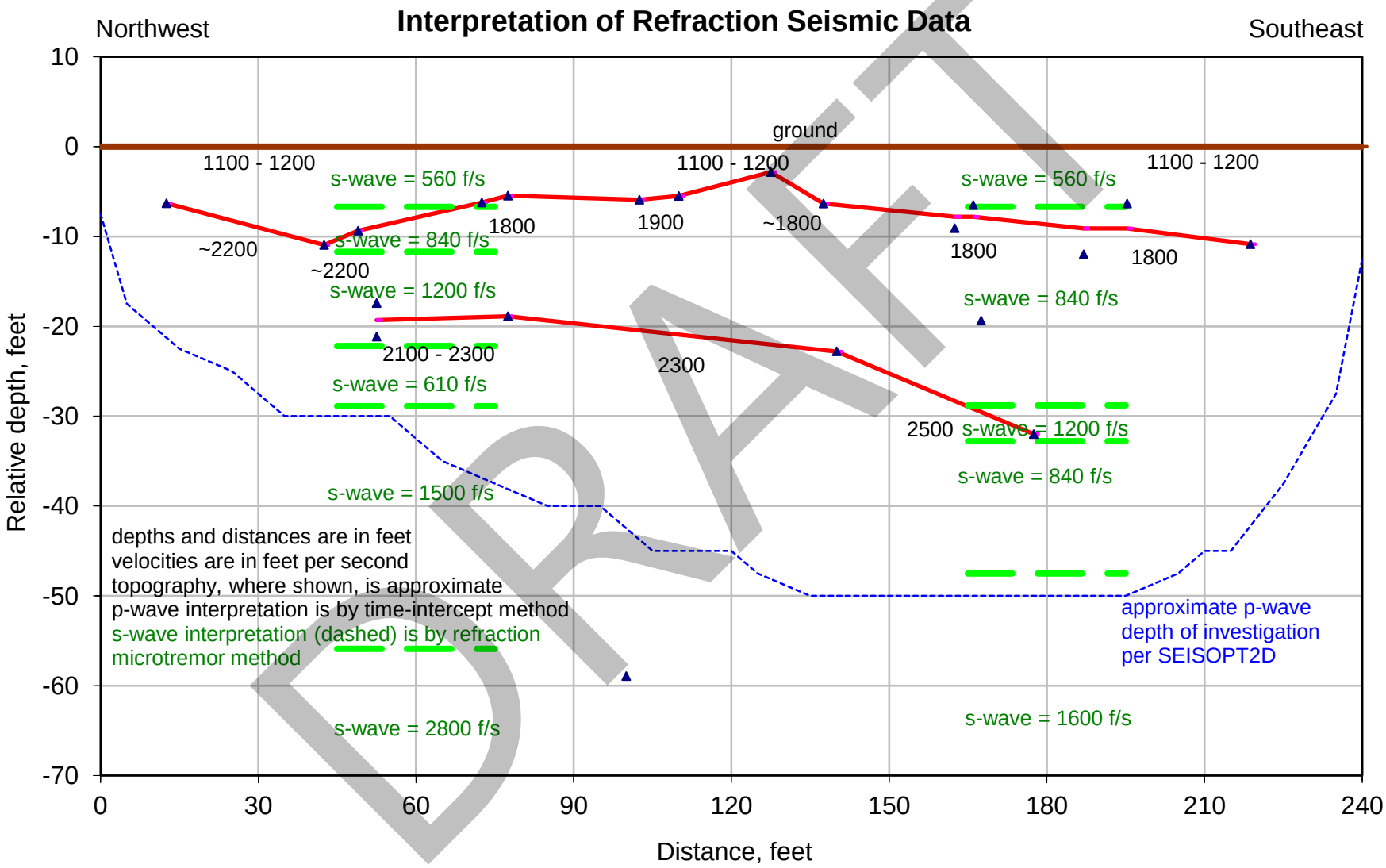

Seismic Refraction Interpretation
Time-Distance Plots

Line 02
(SL20-02)

Wood Job No. 17-2020-4004

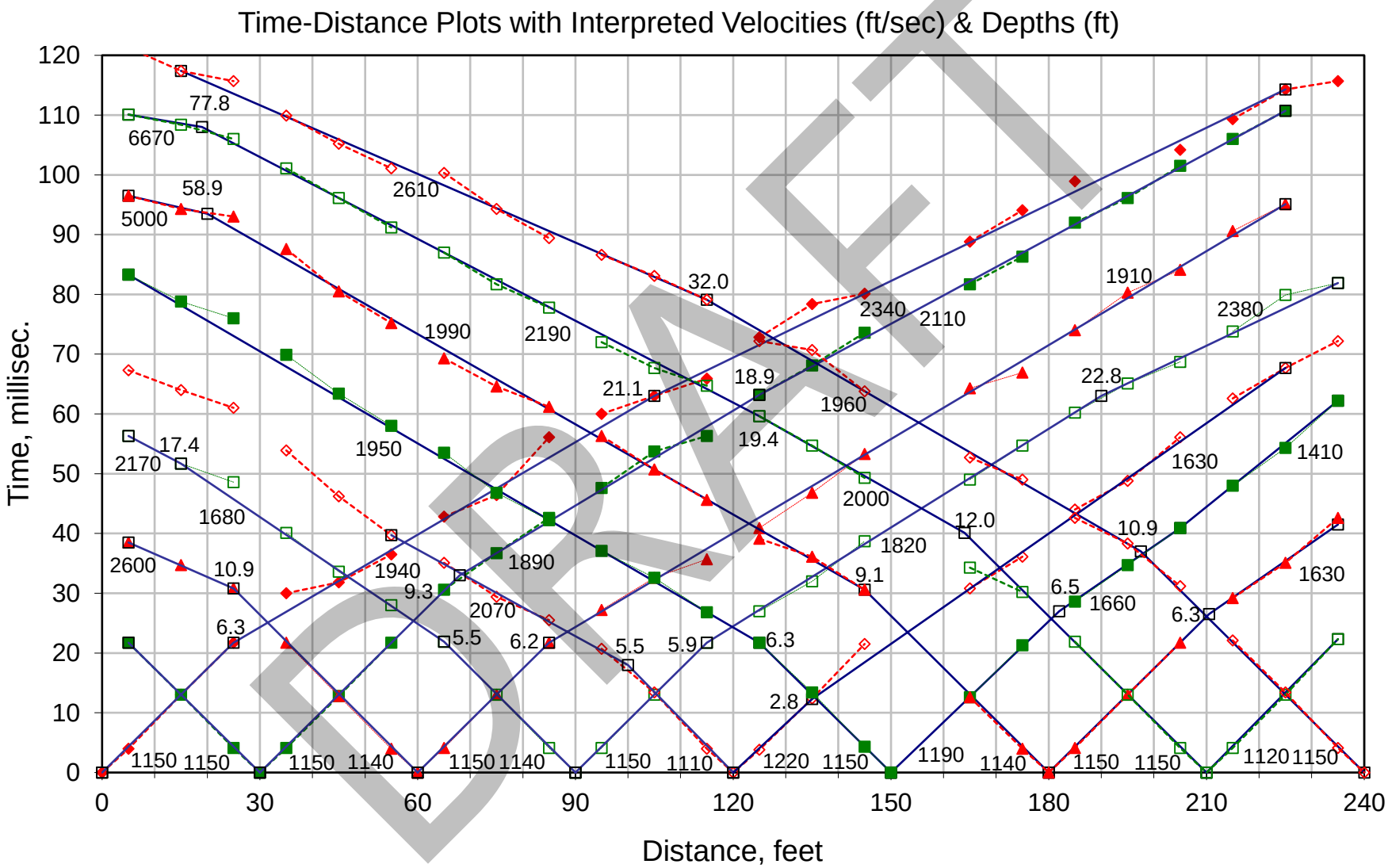

Refraction Microtremor S-wave Interpretation

Line 02A
(SL20-02A)

Wood Job No. 17-2020-4004

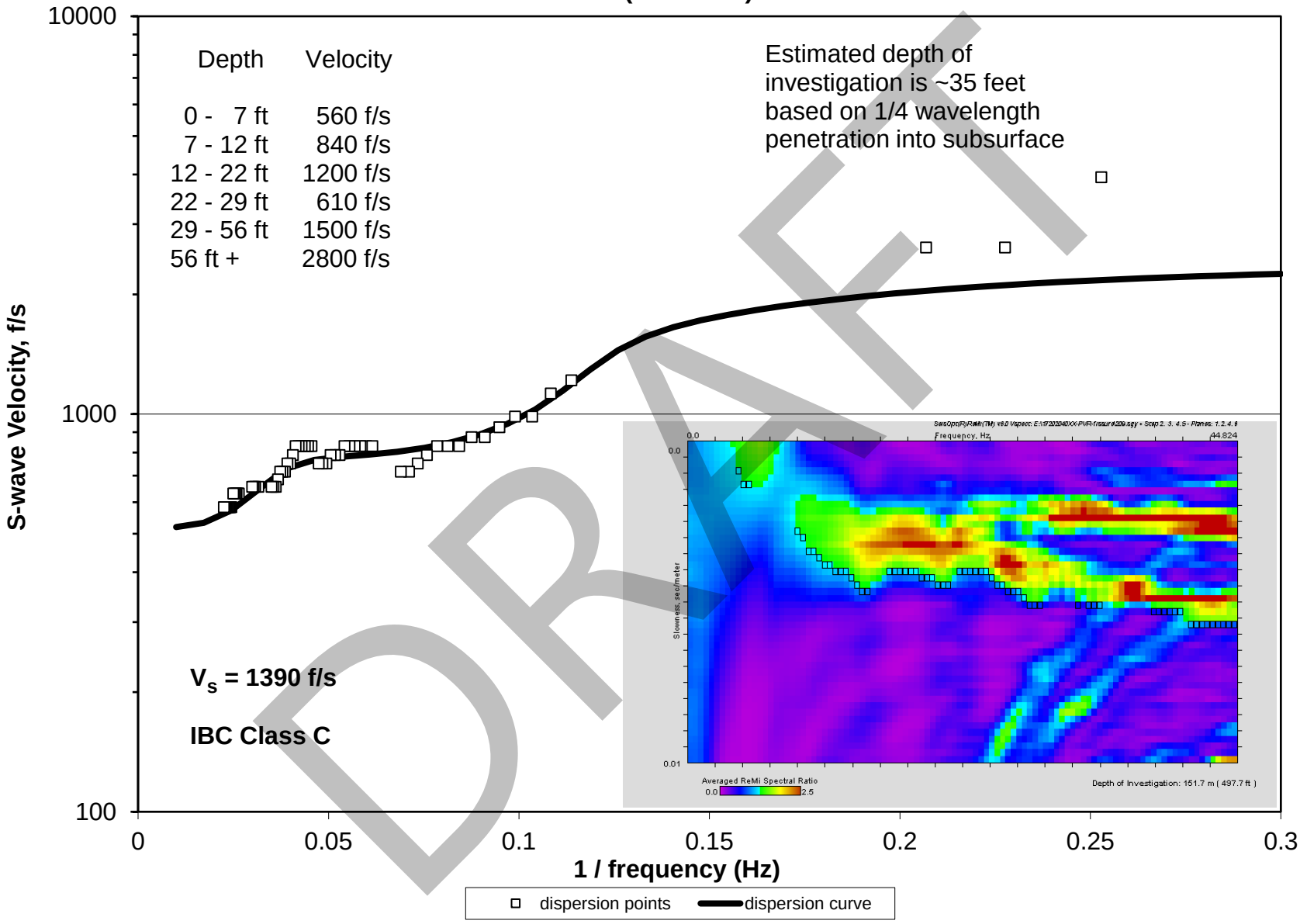

Refraction Microtremor S-wave Interpretation

Line 02B
(SL20-02B)

Wood Job No. 17-2020-4004

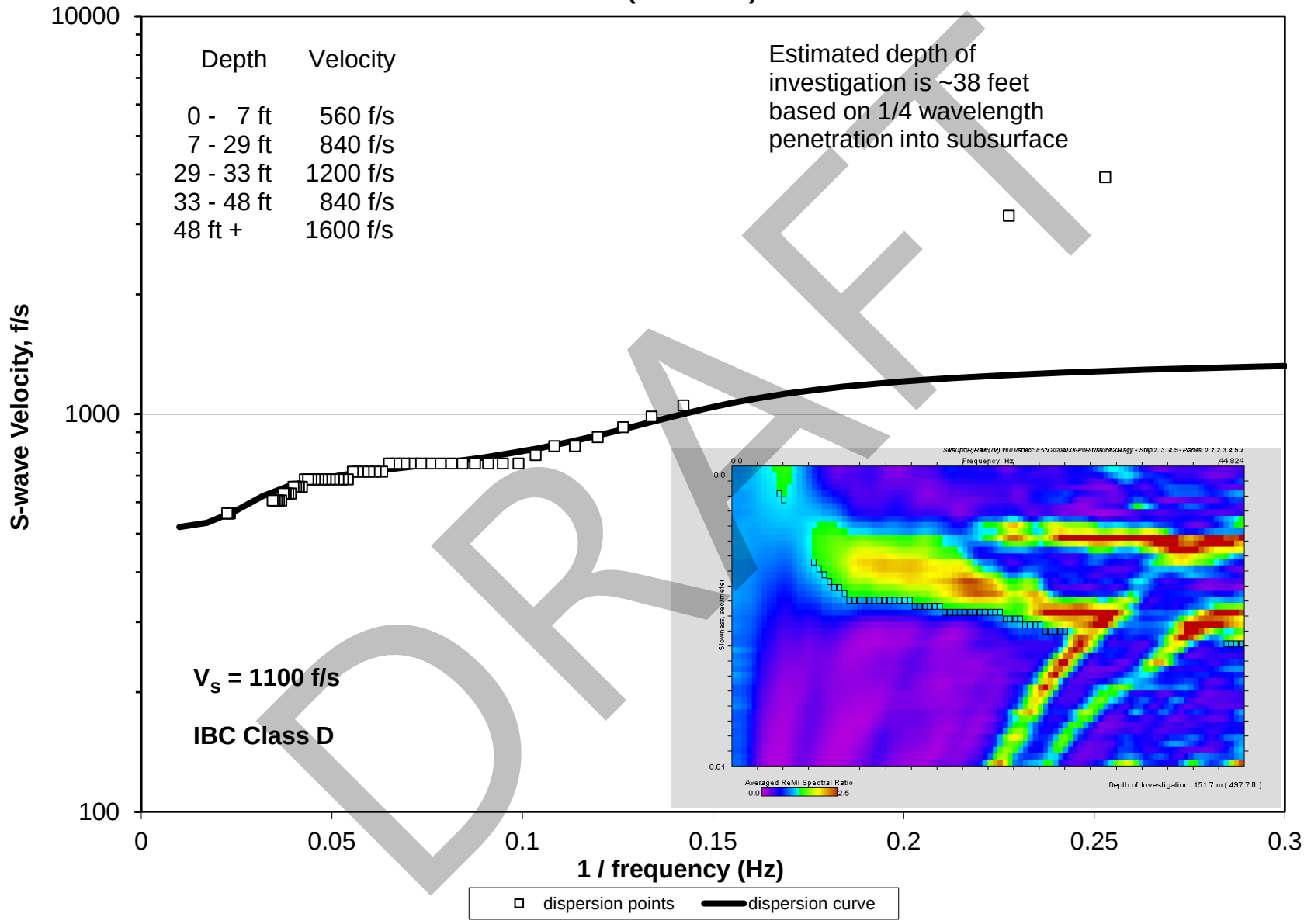

Seismic Refraction and Refraction
Microtremor Interpretation

Line 03
(SL20-03)

Wood Job No. 17-2020-4004

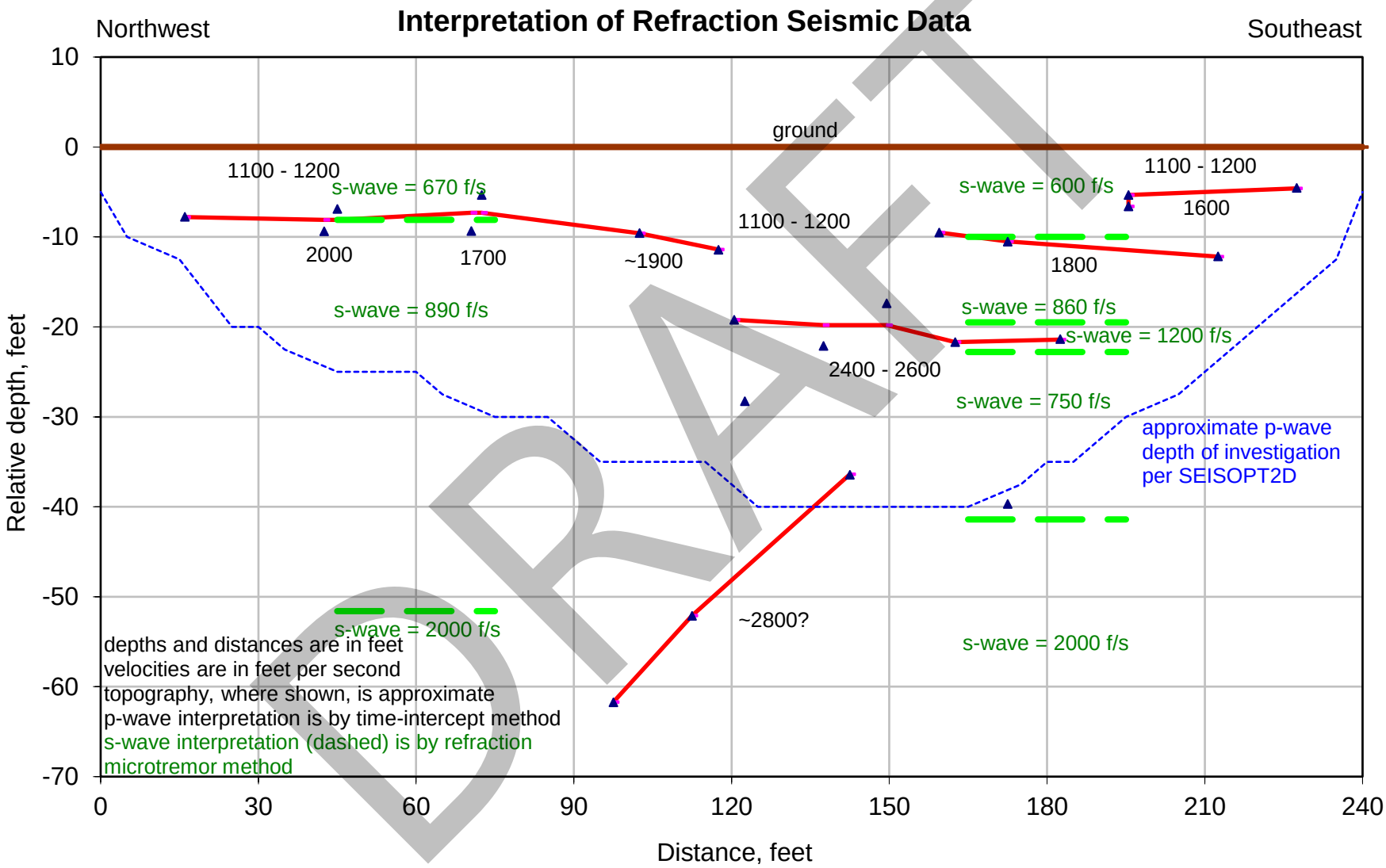

Seismic Refraction Interpretation
Time-Distance Plots

Line 03
(SL20-03)

Wood Job No. 17-2020-4004

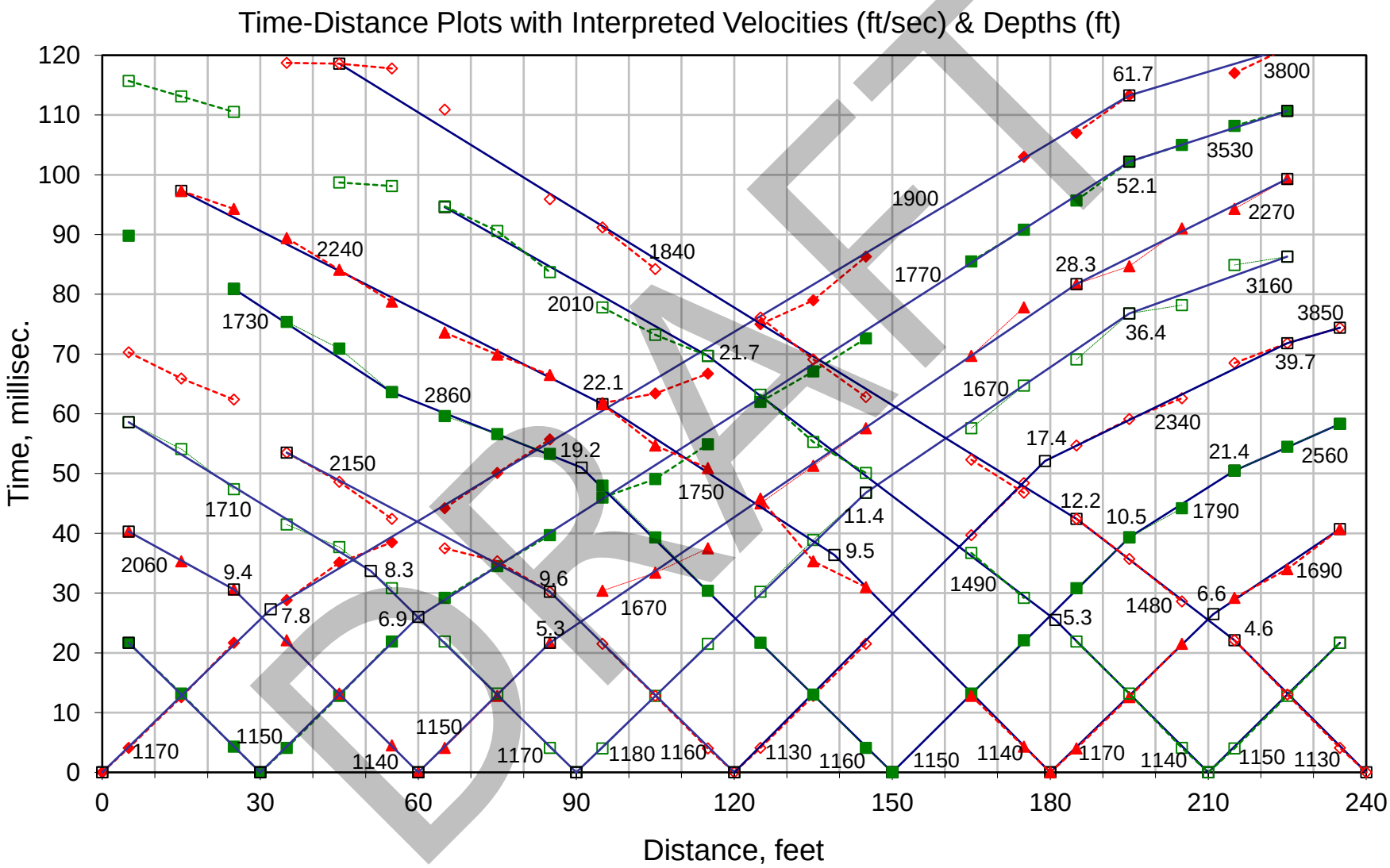

Refraction Microtremor S-wave Interpretation

Line 03A
(SL20-03A)

Wood Job No. 17-2020-4004

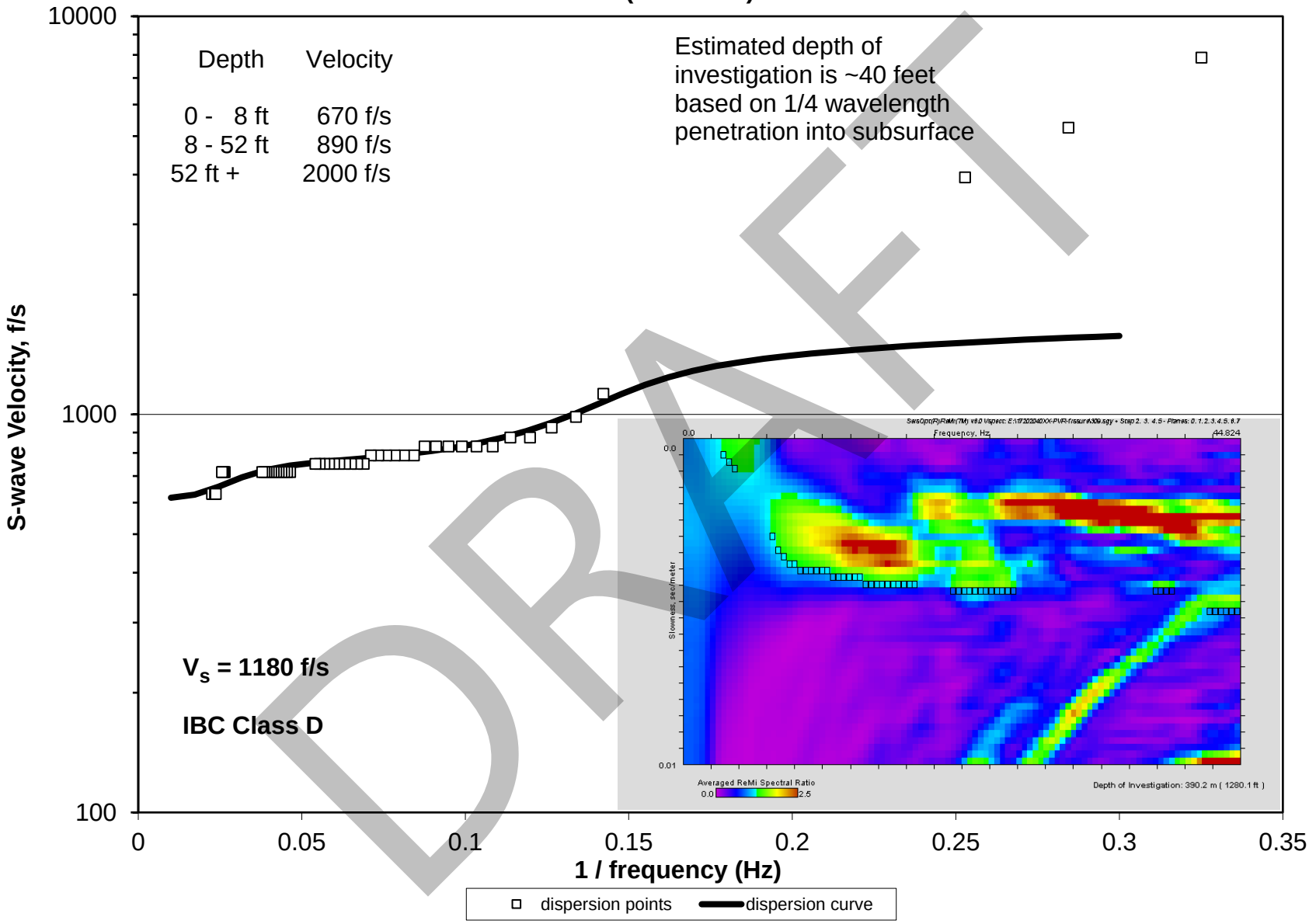

Refraction Microtremor S-wave Interpretation

Line 03B
(SL20-03B)

Wood Job No. 17-2020-4004

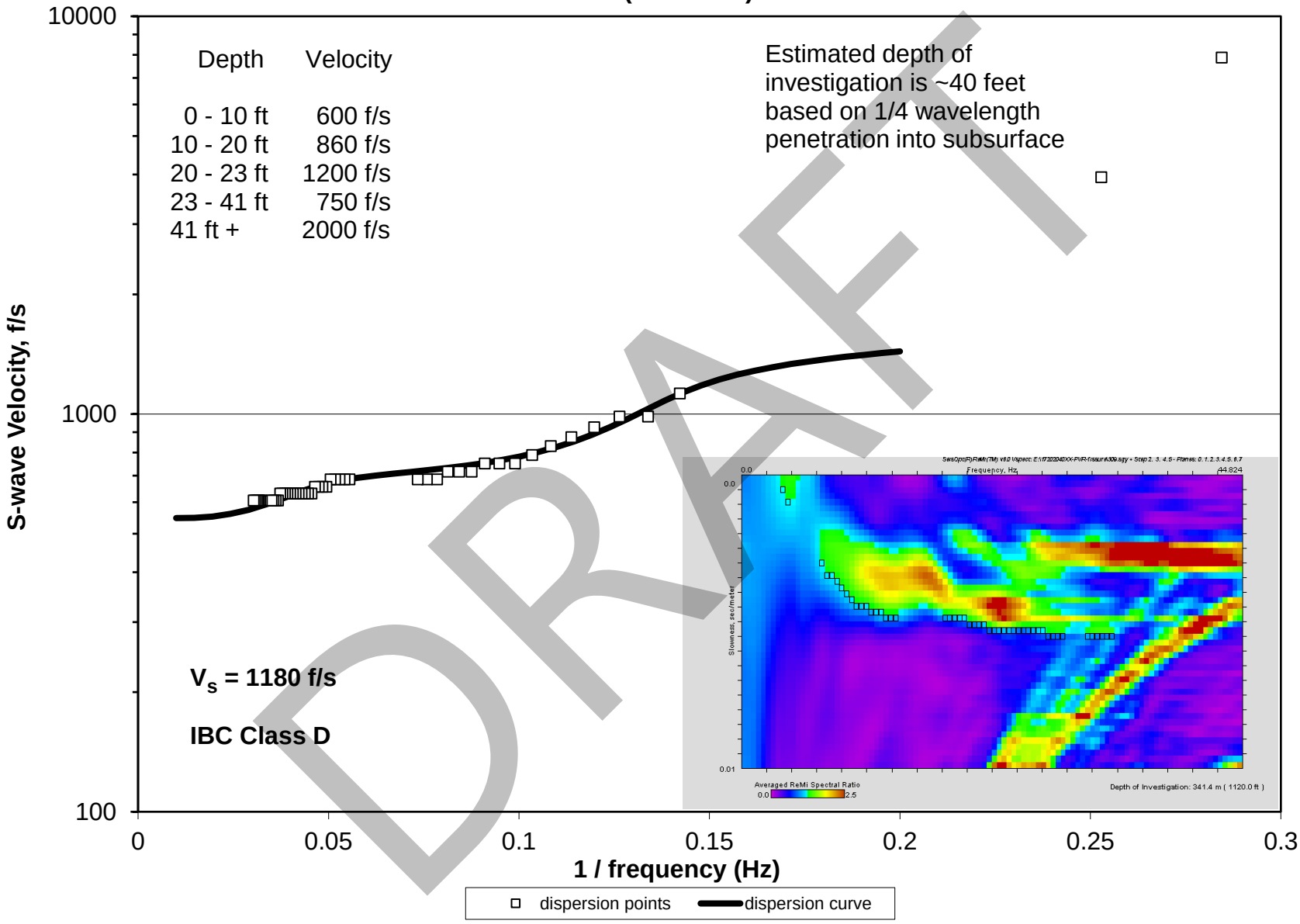

Seismic Refraction and Refraction
Microtremor Interpretation

Line 04
(SL20-04)

Wood Job No. 17-2020-4004

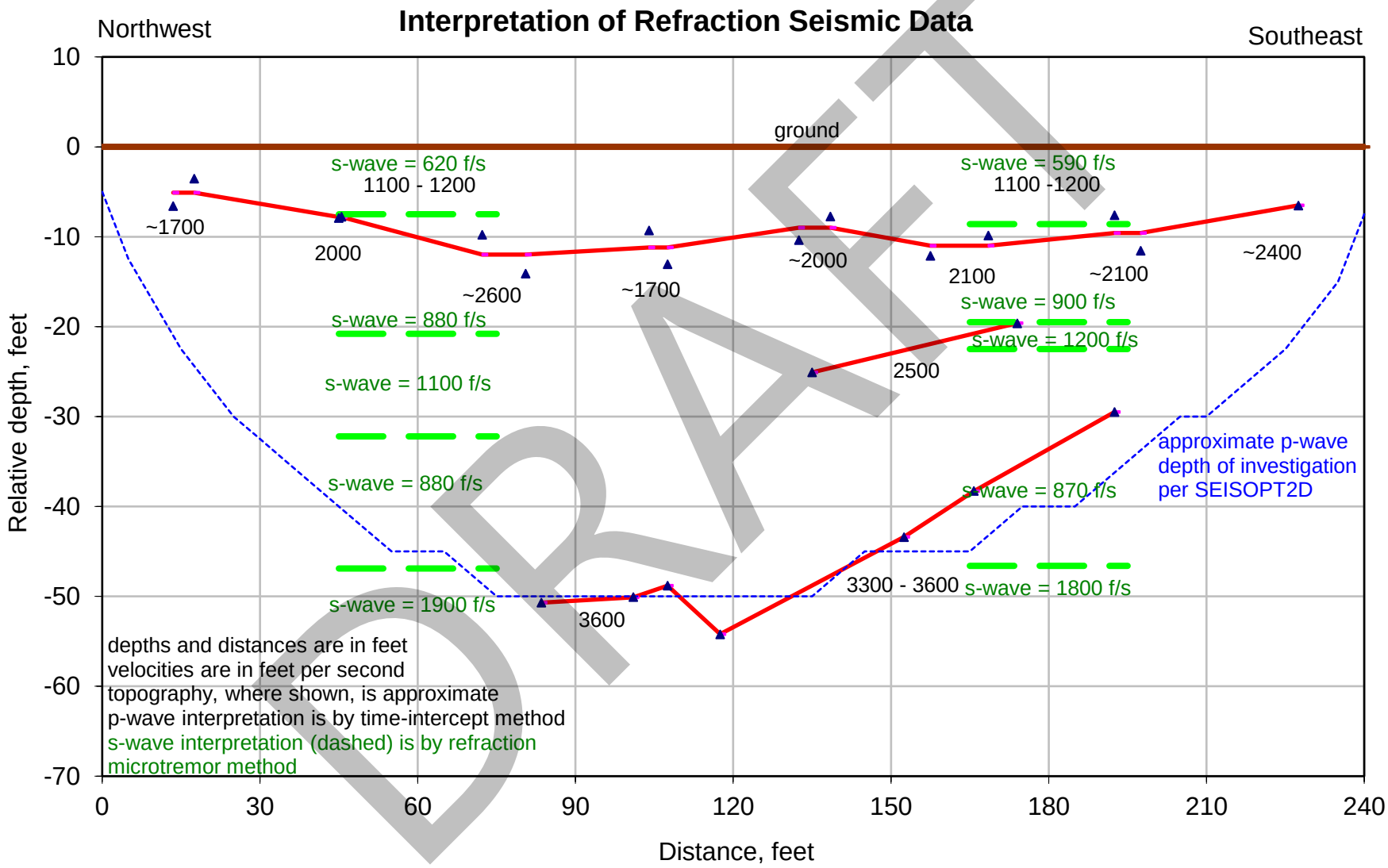

Seismic Refraction Interpretation
Time-Distance Plots

Line 04
(SL20-04)

Wood Job No. 17-2020-4004

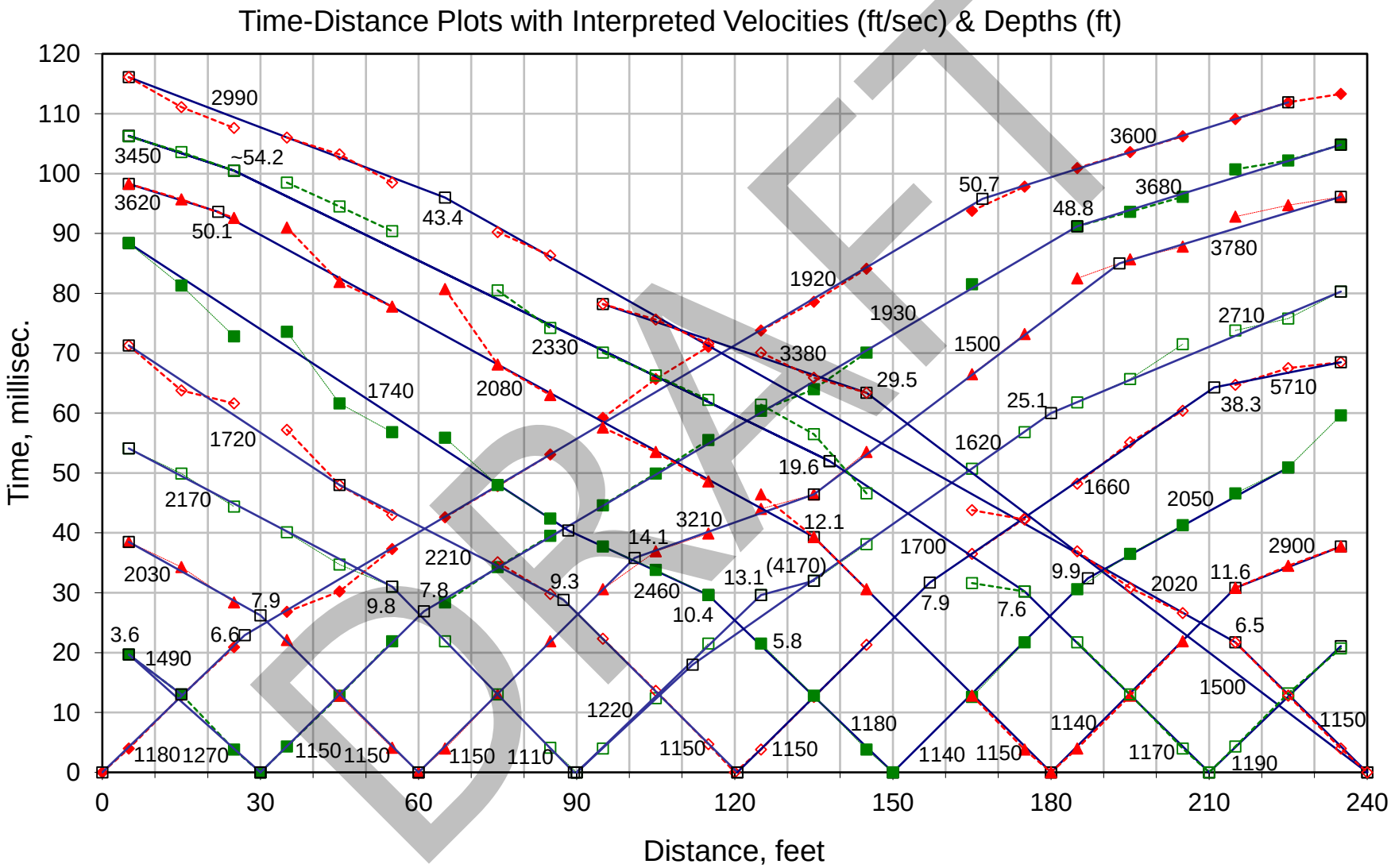

Refraction Microtremor S-wave Interpretation

Line 04A
(SL20-04A)

Wood Job No. 17-2020-4004

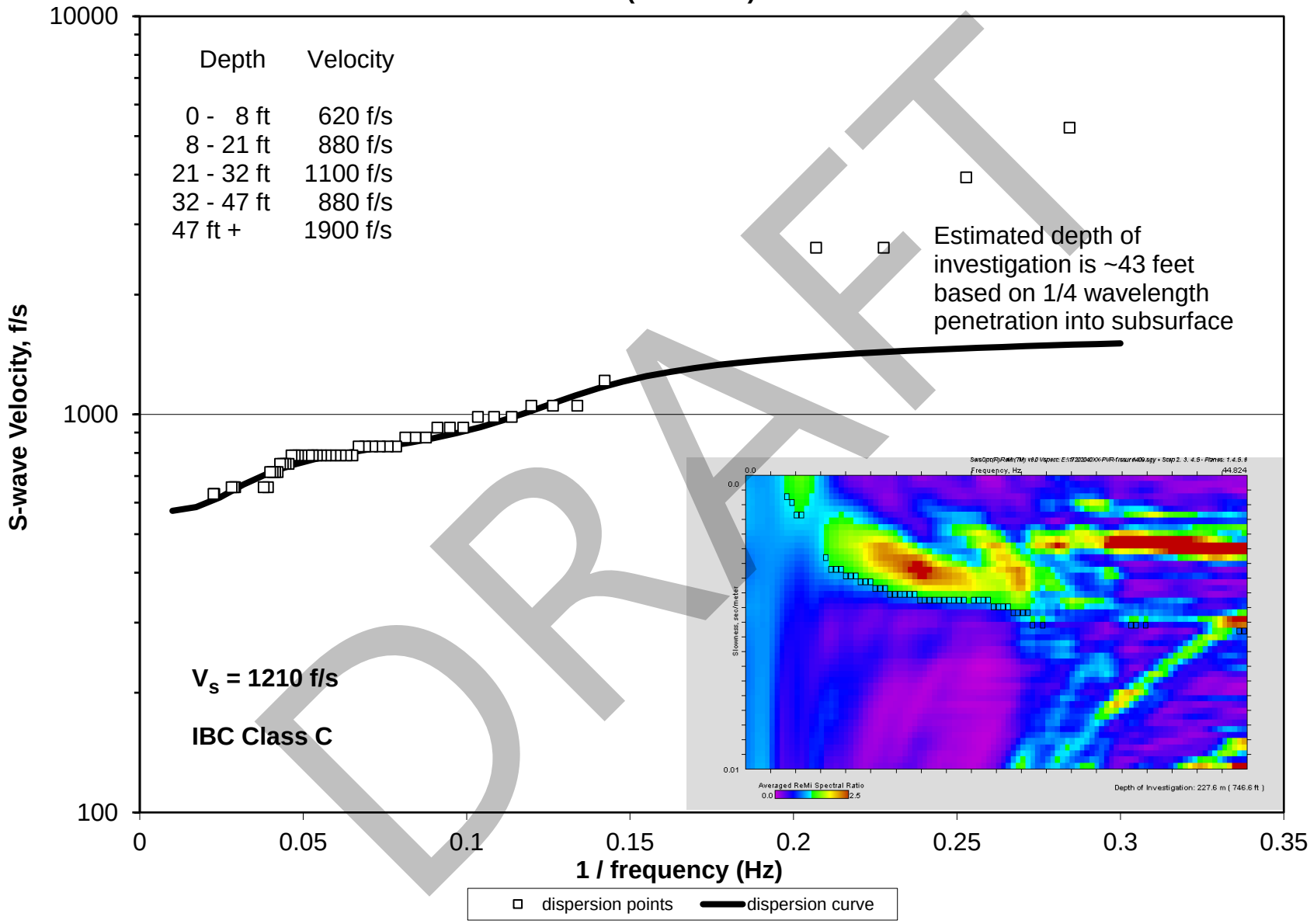

Refraction Microtremor S-wave Interpretation

Line 04B
(SL20-04B)

Wood Job No. 17-2020-4004

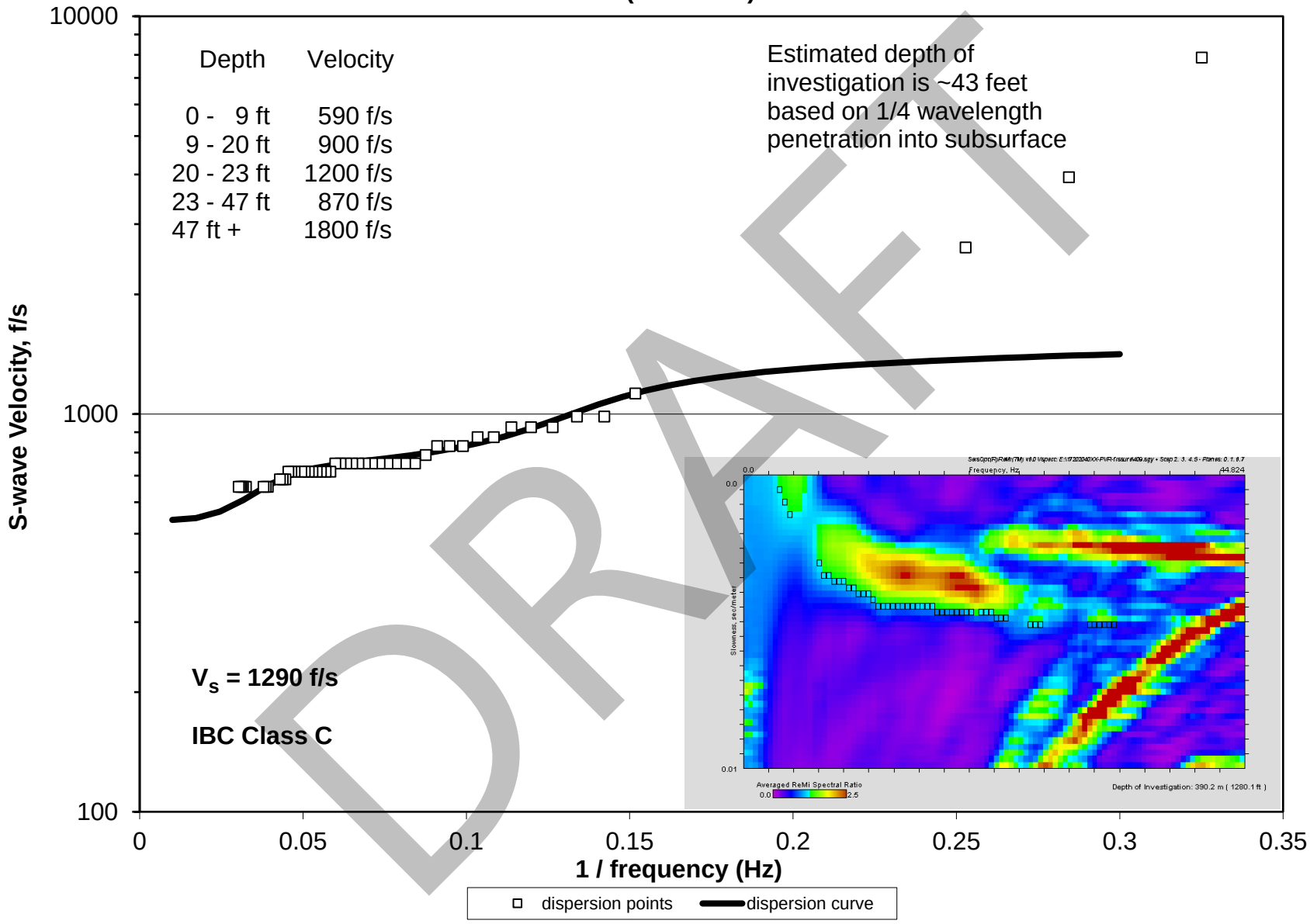

INTERPRETATION AND ANALYSIS OF SEISMIC ANOMALY TRACES

An initial definition and description of seismic anomalies as used in 1994 when the method was developed and applied to earth fissure detecting and tracing in the field is presented in Rucker and Keaton (1998) as follows:

> *Qualitative interpretation of isolated attenuation data is separated into four semi-empirical categories: excellent, good, poor and none. An excellent indication is given by an amplitude ratio in excess of about 4 (12 db) for adjacent geophones and 3 for equidistant geophones, or by cycle skipping… A good indication is given by an amplitude ratio in excess of about 3 for adjacent geophones and 2 (6 db) for equidistant geophones… A poor indication has a lower amplitude ratio, which may or may not be due to isolated attenuation… Absence of attenuation results in an interpretation that no fissure is present.*

Continuing experience has modified the empirical interpretations somewhat as the field seismic methods have evolved and additional subsurface conditions have been encountered and interpreted, and then verified and evaluated, using test pits and trenches. Improved seismic methods include the use of 5 shotpoints along a 120-foot seismic line at 30-foot intervals (10-foot geophone spacing) and the introduction of surface wave data collection for ReMi as an additional means of empirically evaluating seismic amplitude attenuation. The introduction of 24-channel seismic equipment, using 9 shotpoints at 30 foot shotpoint intervals and 240-foot arrays at 10-foot geophone spacing, has further improved seismic anomaly detection as less overlap of adjacent seismic lines is required. The inclusion of a distinct lateral reduction in seismic velocity is now also included in the interpretation of a weak to possible seismic anomaly. Additional subsurface conditions include encountering, interpreting and verifying buried (paleo-) stream channels and collecting data across observed surface desiccation cracks typical of areas with giant polygonal desiccation features.

The presence of a velocity reversal condition in the subsurface can generate seismic anomalies that could easily be confused with earth fissure-type seismic anomalies. Typically, such velocity reversal-induced seismic signal attenuation and apparent cycle skipping can be generated due to subsurface conditions involving a cemented or cohesive horizon overlying a less cemented or uncemented (or cohesionless) horizon. Very rapid attenuation of p-wave refraction signals in thin high velocity layers, about 5 to 10 db per wavelength when the layer is less than about one-half wavelength in thickness, has been presented in the literature (O'Brien, 1967; Sherwood, 1967). Vertical s-wave profiles and signal attenuation patterns that repeat at the same apparent distance from the shotpoints across multiple shot trends can help to discriminate between a relatively thin cemented horizon and a significant discrete anomaly, including an earth fissure. Examples of combined seismic refraction and refraction microtremor interpretation under such velocity reversal conditions are discussed by Rucker (2006).

Given these considerations, a current definition of seismic anomalies in native ground and embankments, tempered with engineering judgment, may be considered as follows.

Strong seismic anomaly – would typically be an excellent to good (Rucker and Keaton, 1998) seismic signal indication obtained in multiple seismic shot trends (i.e.: fore-shot, forward quarter-shot and back quarter-shot). This interpretation typically indicates the presence of a significant and discrete subsurface anomaly. Such an anomaly in native ground could be an earth fissure, or in an embankment could be a significant crack. An example of a strong seismic anomaly in an embankment is presented in Figure 9 of Rucker and Holmquist (2006).

Early air wave signals masking first arrivals at a deep low velocity surficial horizon, or the presence of considerable background noise, may complicate a 'strong' seismic anomaly interpretation. A seismic anomaly may be masked within what appears to be noise in the seismic refraction trace data. Additional trace data obtained using 24-geophone arrays rather than 12-geophone arrays provides additional 'looks' at the subsurface profile at a greater variety of distances in these noisy environments to enhance the seismic anomaly interpretation.

Weak seismic anomaly – would typically be a poor (Rucker and Keaton, 1998) seismic signal indication obtained in multiple seismic shot trends (i.e.: forward quarter-shot, mid-shot and back-shot). There may be one good (Rucker and Keaton, 1998) seismic shot trend in the group, but the other shot trends do not support a strong seismic anomaly interpretation. A distinct or discrete reduction in lateral seismic velocity at multiple seismic shot trends, perhaps over an apparent lateral distance of perhaps two to three geophones, with or without significant attenuation, can also contribute to the interpretation of a weak seismic anomaly. In native ground, this interpretation more likely indicates the presence of a subsurface anomalous condition that influences seismic velocity, such as a distinct zone of cohesionless material in a geologic setting of cemented materials, rather than a discrete earth fissure-type feature. Although this type of feature is typically a **buried paleo-channel**, a **sediment-filled earth fissure**, where tension has been relieved over time by ground cracking through a zone of adjacent ground, has been identified at one location in the western Salt River Valley. In an embankment, this interpretation is more likely consistent with a zone of desiccation cracking that is relatively shallow in extent.

Possible seismic anomaly – would typically be less distinct than a weak seismic anomaly, but still expresses sufficient character that it would be imprudent to ignore in an investigation to evaluate the presence or absence of subsurface anomalies.

P-wave interpretations for seismic velocities of horizons and depths of horizon interfaces typically utilize first arrival picks as far as can be determined from each energy point. Under normal conditions, data for a minimum distance of at least 9 to 12 geophones of a 24-geophone array can be picked for each energy point. Attenuation of the seismic signal eventually degrades the signal traces such that usable signals are not expected across an entire 24-geophone array. Multiple energy points along each seismic line provide multiple opportunities to interpret the potential for anomalous signal loss, depths to subsurface interfaces, possible velocity reversals, and laterally variable velocity conditions.

ReMi surface wave signal traces also provide opportunity to evaluate potential anomalous signal attenuation under some conditions. However, anomalous time delays may not be readily

discernable or interpretable using this method. ReMi's s-wave use has not been as extensively tested as p-wave seismic refraction, but may be effective in some conditions.

Discussion of Example Seismic Line Traces

A 120-foot long 12-geophone seismic line was completed along the Northern Avenue south right-of-way fence across a known earth fissure by Michael L. Rucker, P.E. and Kenneth C. Fergason, P.G. of AMEC on March 10, 2009. The seismic line, labeled "L3" on the scanned traces, was centered on the known earth fissure crossing Northern Avenue about one-half mile east of Dysart Road in Glendale, Arizona (AZGS, 2009). The fissure trend crosses the seismic line in the vicinity of geophones 6 to 8. Copies of the p-wave traces and traces of a selected ReMi surface wave data set are attached.

Based on visual examination without quantitative interpretation, p-wave traces are typically formed throughout only part of the data set, with time offset delays and degradation of trace quality, attenuation or total loss of signal typically apparent. The fore-shot traces (file 3017) show a first arrival trend at geophones 2 to 6 that begins to degrade at geophone 6. Beginning at geophone 7 and continuing through geophone 12, the downward portion of the first arrivals are severely attenuated or lost, and the upward portion of the first arrival trend slows significantly. The forward quarter-shot (file 3018) shows time delay and / or lateral reduction in p-wave velocity beginning at geophone 7. The mid-shot (file 3019) shows loss of signal at geophones 7 through 12. The back quarter-shot (file 3020) shows slow p-wave velocities (lower than the speed of sound in air) with normal trace shapes only clearly identifiable between geophones 5 and 3. The back-shot (file 3021) shows only air wave noise and no clear, well formed first arrivals. Based on the seismic traces, a strong seismic anomaly is indicated in the vicinity of geophones 6 to 7, with the anomaly further indicated to be between the midshot point and geophone 7. The anomaly is consistent with the interpretation of an active earth fissure at this location.

A 240-foot long 24-geophone seismic line was completed on the northern right-of-way of Olive Avenue across a known earth fissure by Mr. Rucker on May 3, 2011. The seismic line, labeled "L19" on the scanned traces, was centered on the known fissure crossing Olive Avenue just east of State Route (SR) 303 in the western Salt River Valley, Arizona (AZGS, 2009). Three seismic lines were completed on the earth fissure trend to the southwest of this line, seismic traces from these lines did not indicate the presence of fissuring, although complete interpretations of the p-wave data indicated a localized low-velocity feature at the fissure trend; without further investigation, that low-velocity feature was consistent with a buried paleo-channel. Copies of two sets of p-wave traces are attached. The fissure trend crosses the seismic line in the vicinity of geophones 11 to 12. Traffic on SR 303 generated considerable background noise that reduced the visual quality of the p-wave traces. The surficial soil horizon has interpreted p-wave velocities at or less than the speed of sound in air and interpreted depths of about 10 to over 20 feet at the attached traces; apparent p-wave first arrivals at the geophones nearest the shotpoint, perhaps as far as 4 to 6 geophones, may be air-wave rather than ground p-wave arrivals. The use of 24 geophone channels provides effective trace information at L19 that could not be obtained using only 12 geophone channels.

Based on visual examination without quantitative interpretation, quality p-wave traces are typically formed throughout only a portion of the L19 data sets. Typically, only the uppermost 8 to 9 seismic traces (about geophones 16 through 24) show well-defined first arrival waveforms. Higher-frequency noise associated with the sledgehammer impact dominates traces in the vicinity of the shotpoint, sometimes out to perhaps 4 to 6 geophone traces. Low-frequency 'ground-roll' ambient noise is significant in the lowermost seismic traces that are both closest to SR 303 and set to the highest gains. Nonetheless, a strong anomaly interpretation can be made at the lower L19 trace set with the shotpoint at the geophone array center. With the fissure located just west of the shotpoint, at least 6 well-formed first arrival traces can be identified to the east in the upper portion of the trace set. That seismic energy does not have to cross the earth fissure. No similar pattern of well-formed first arrival traces is present to the west of the shotpoint where the seismic energy has to cross the earth fissure. The same pattern of well-formed first arrival traces to the east and missing first arrival traces to the west is present in the trace set for the adjacent L19 shotpoint 30 feet to the east (L19 upper trace set). Due to the air wave interference at traces near to the shotpoints, the location of the earth fissure cannot be effectively determined to the nearest geophone pair.

References:

Arizona Geological Survey (AZGS), 2009, Earth Fissure Map of the Luke Study Area: Maricopa County, Arizona, Digitial Map Series – Earth Fissure Map 8 (DM-EF-8), February.

O'Brien, P.N.S., 1967, The use of amplitudes in seismic refraction survey, in Musgrave, A.W. (ed), Seismic Refraction Prospecting, Society of Exploration Geophysicists, Tulsa, Oklahoma, 85-118.

Rucker, M.L. and Keaton, J.R., 1998, Tracing an earth fissure using refraction-seismic methods with physical verification, in Land Subsidence, Case Studies and Current Research, Proceedings of the Joseph F. Poland Symposium on Land Subsidence, ed. J.W. Borchers, Special Publ. No. 8, Association of Engineering Geologists, pp. 207-216.

Rucker, M.L., 2006, Integrating Seismic Refraction and Surface Wave Data Collection and Interpretation for Geotechnical Site Characterization, presented at FHWAGeophysics2006, St. Louis, Mo., Dec. 4-7. http://www.optimsoftware.com/white_papers/images/FHWA2006RuckerP-waveS-wave.pdf Accessed August 25, 2010.

Rucker, M.L. and Holmquist, O.C., 2006, Surface seismic methods for locating and Tracing earth fissures and other significant discontinuities in cemented unsaturated soils and earthen structures, in Unsaturated Soils, Miller, G.A., Zapata, C.E., Houston, S.L. and Fredlund, D.G., eds, Geotechnical Special Publication No. 147, ASCE, Reston, Va., pp. 601-612.

Sherwood, J.W.C., 1967, Refraction along an embedded high-speed layer, *in* Musgrave, A.W. (ed), Seismic Refraction Prospecting, Society of Exploration Geophysicists, Tulsa, Oklahoma, 138-151.

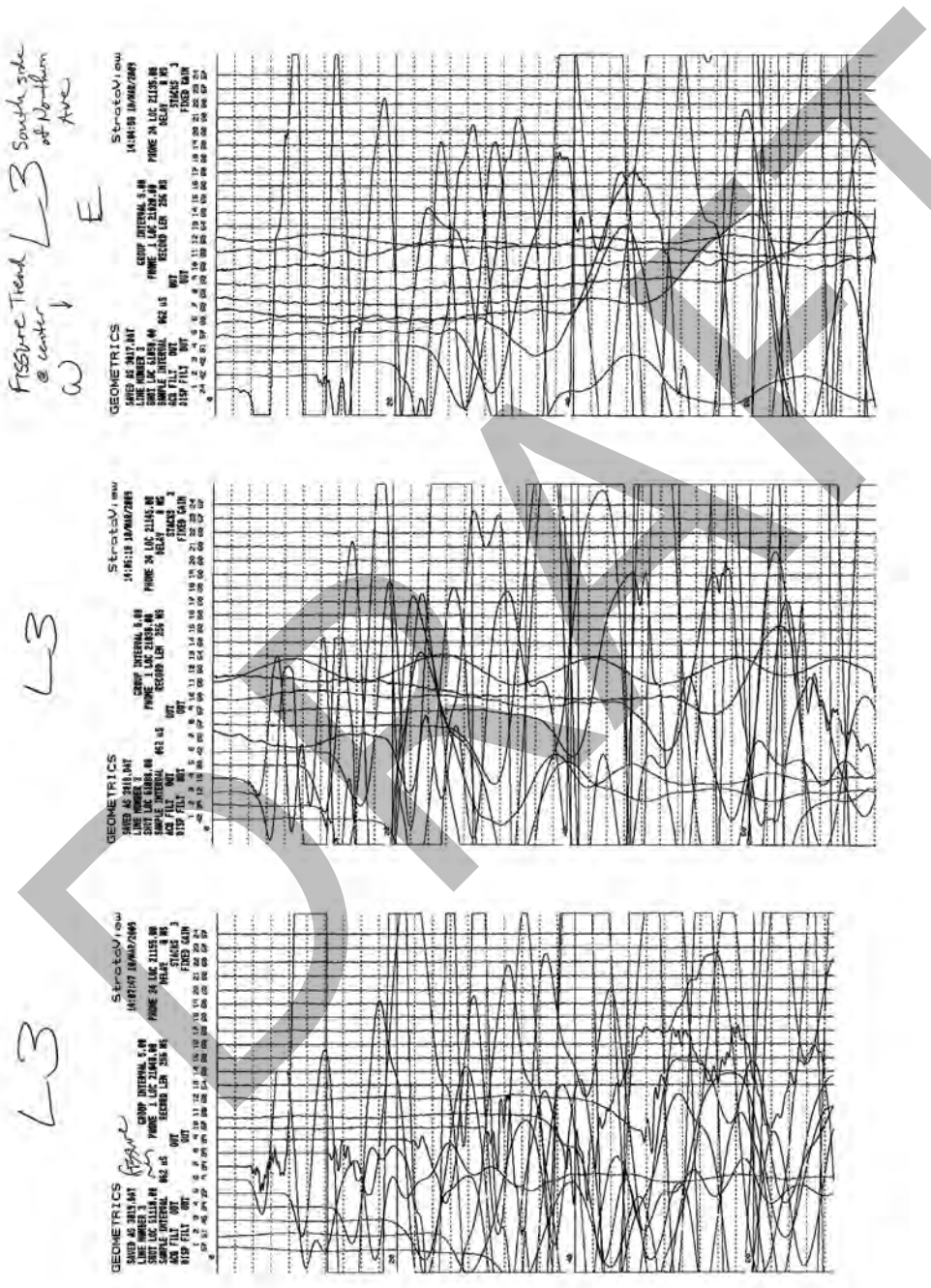

Seismic Line L3 fore-shot, forward quarter-shot and mid-shot traces across known earth fissure.

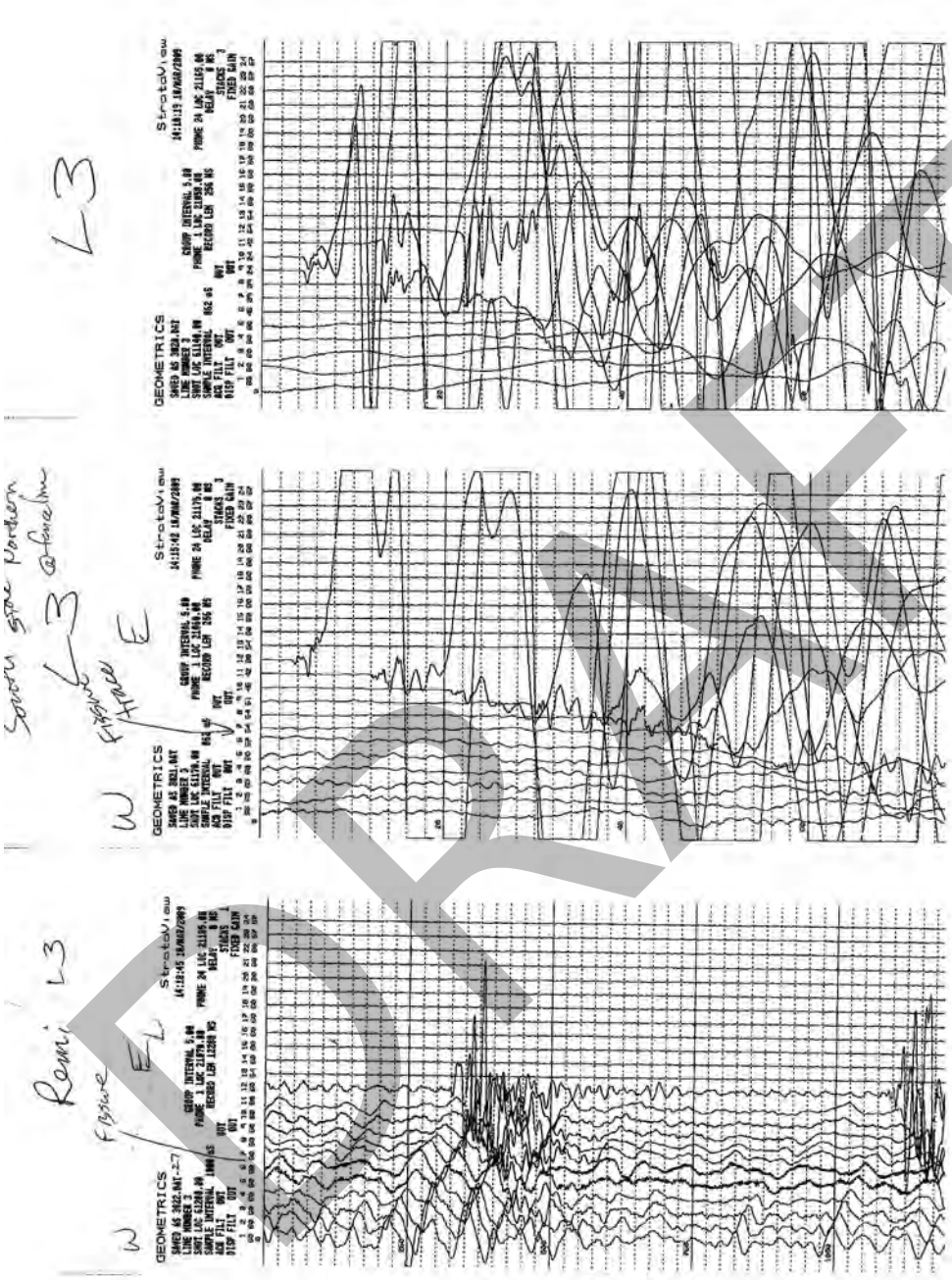

Seismic Line L3 back quarter-shot, back-shot and refraction microtremor traces across known earth fissure.

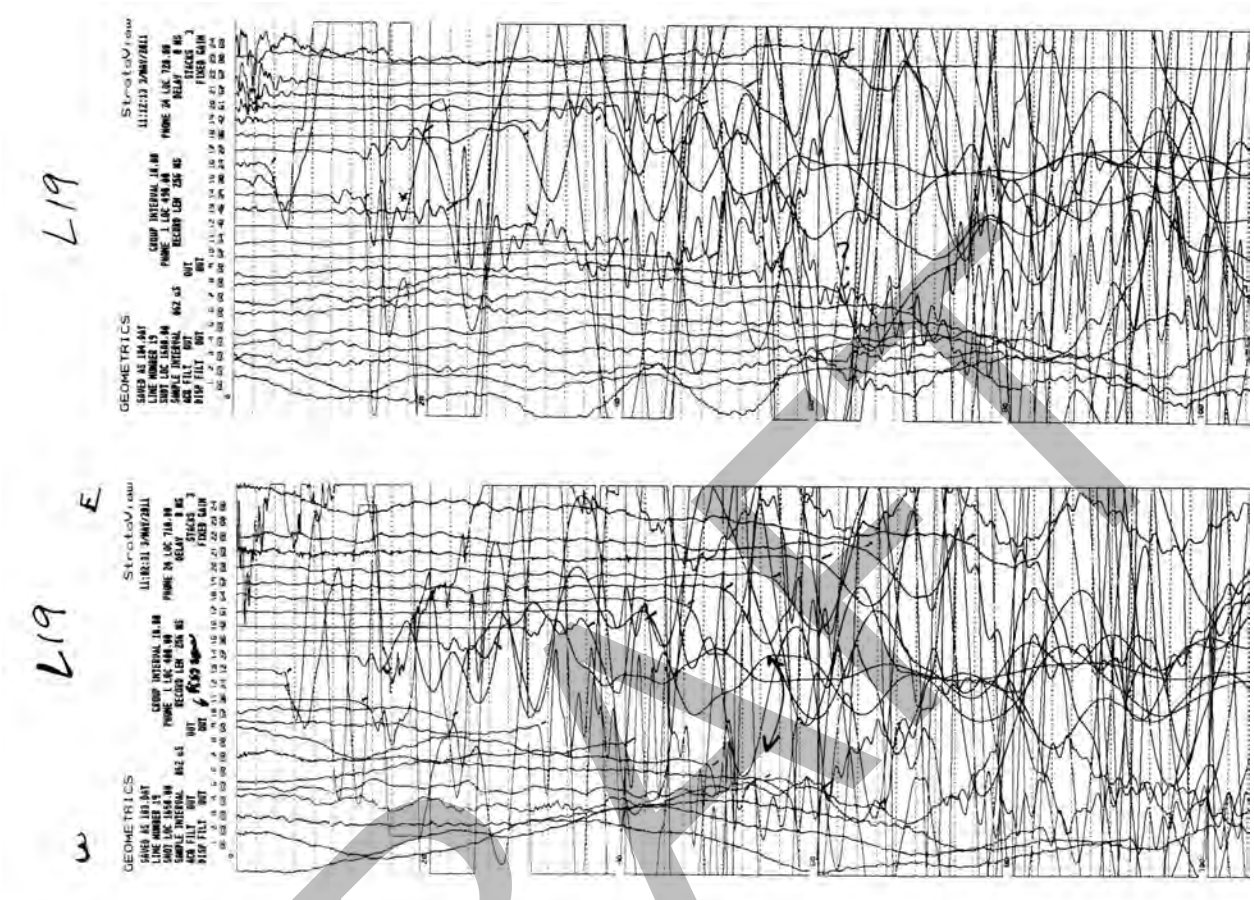

Seismic Line 19 midshot (lower trace set) and shotpoint 30 feet to the east (upper trace set) across known earth fissure.

Line 1 – shotpoint 1

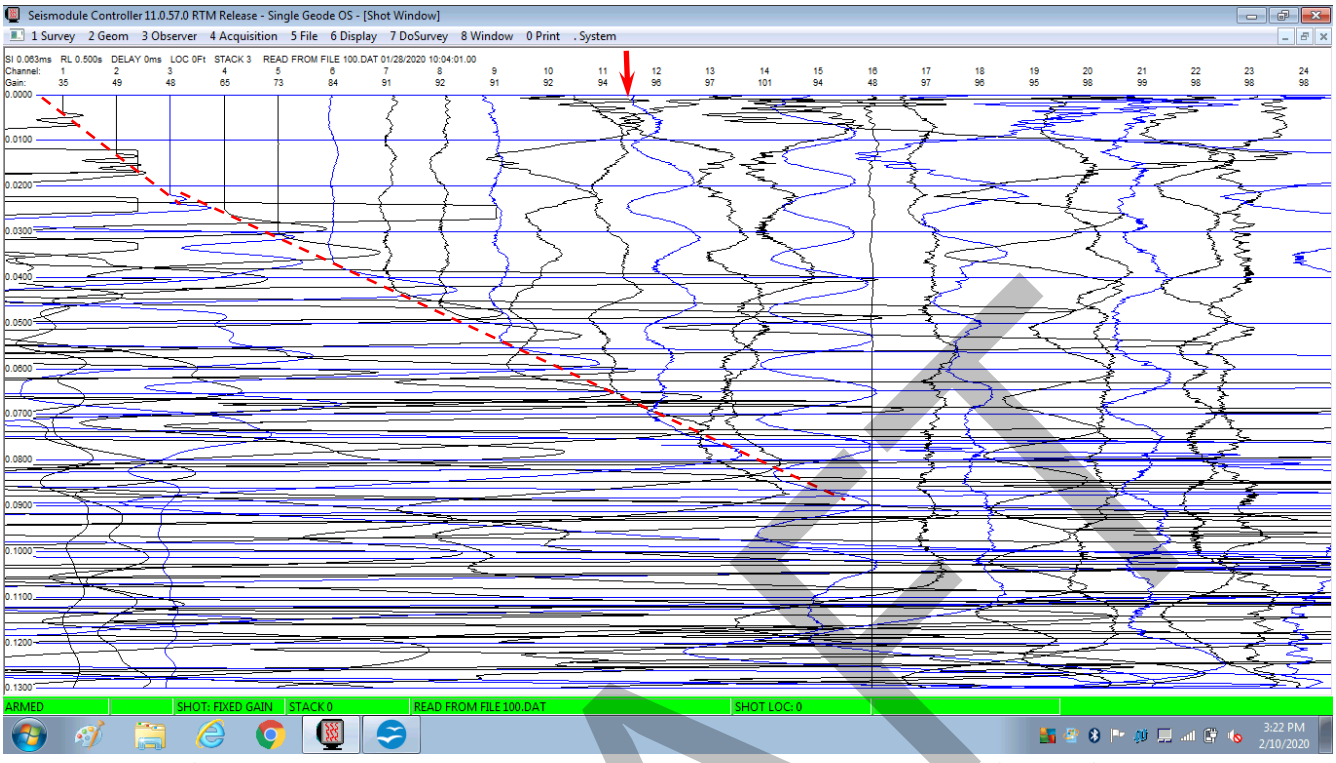

Line straddles fissure end near phone 12. Attenuation and signal loss is significant after geophone 14. Air wave dominates first 3 geophones from shotpoint..

Line 1 – shotpoint 2

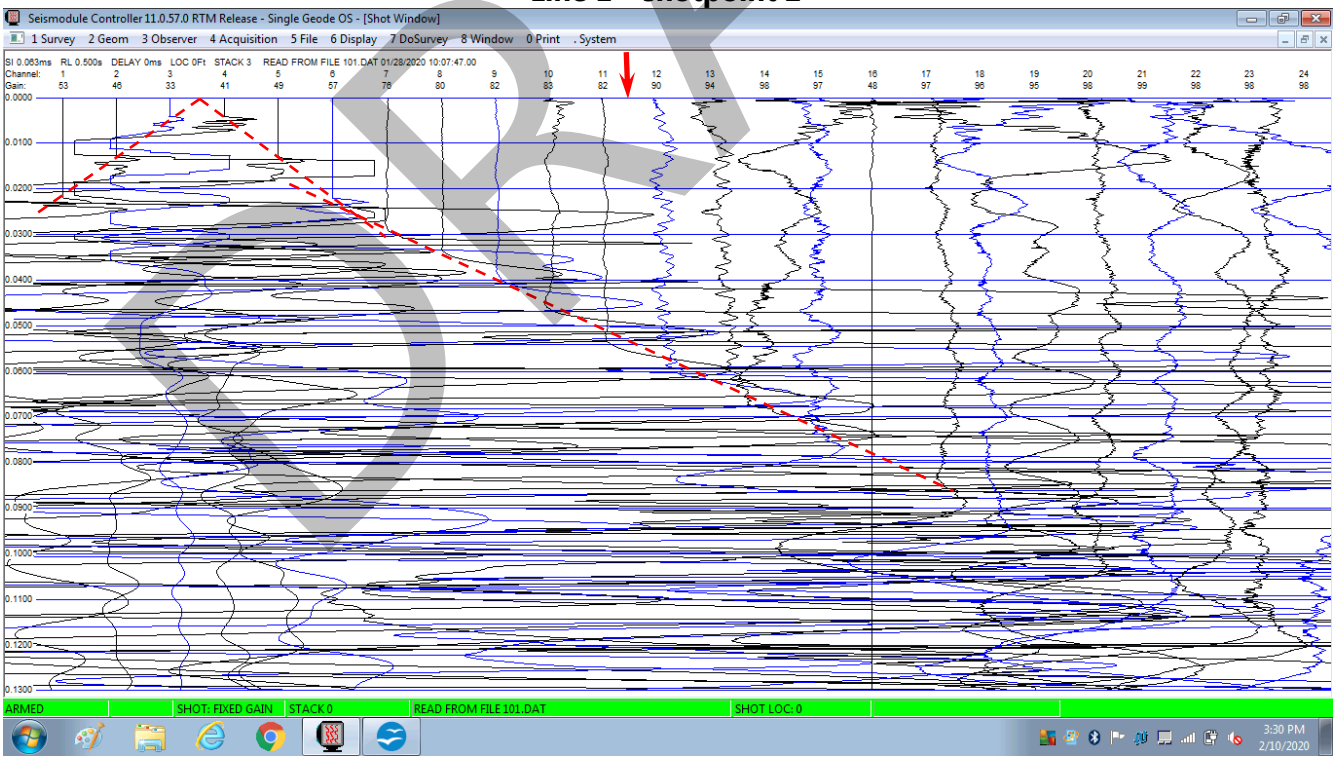

Attenuation is significant after geophone 14. Air wave dominates first 3 geophones from shotpoint.

Line 1 – shotpoint 3

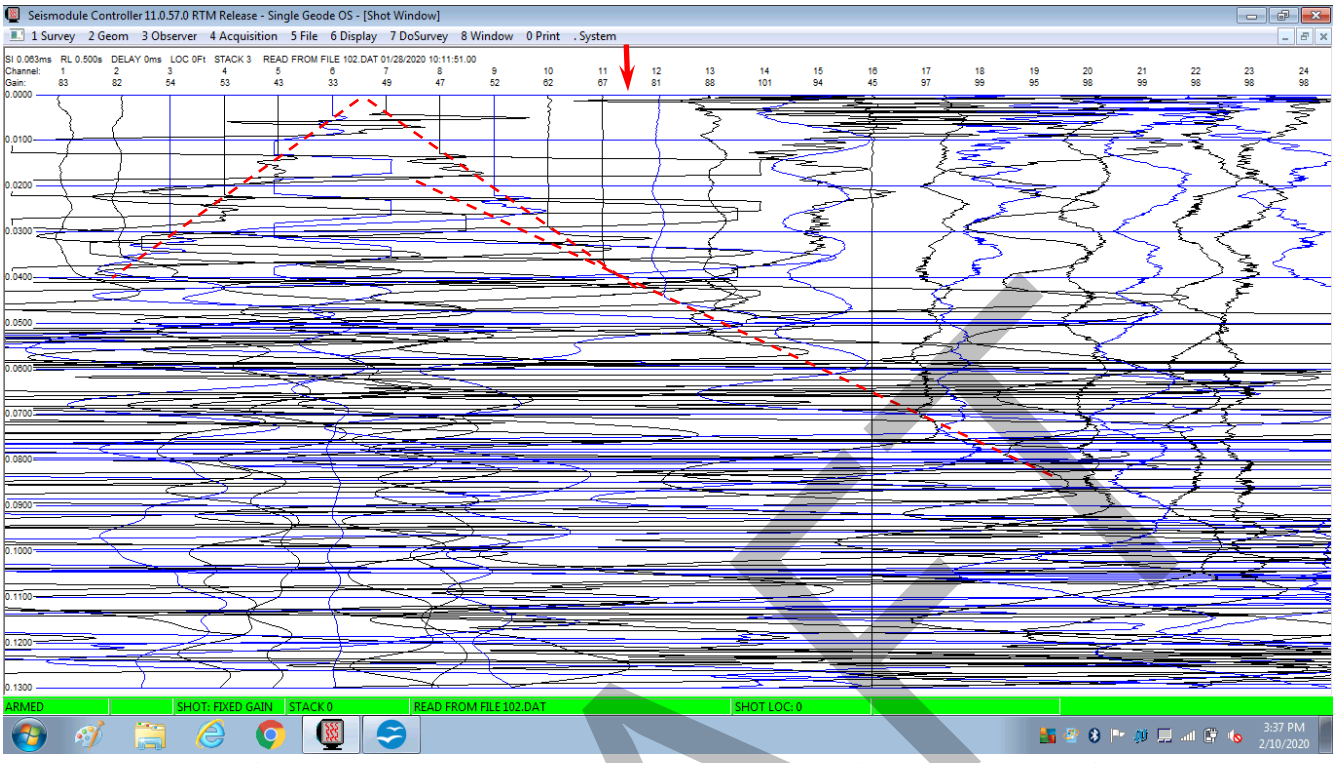

Attenuation is significant after geophone 14. Air wave dominates first 4 geophones from shotpoint.

Line 1 – shotpoint 4

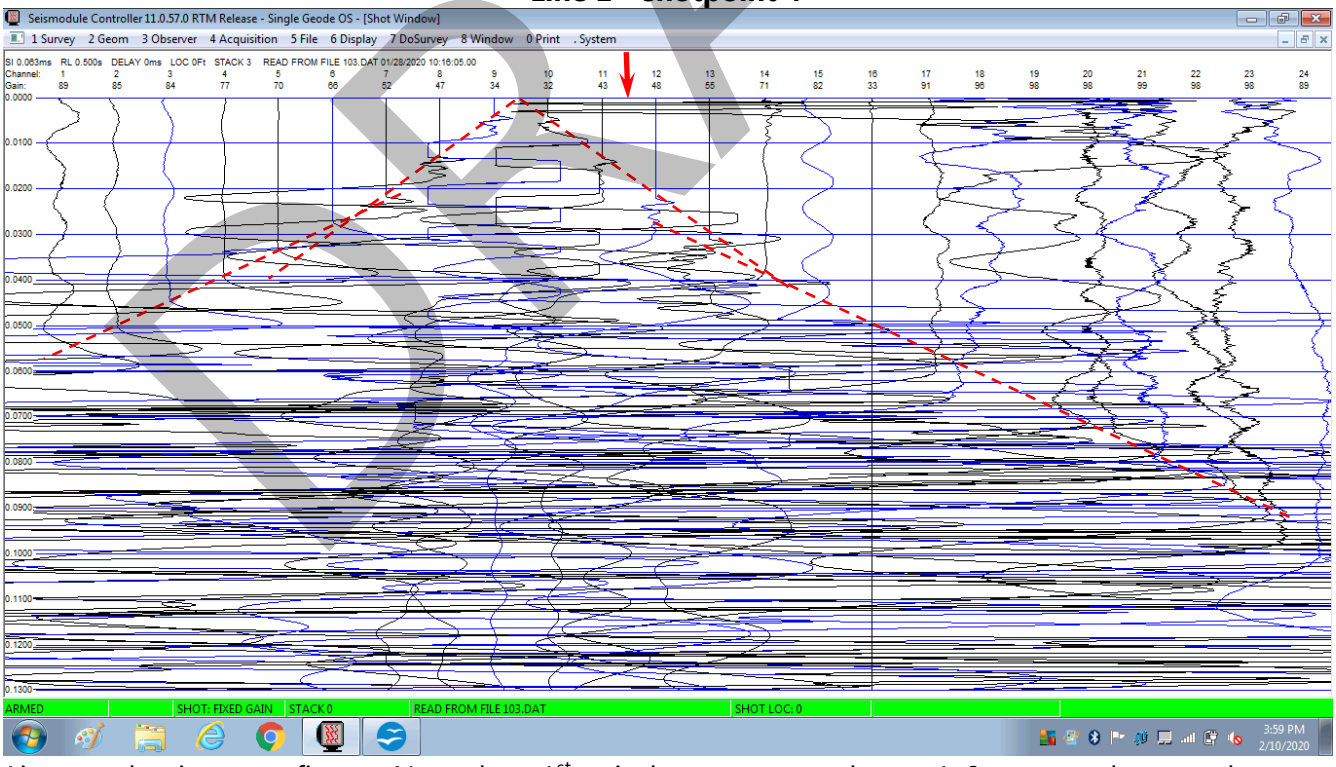

Air wave dominates at fissure. Note clean 1st arrival traces at geophones 1-6 compared to geophones 13-18.

Line 1 – shotpoint 5

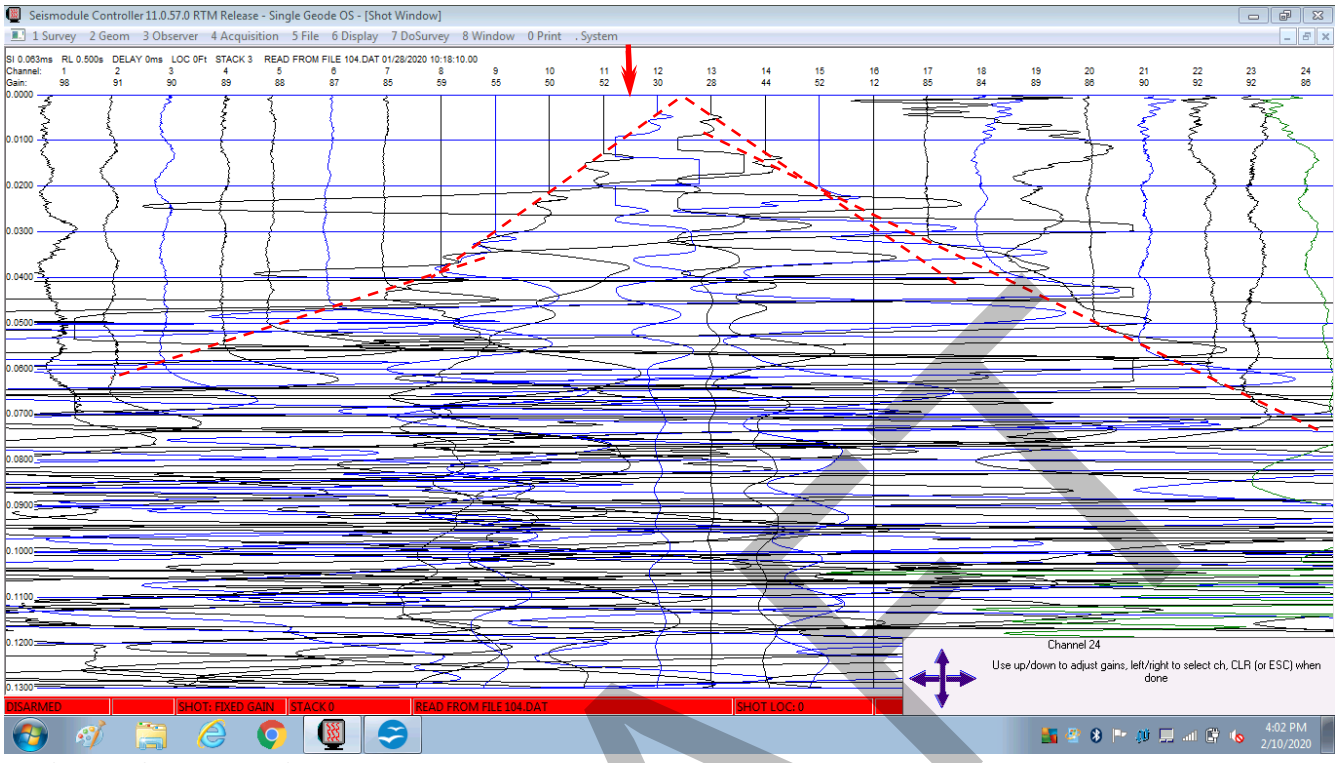

Surficial infill bridges fissure so that traces are well developed in both directions.

Line 1 – shotpoint 6

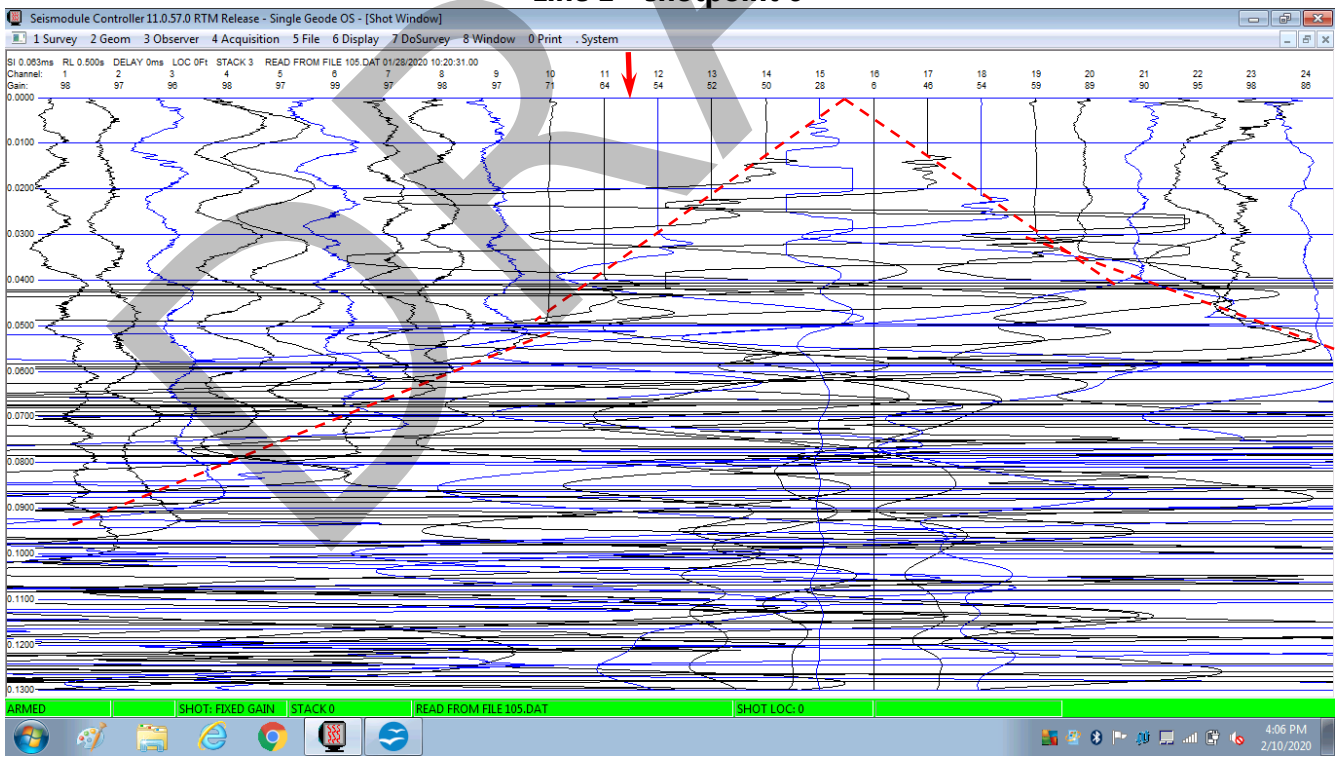

Significant attenuation at geophones 1-9 before fissure as shotpoint moves past fissure.

Line 1 – shotpoint 7

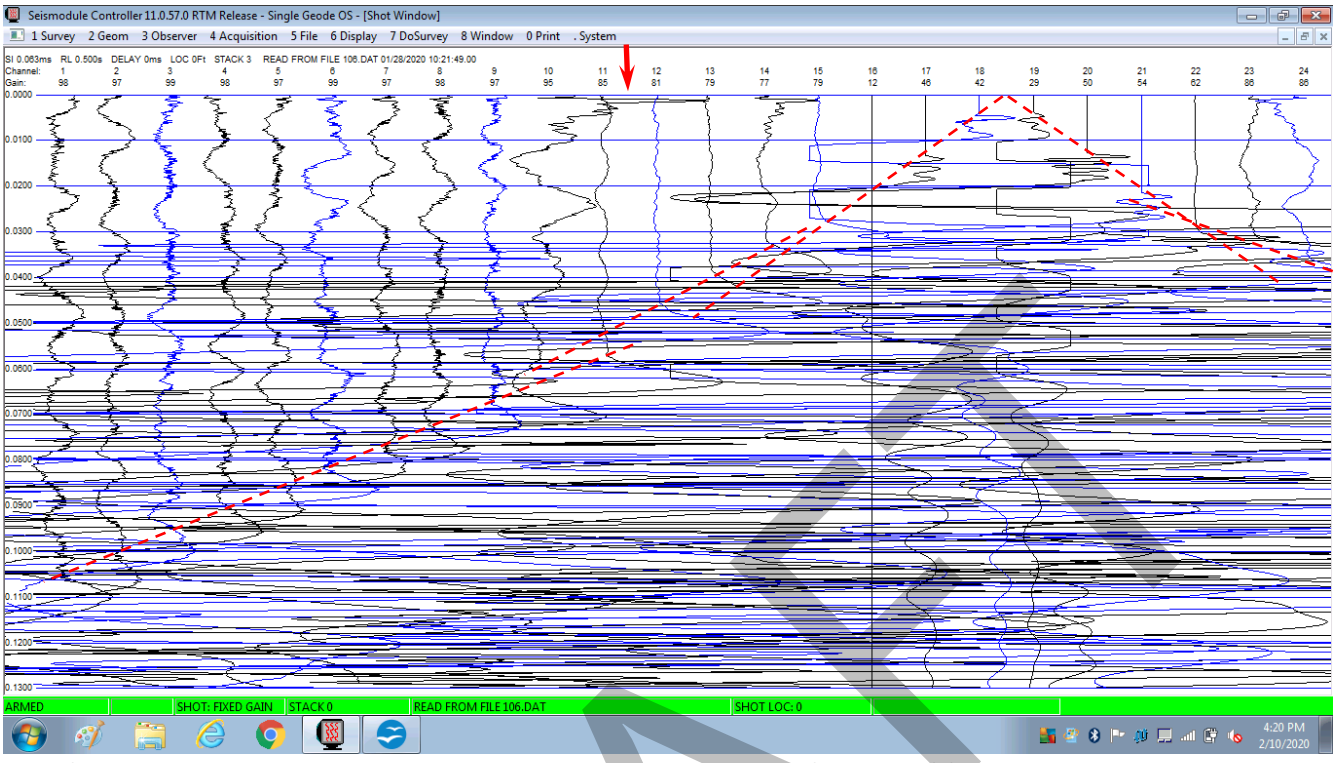

Significant attenuation and some time delay at geophones on far side of fissure.

Line 1 – shotpoint 8

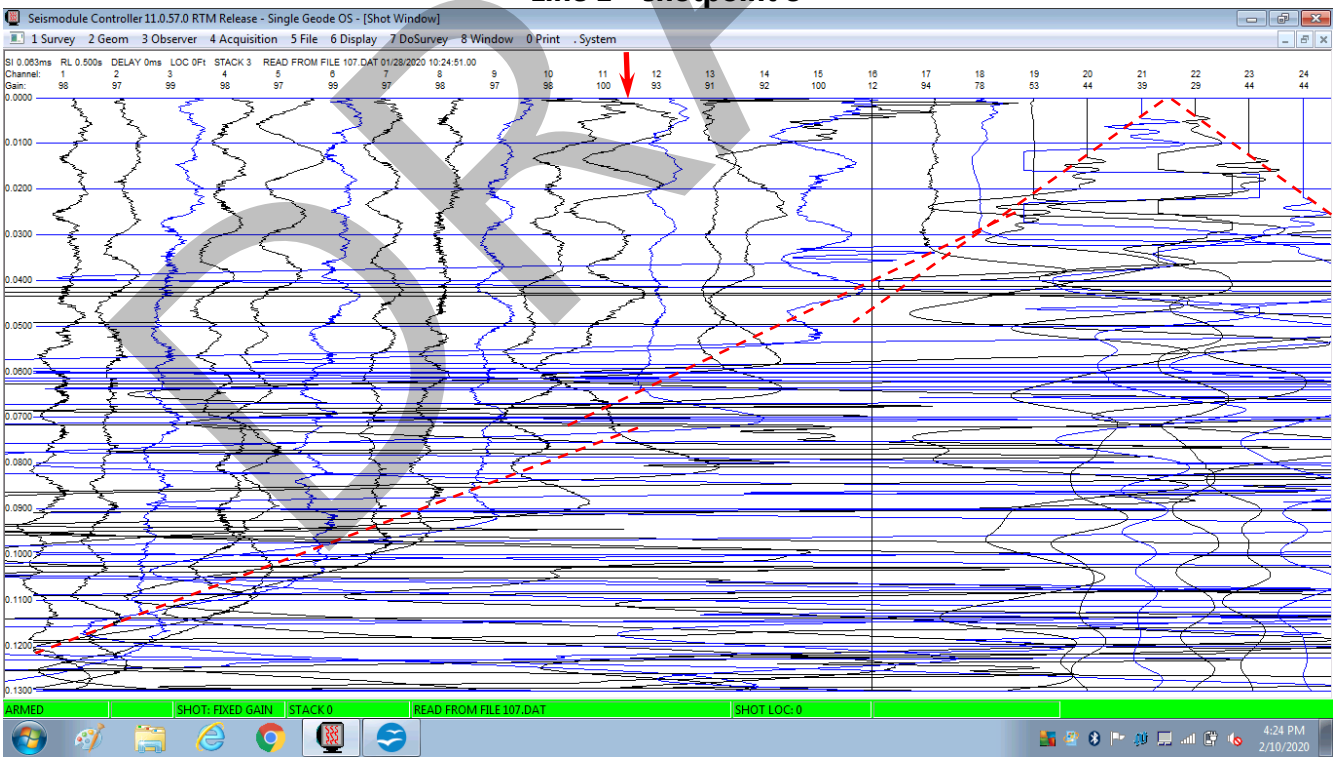

General attenuation is obscuring possible fissure signatures.

Line 1 – shotpoint 9

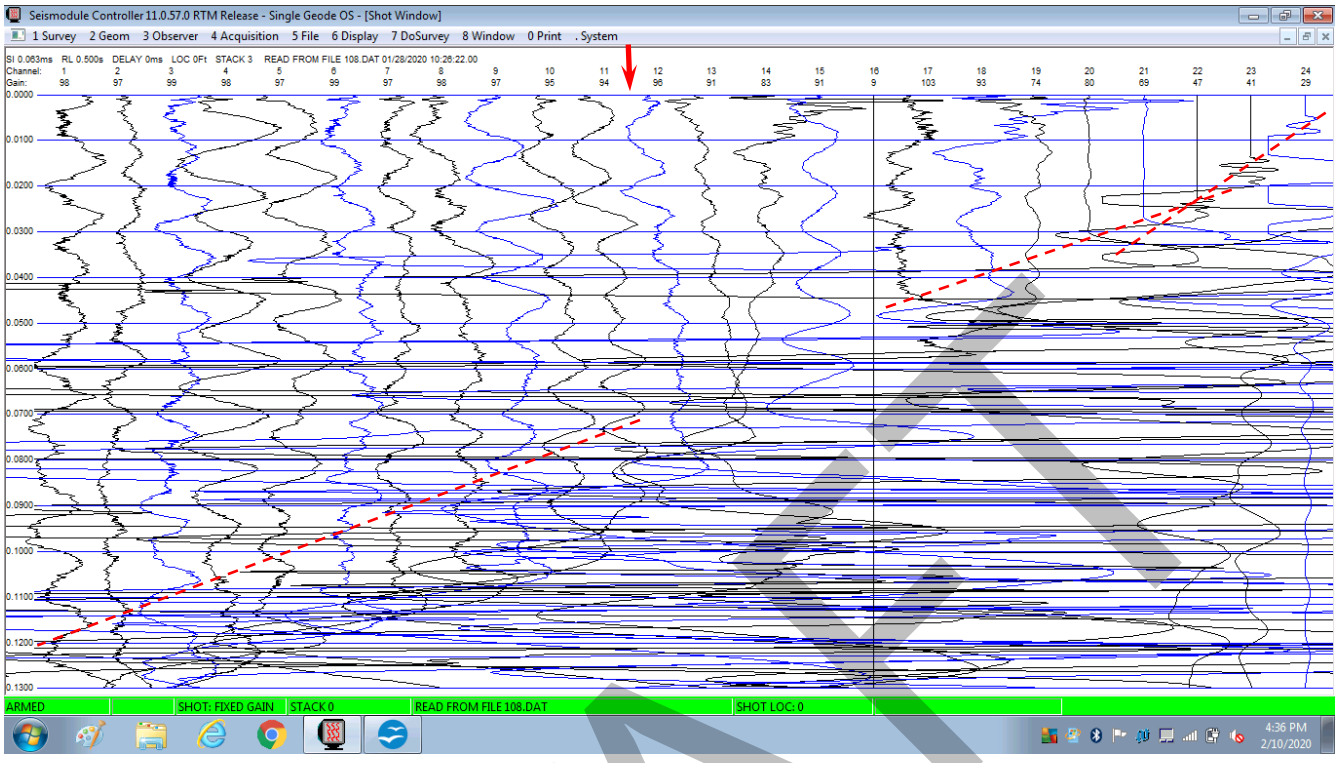

General attenuation is obscuring possible fissure signatures.

Line 2 – shotpoint 1

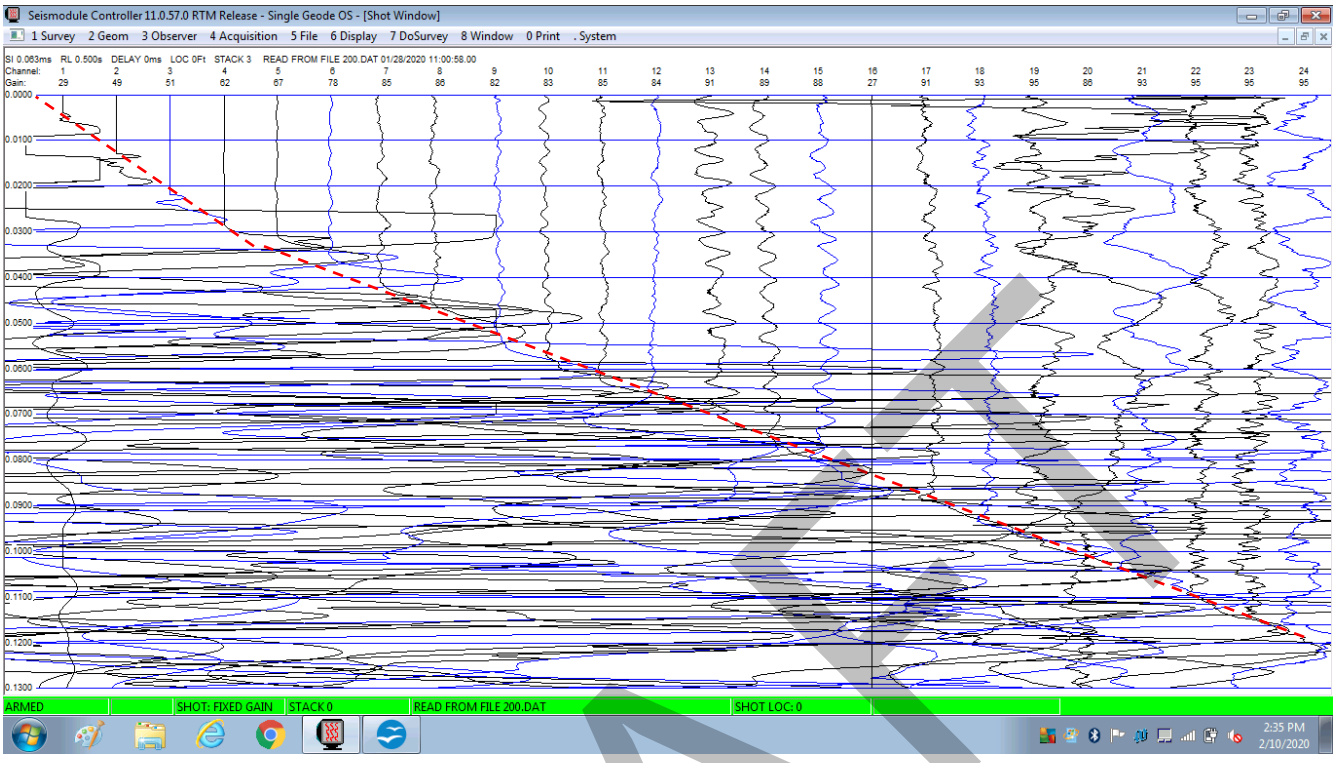

No anomaly is apparent.

Line 2 – shotpoint 2

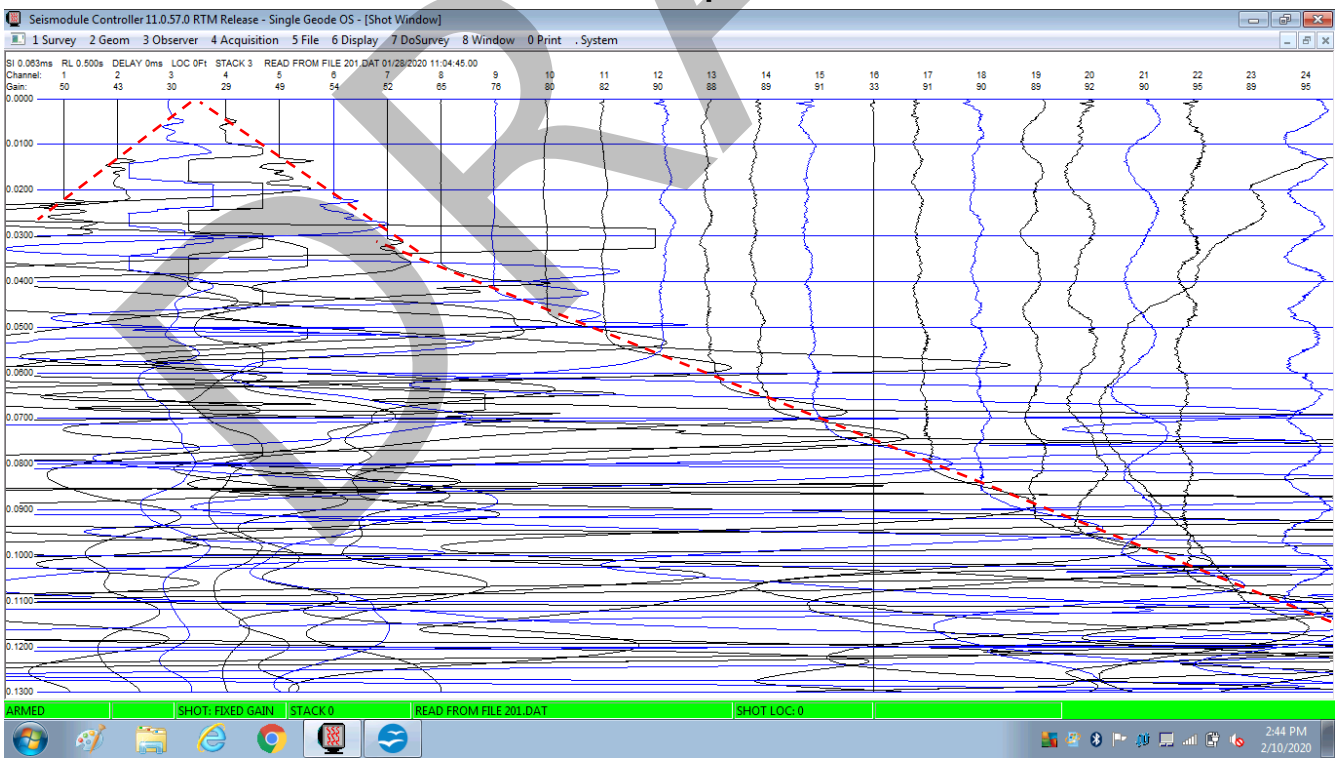

No anomaly apparent

Line 2 – shotpoint 3

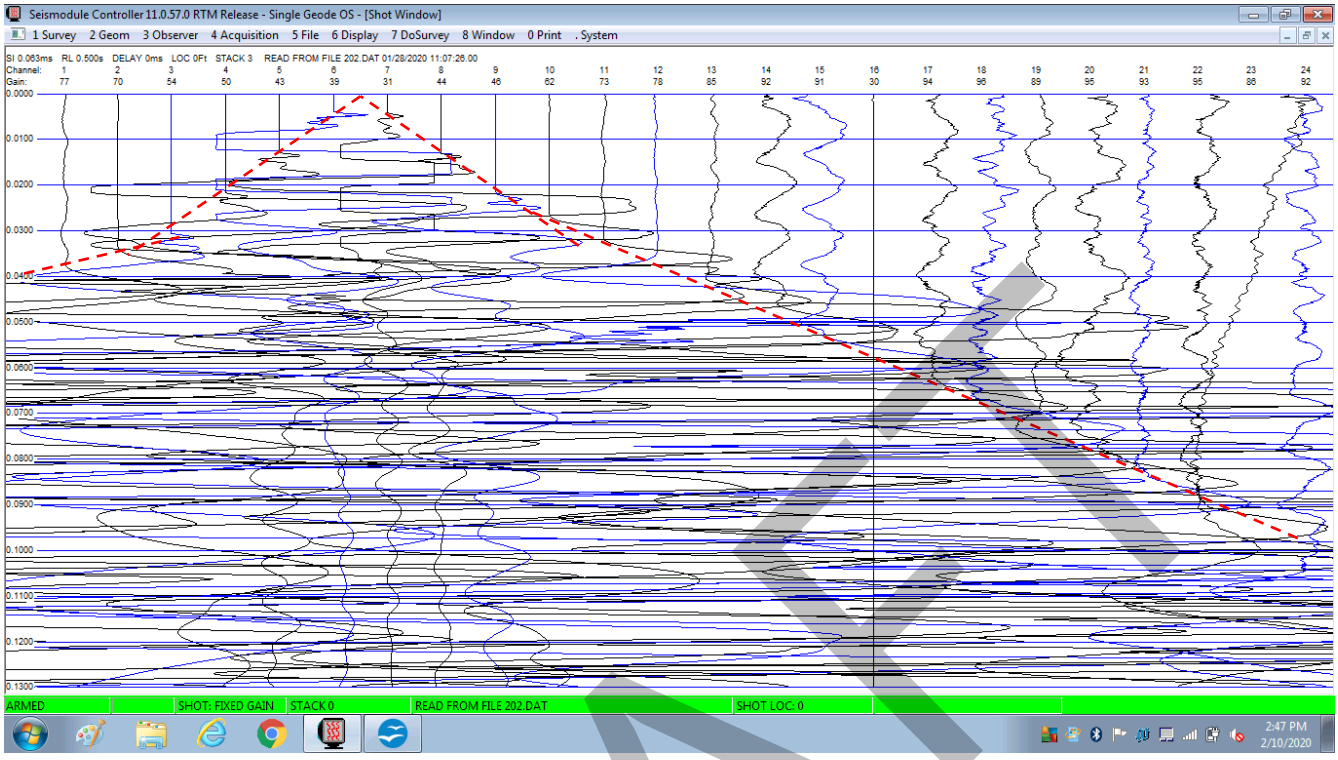

No anomaly apparent.

Line 2 – shotpoint 4

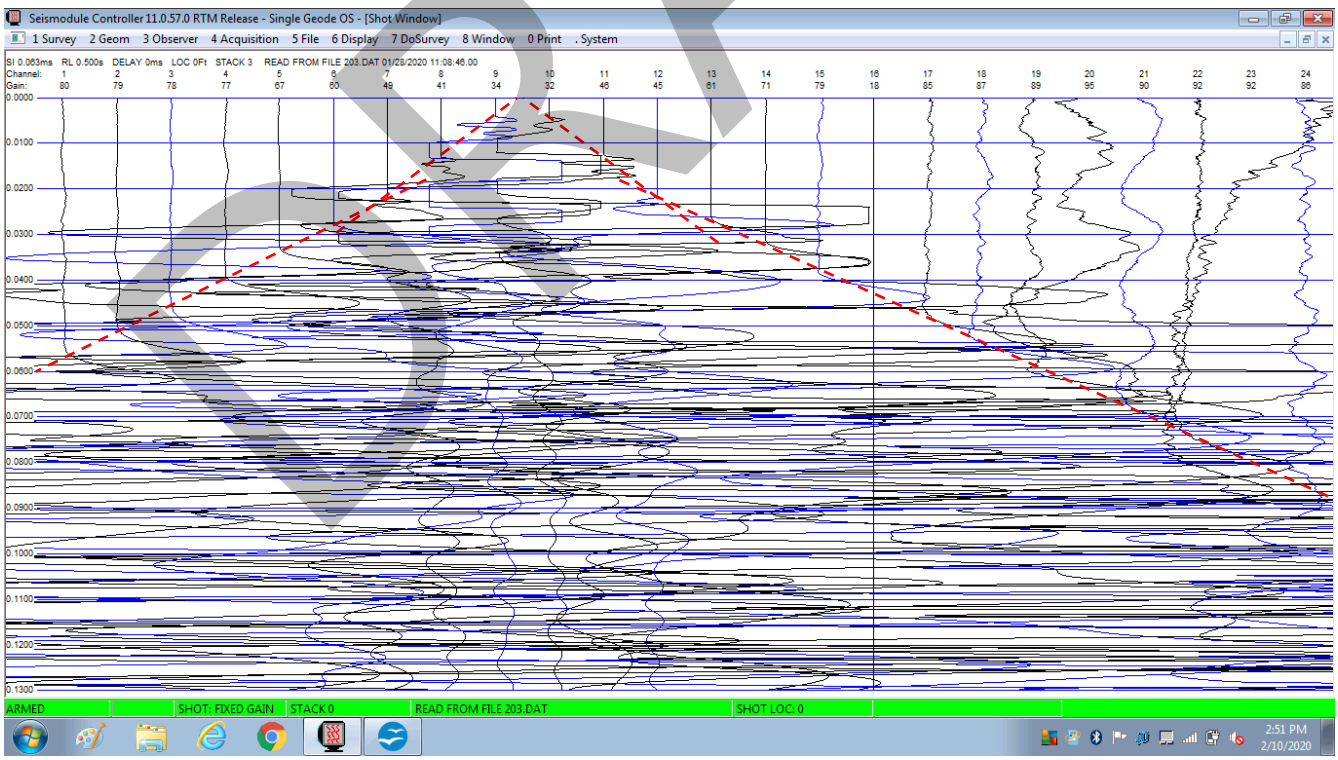

No anomaly apparent

Line 2 – shotpoint 5

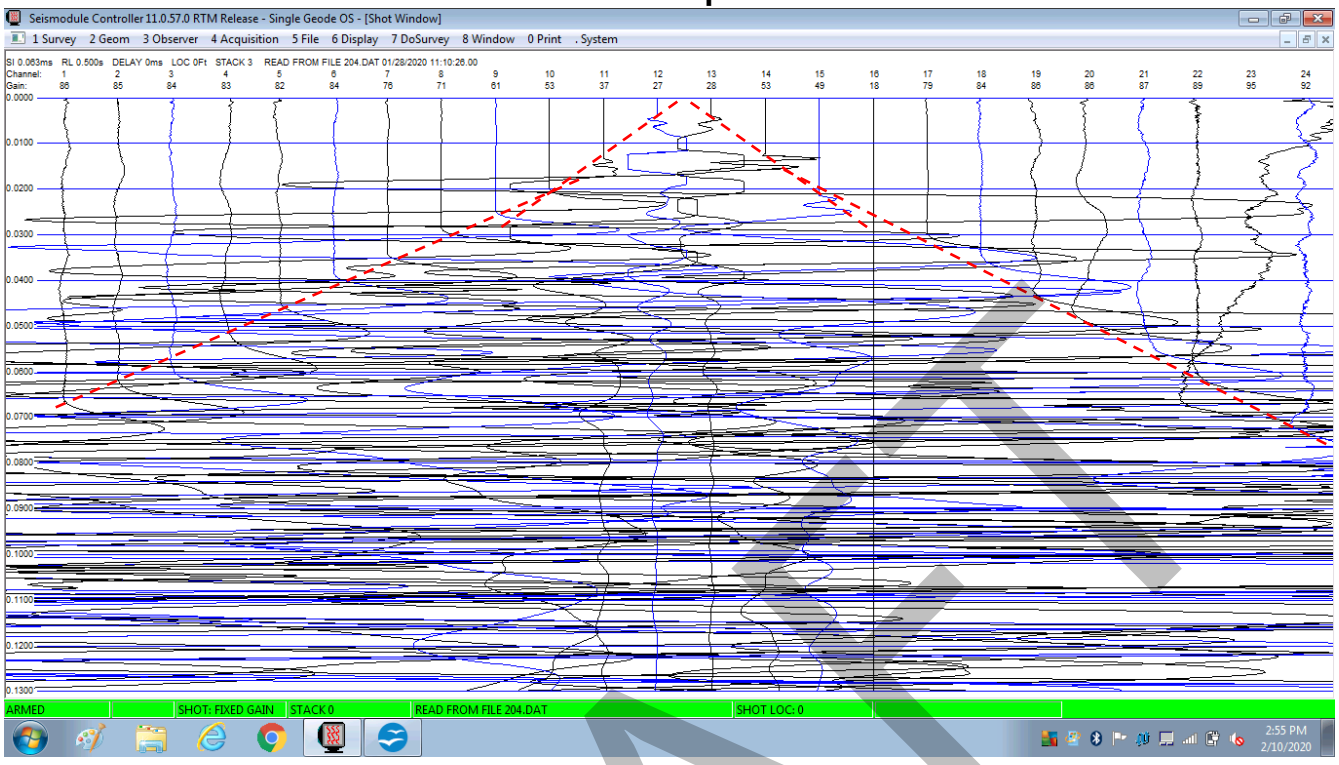

No anomaly apparent

Line 2 – shotpoint 6

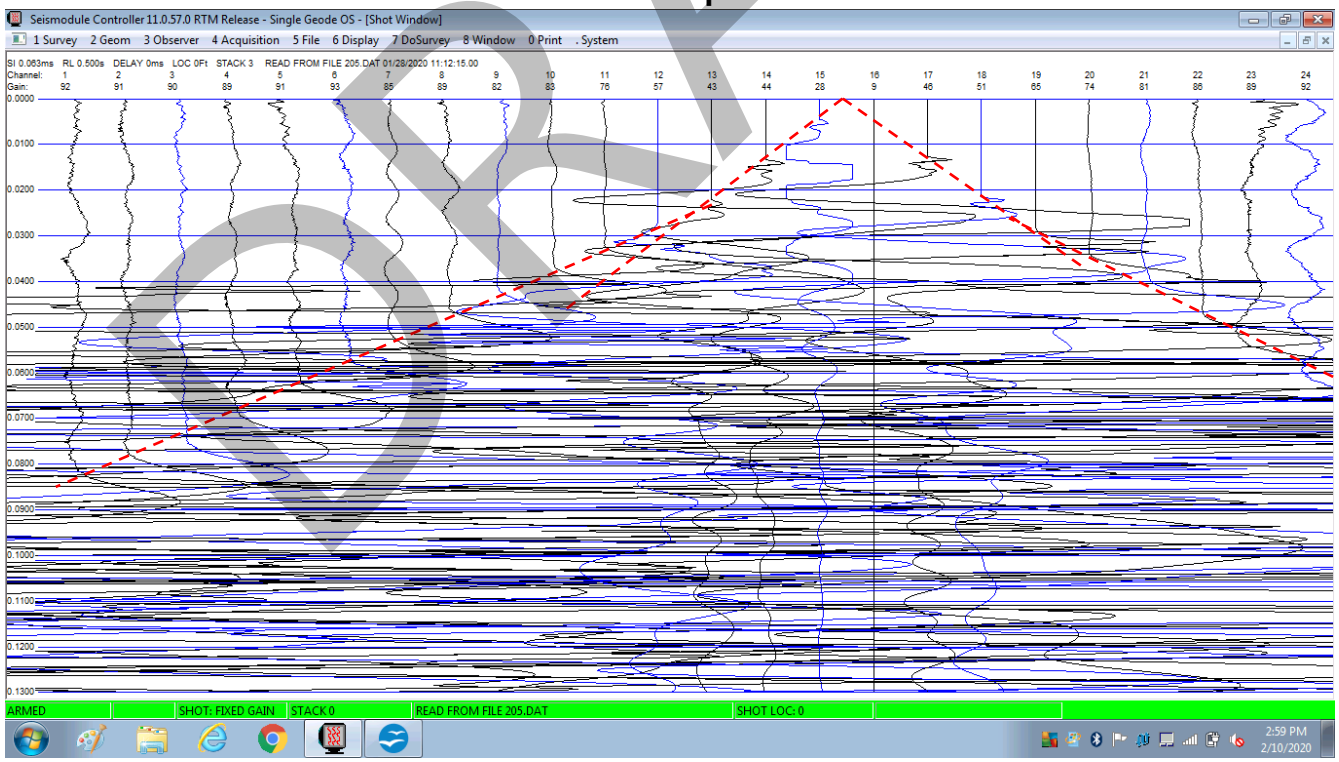

No anomaly apparent

Line 2 – shotpoint 7

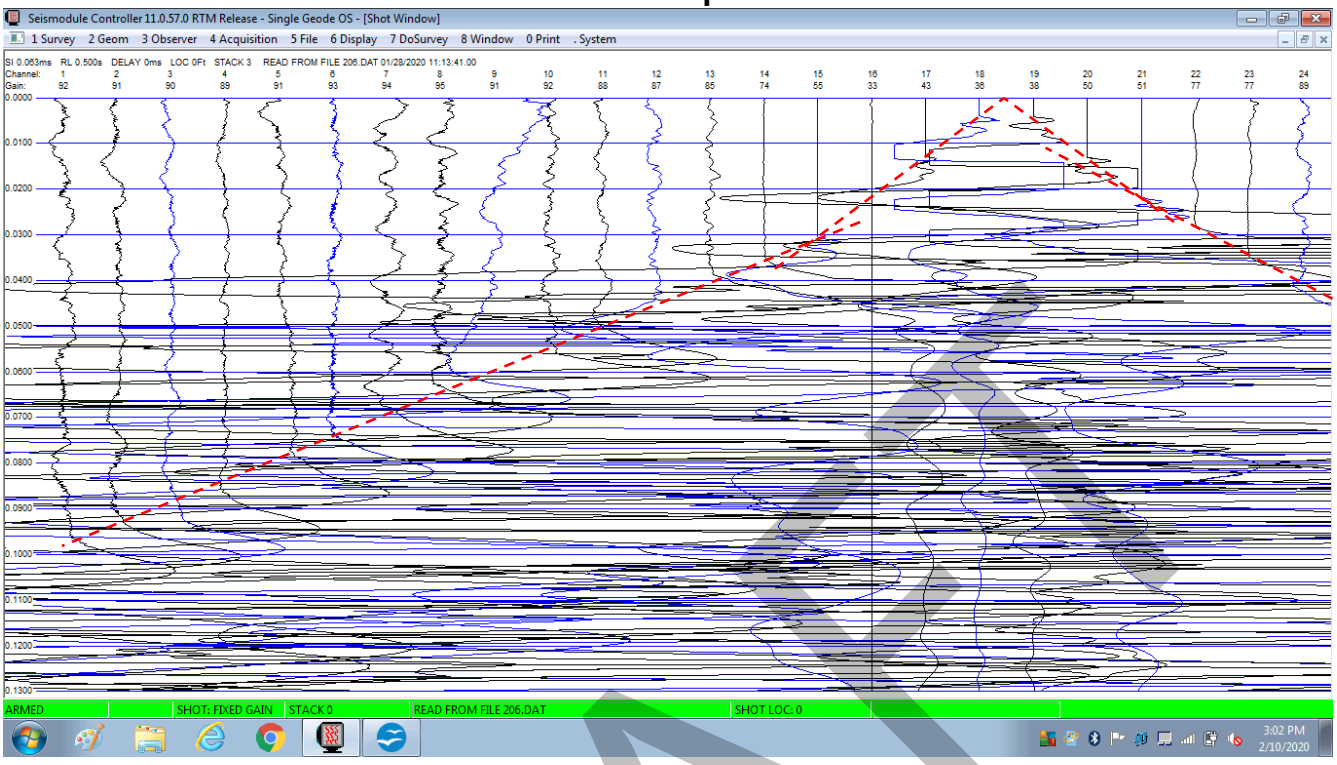

No anomaly apparent

Line 2 – shotpoint 8

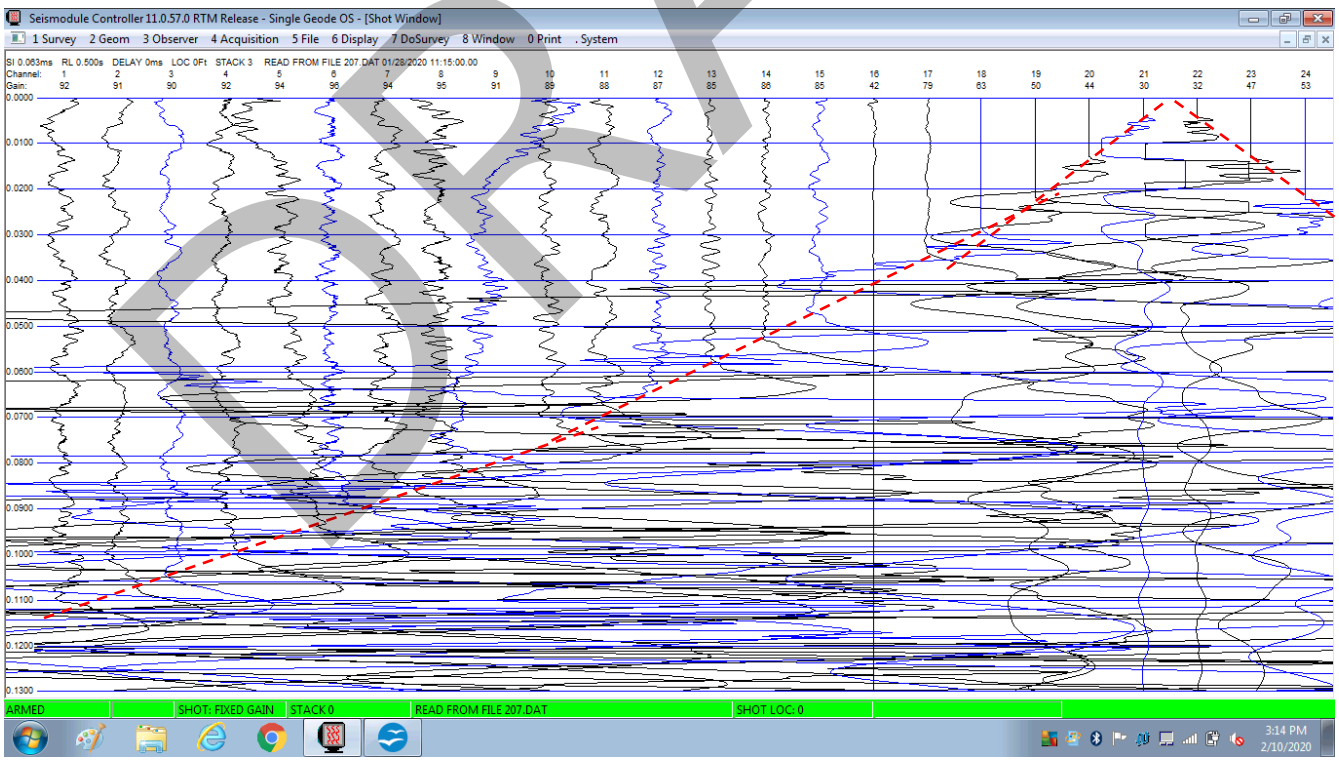

No anomaly apparent

Line 2 – shotpoint 9

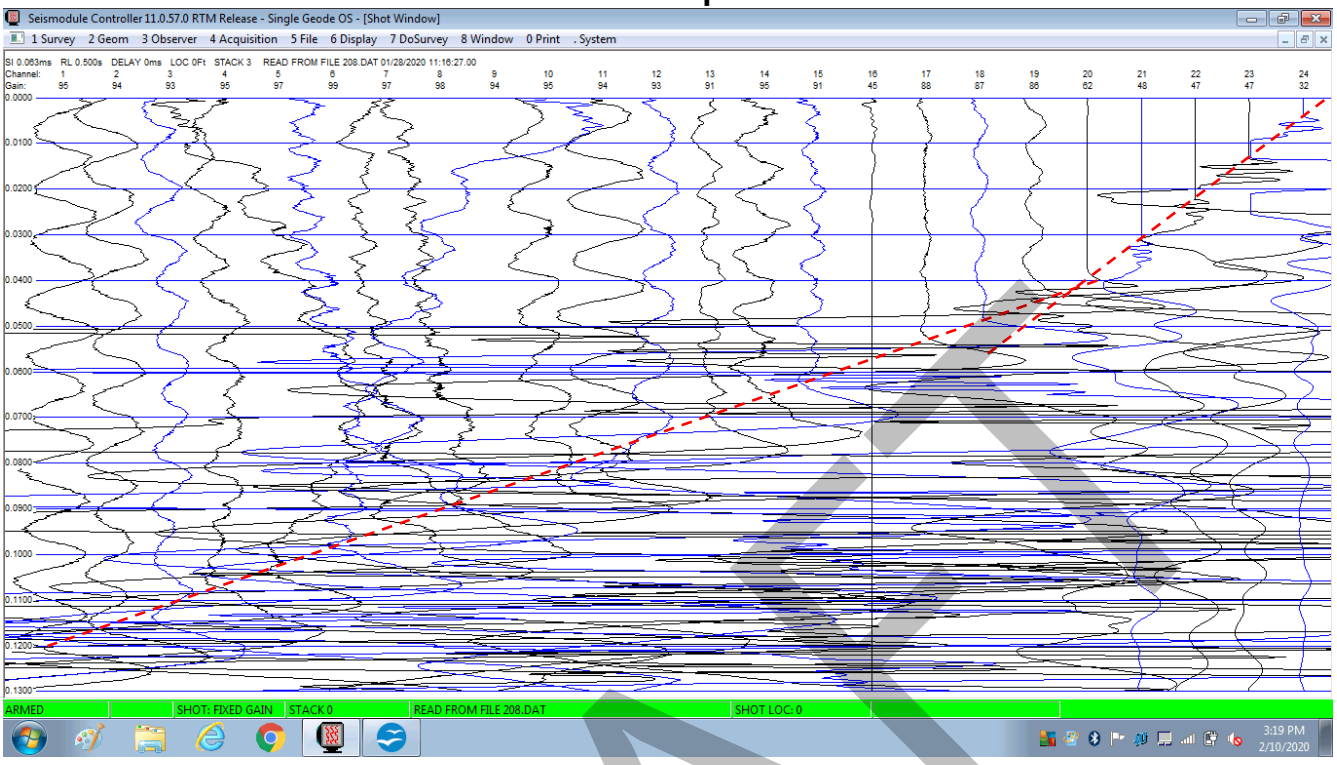

No anomaly apparent

Line 3 – shotpoint 1

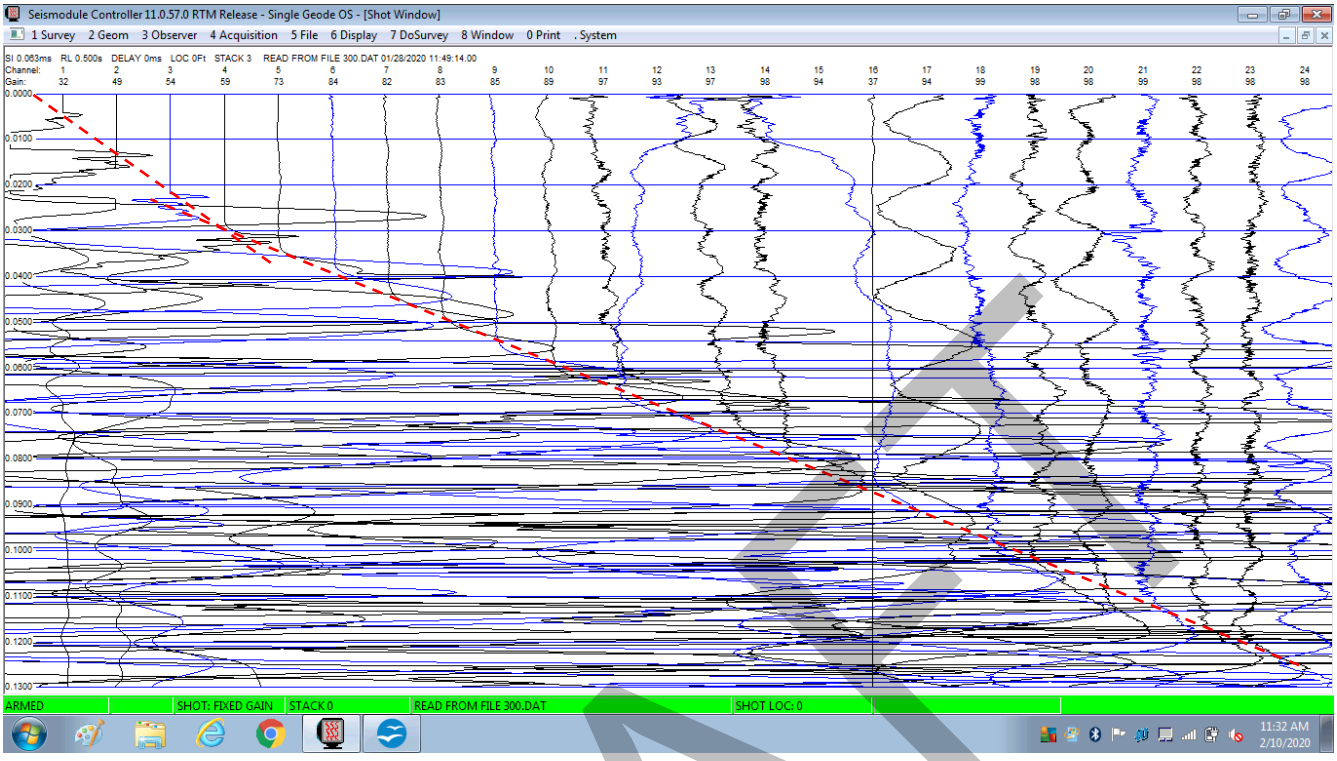

No anomaly apparent

Line 3 – shotpoint 2

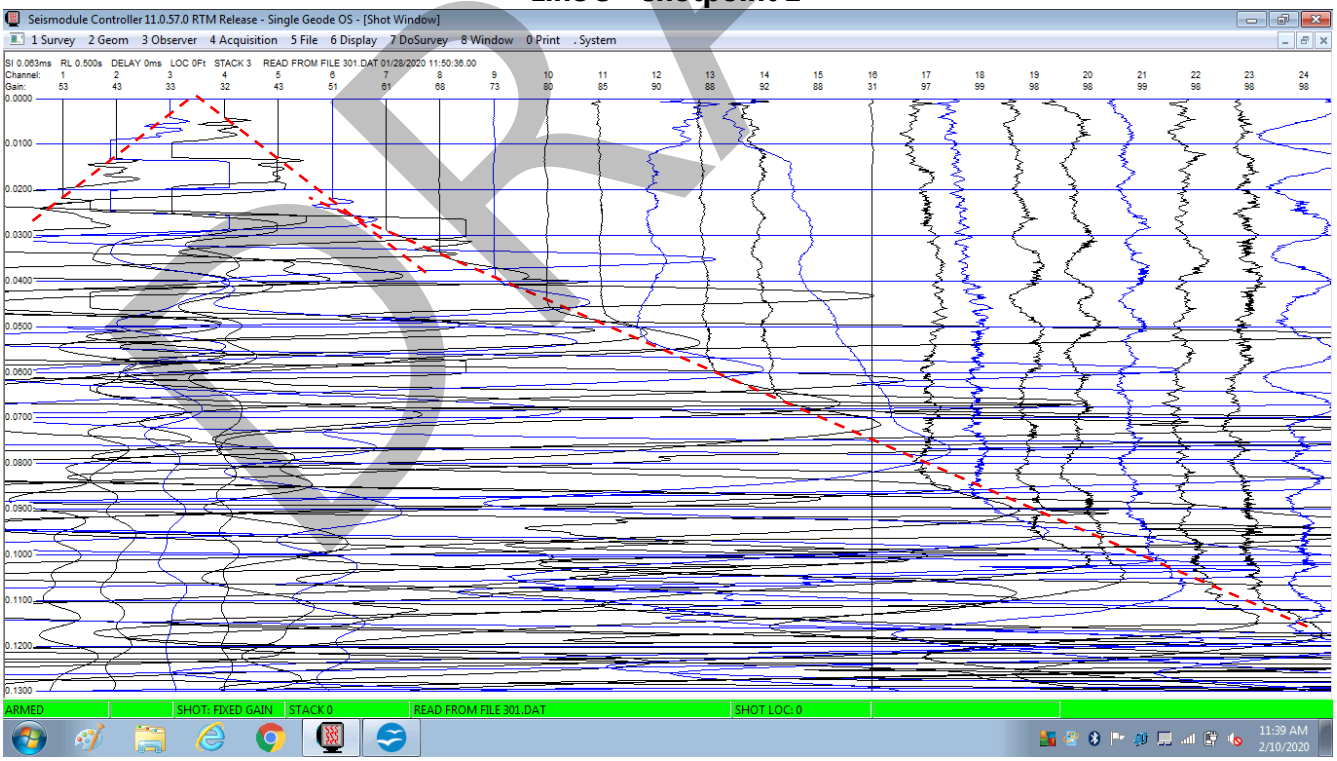

No anomaly apparent

Line 3 – shotpoint 3

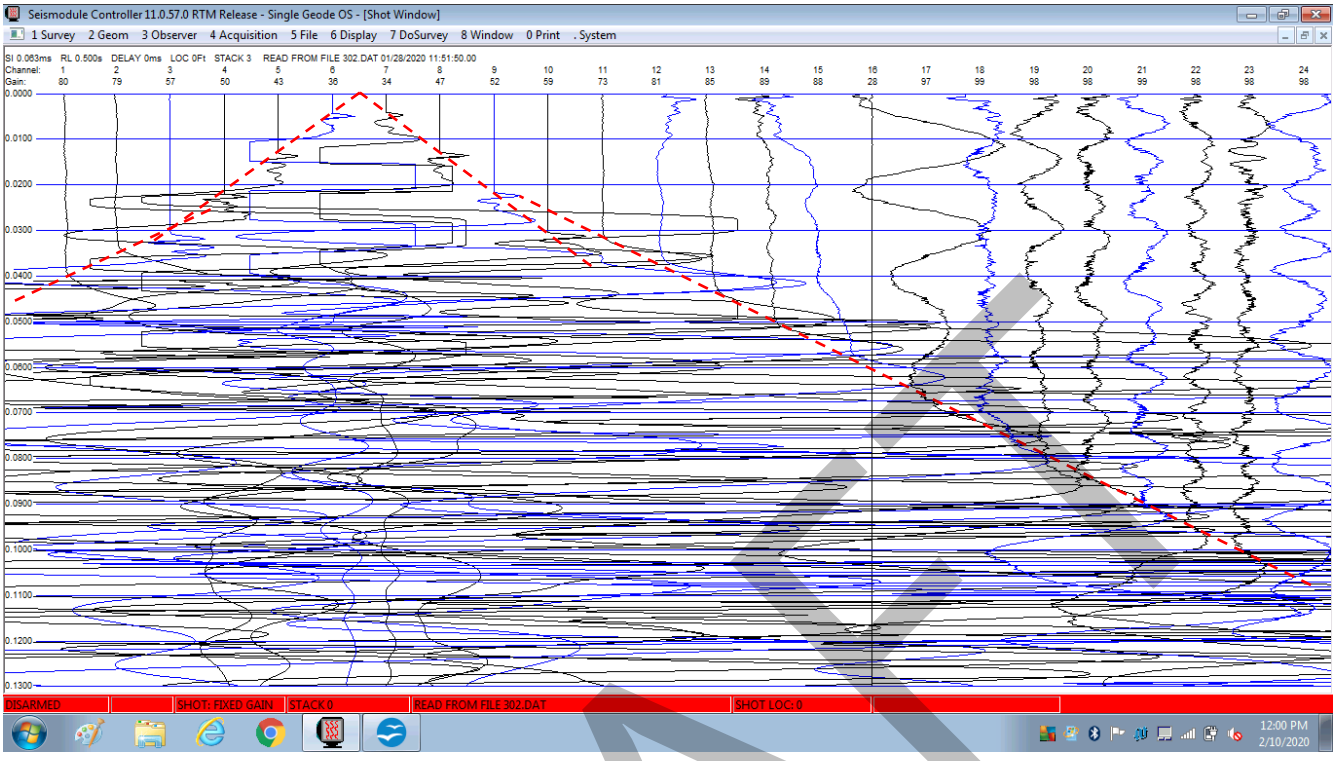

No anomaly apparent

Line 3 – shotpoint 4

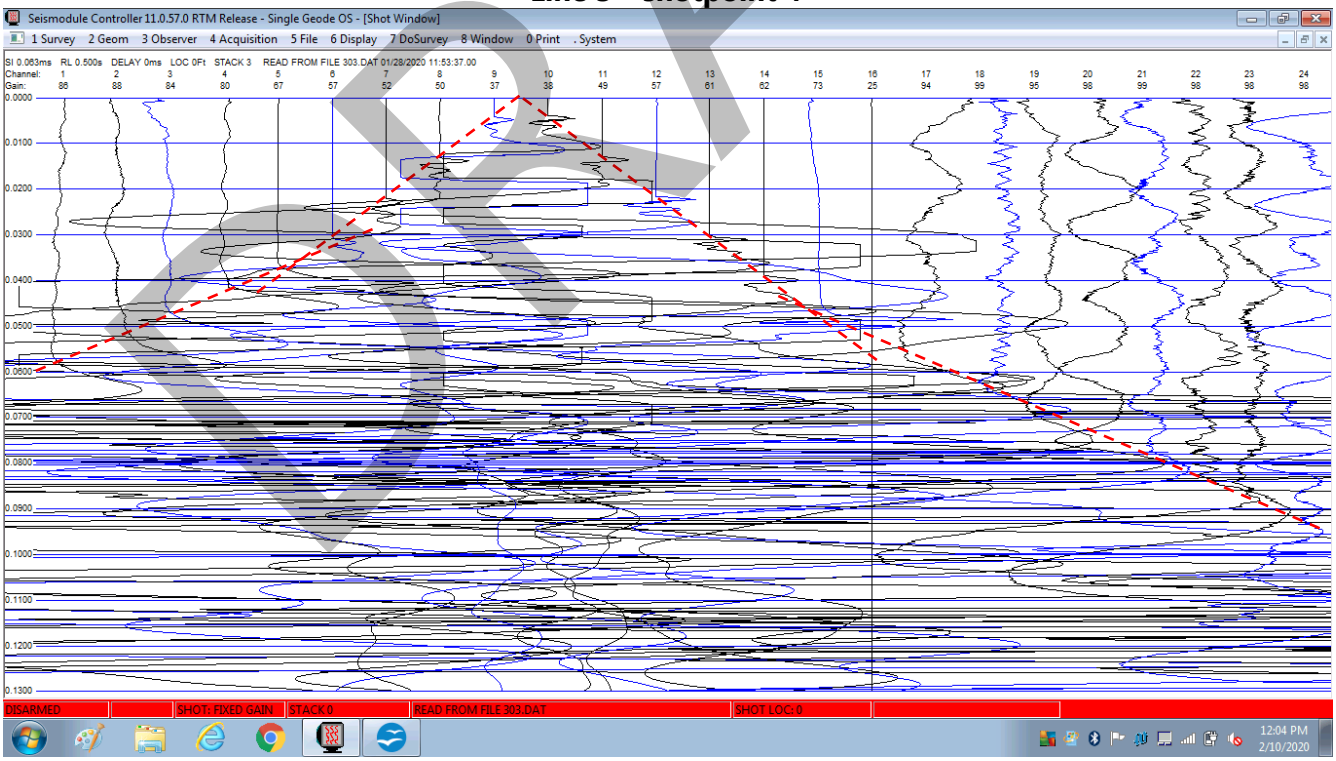

No anomaly apparent

Line 3 – shotpoint 5

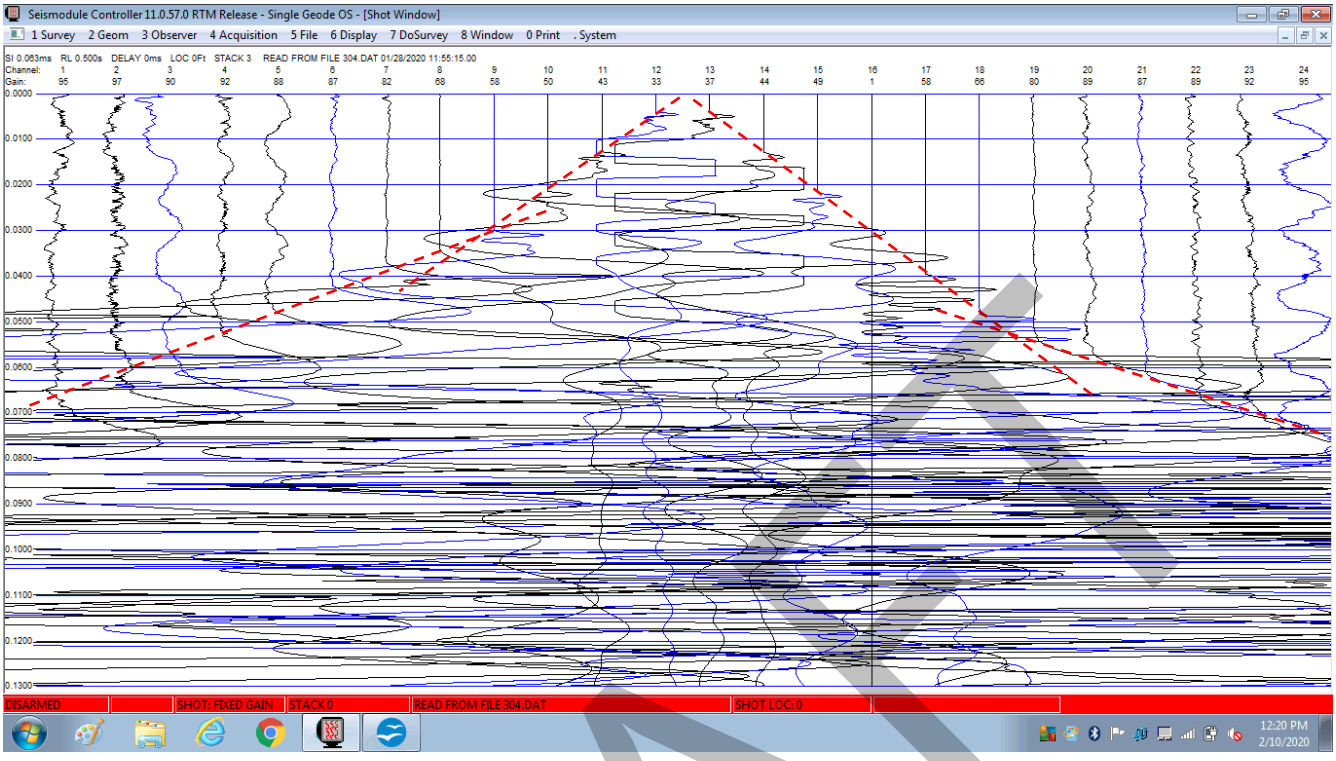

No anomaly apparent

Line 3 – shotpoint 6

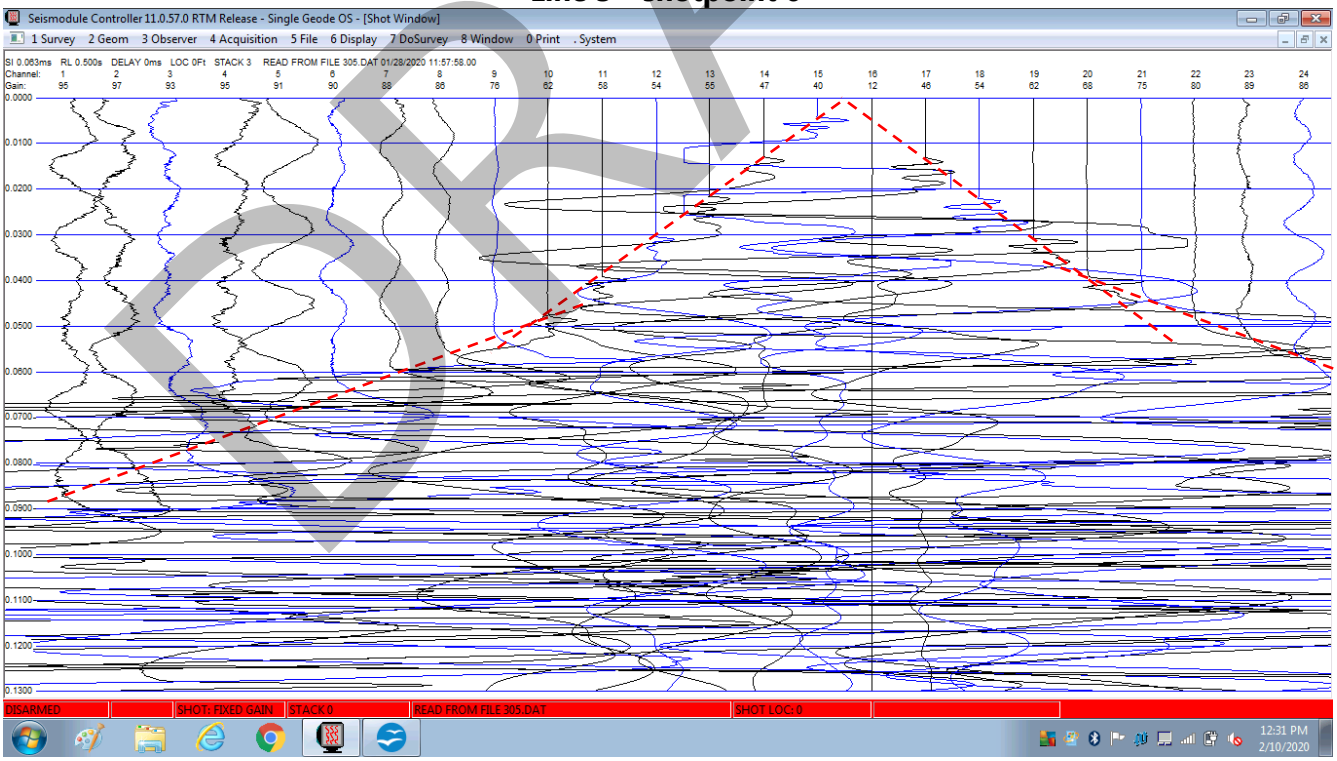

No anomaly apparent

Line 3 – shotpoint 7

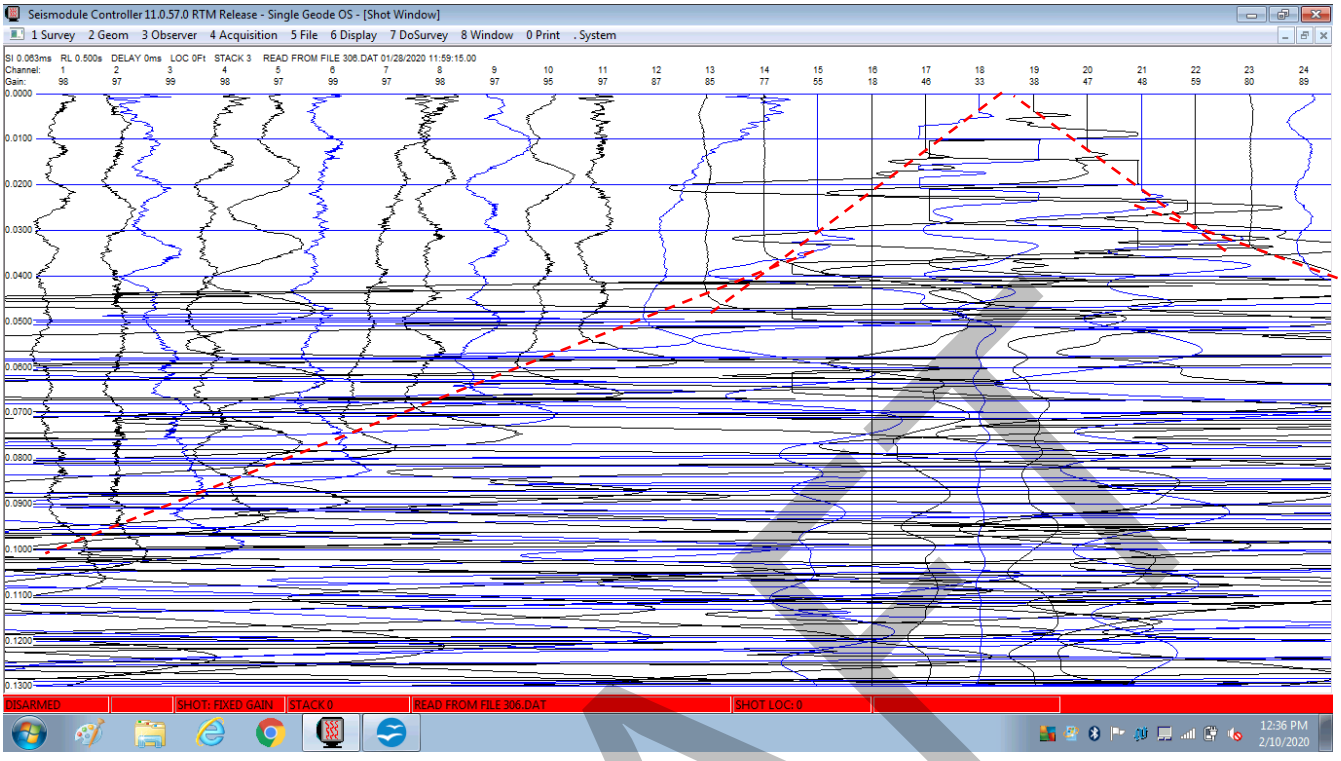

No anomaly apparent

Line 3 – shotpoint 8

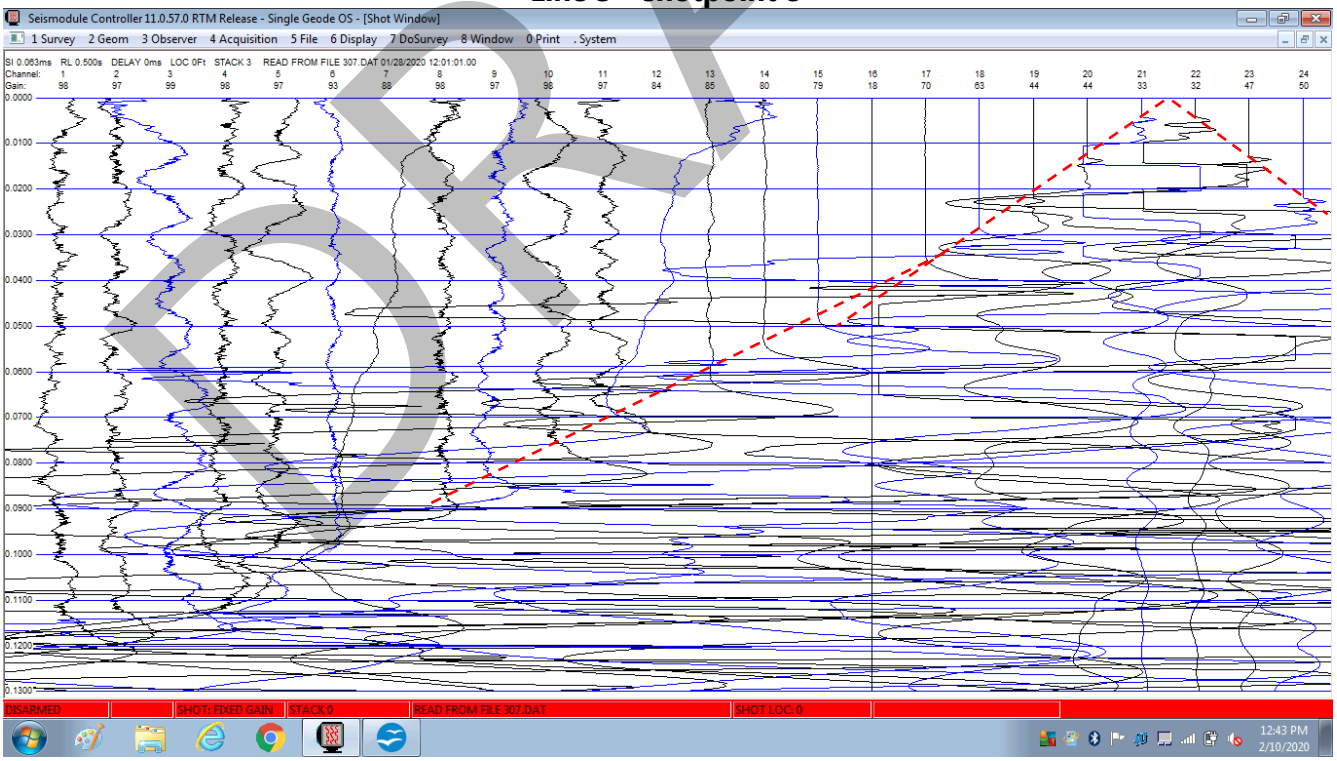

No anomaly apparent

Line 3 – shotpoint 9

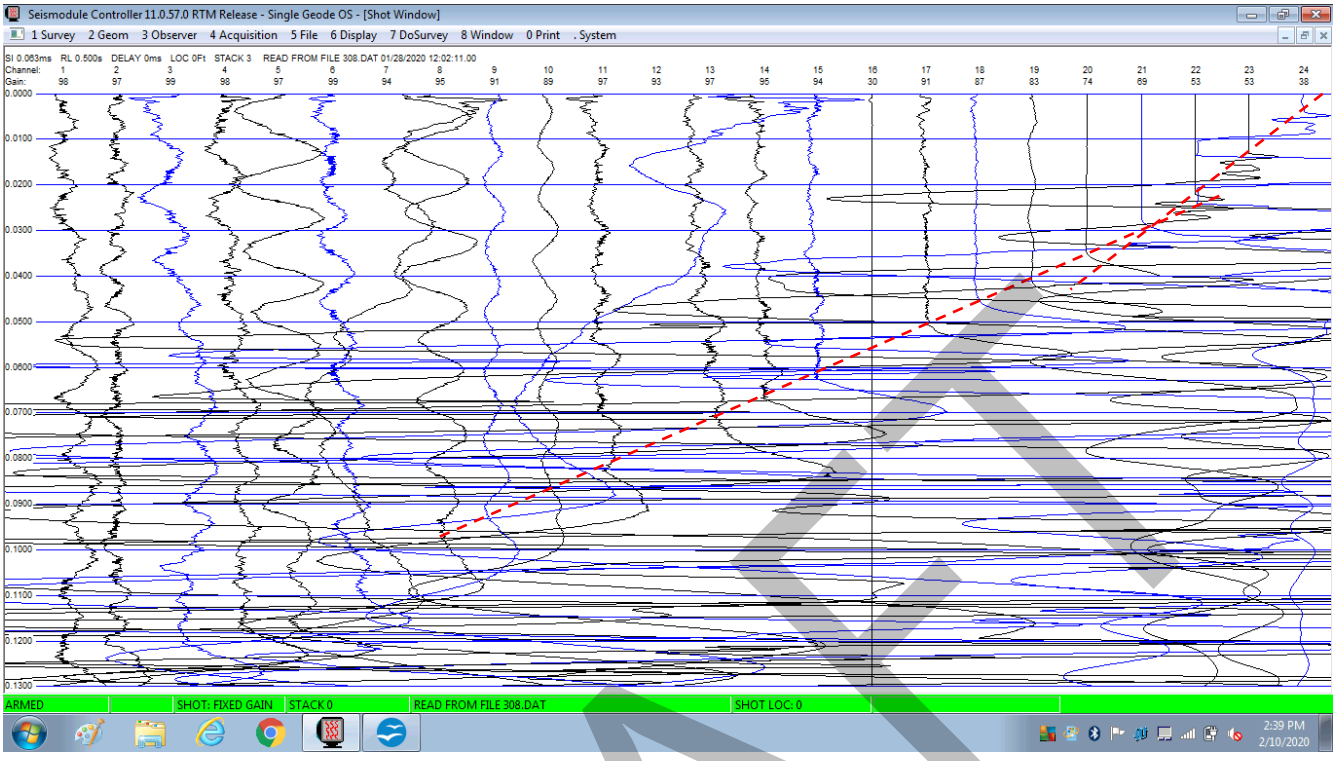

No anomaly apparent

Line 4 – shotpoint 1

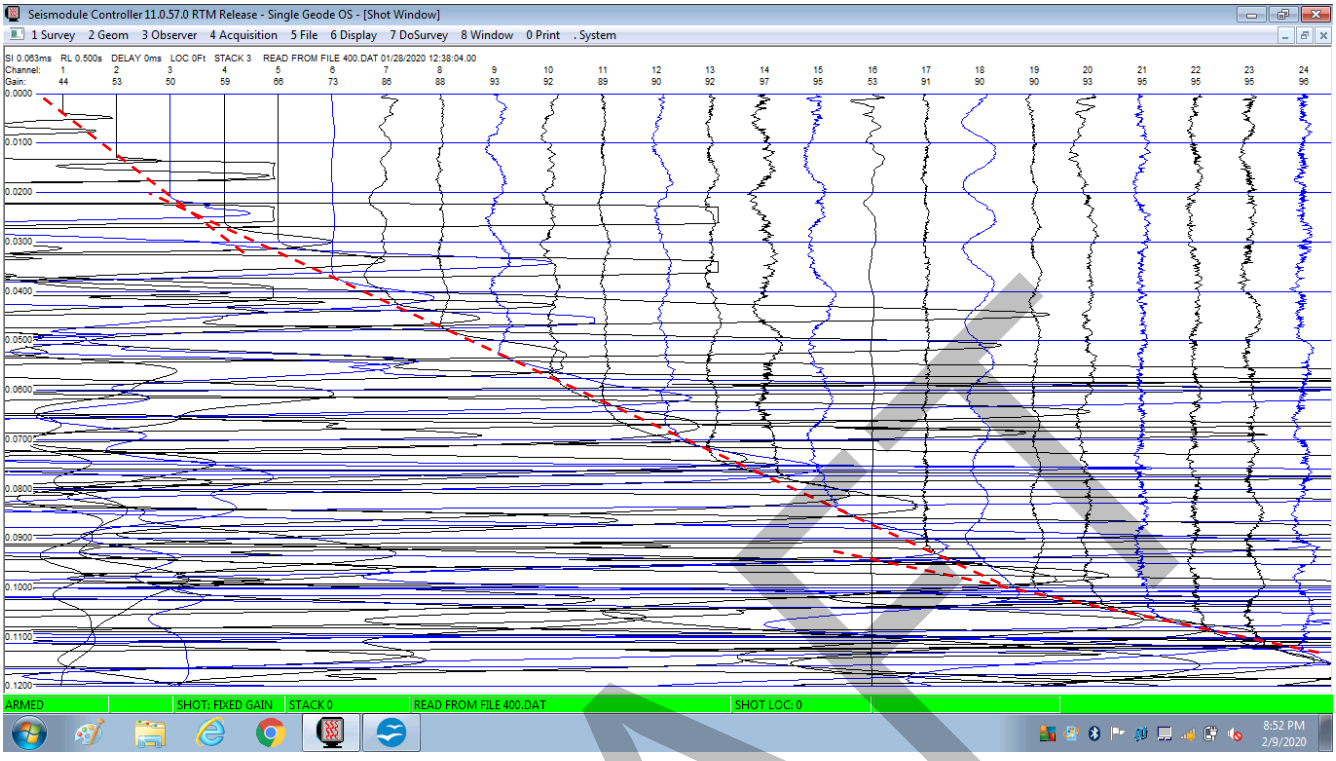

No anomaly apparent

Line 4 – shotpoint 2

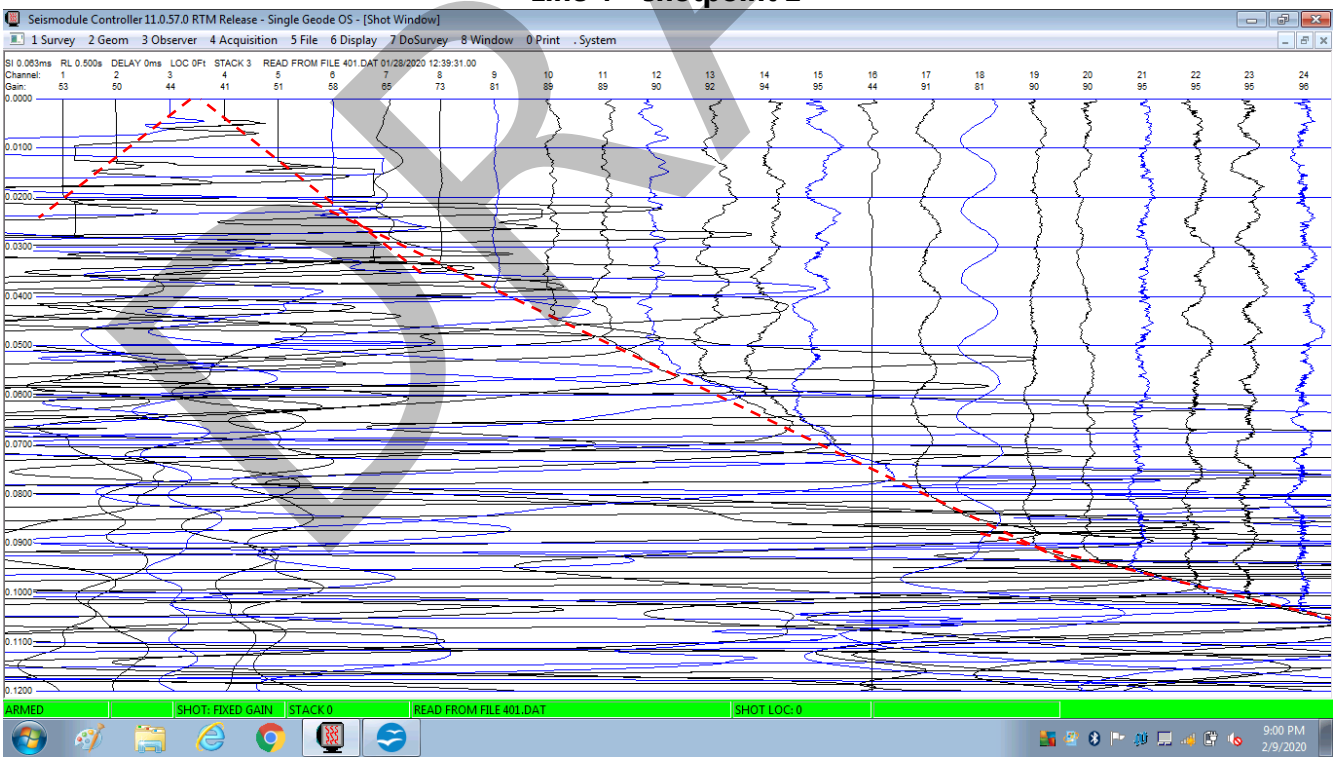

No anomaly apparent

Line 4 – shotpoint 3

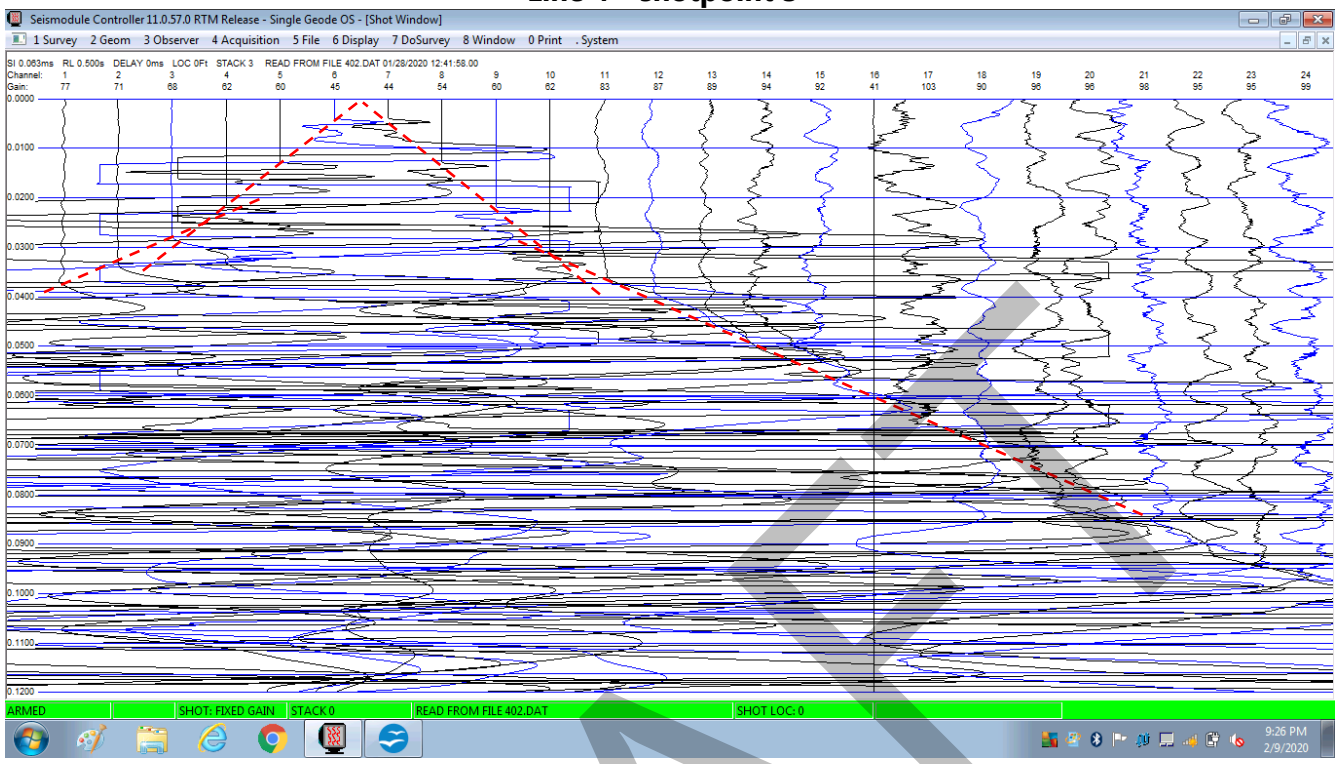

No anomaly apparent; smaller energy source

Line 4 – shotpoint 4

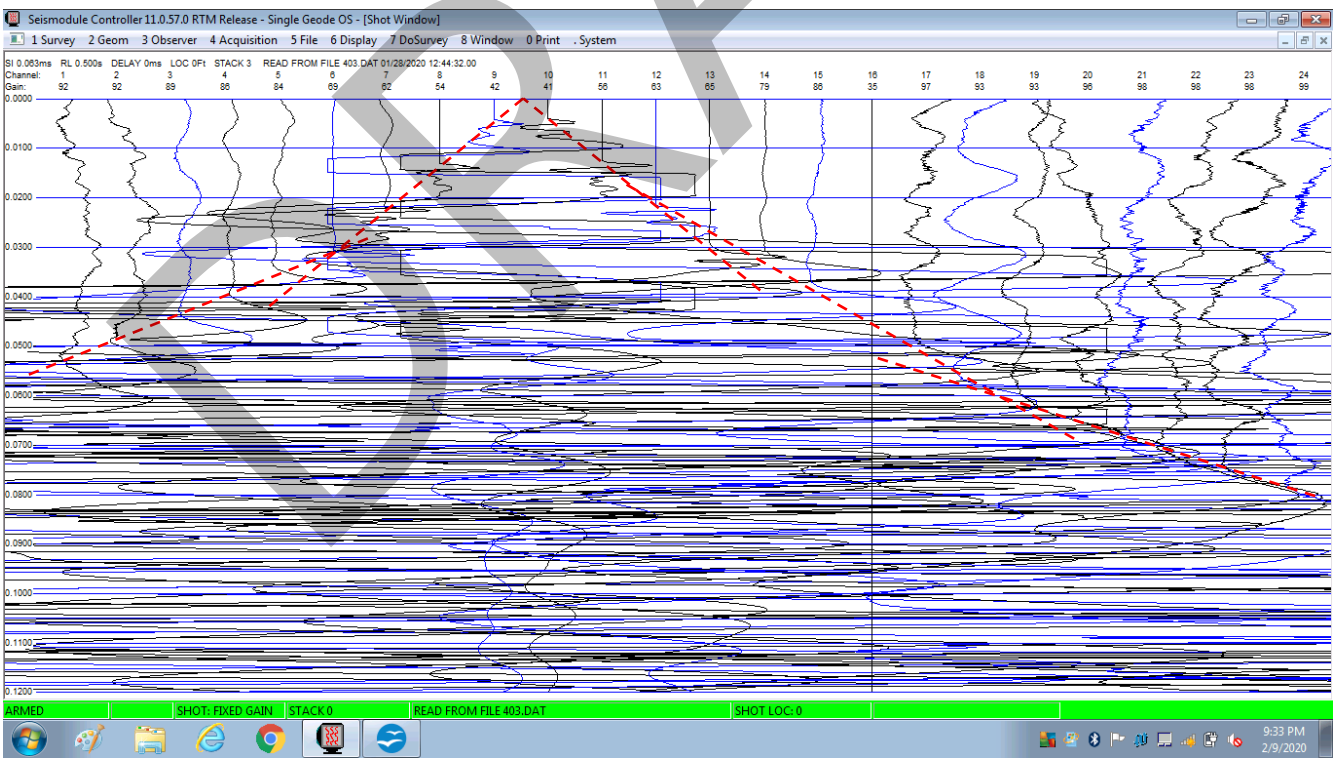

No anomaly apparent

Line 4 – shotpoint 5

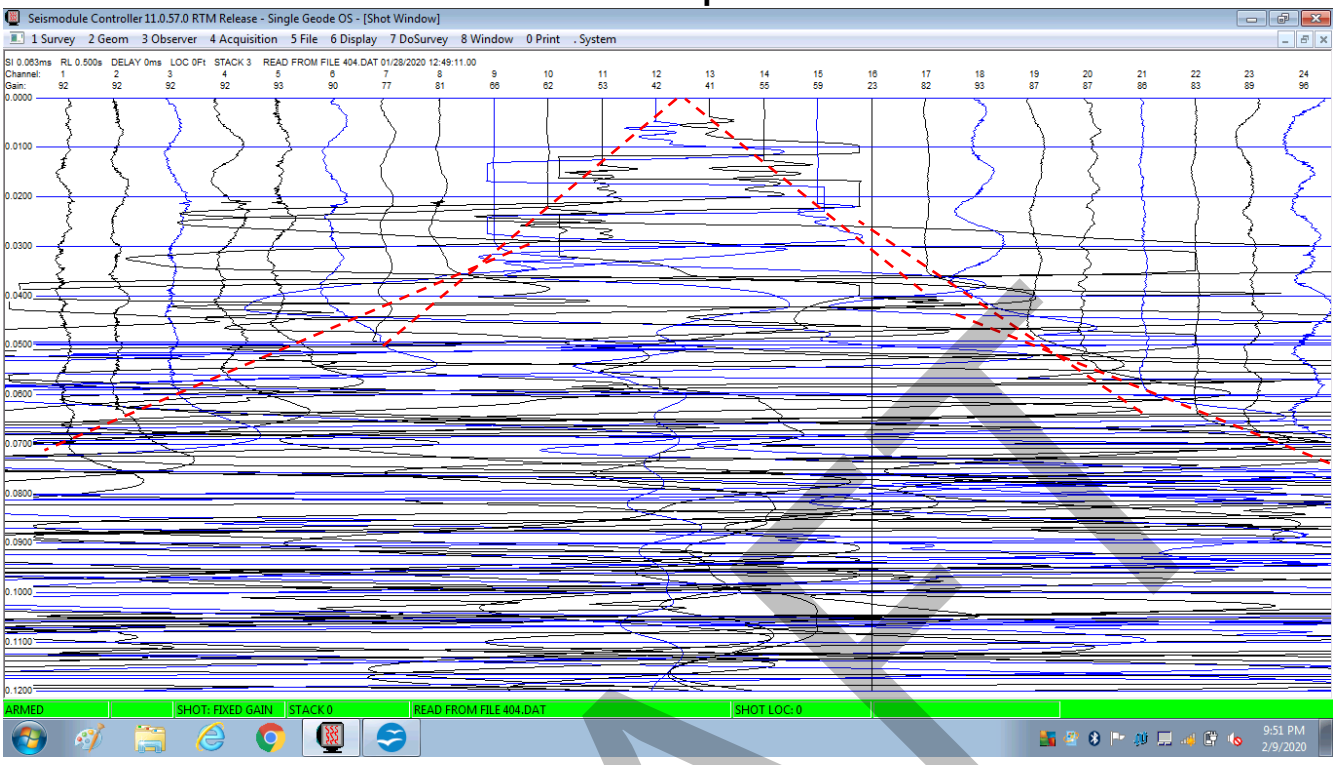

No apparent anomaly

Line 4 – shotpoint 6

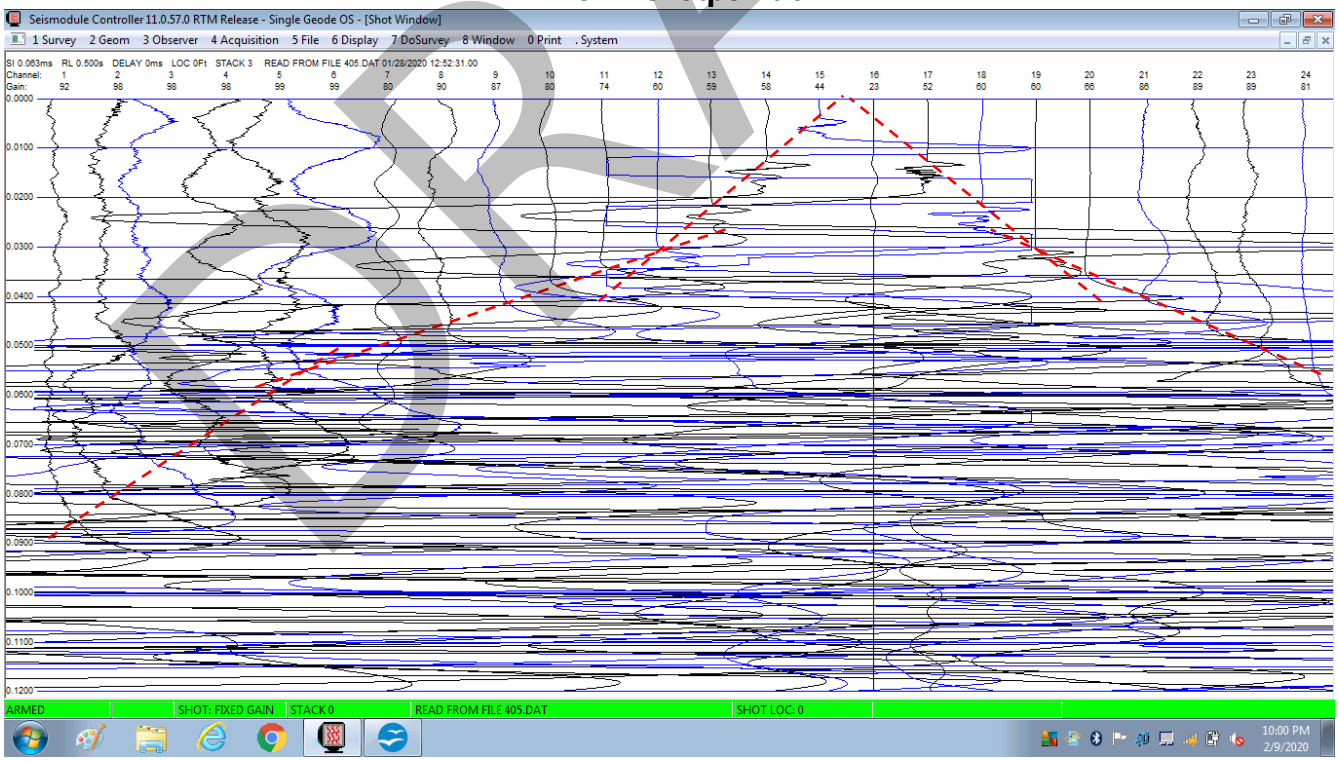

No anomaly apparent

Line 4 – shotpoint 7

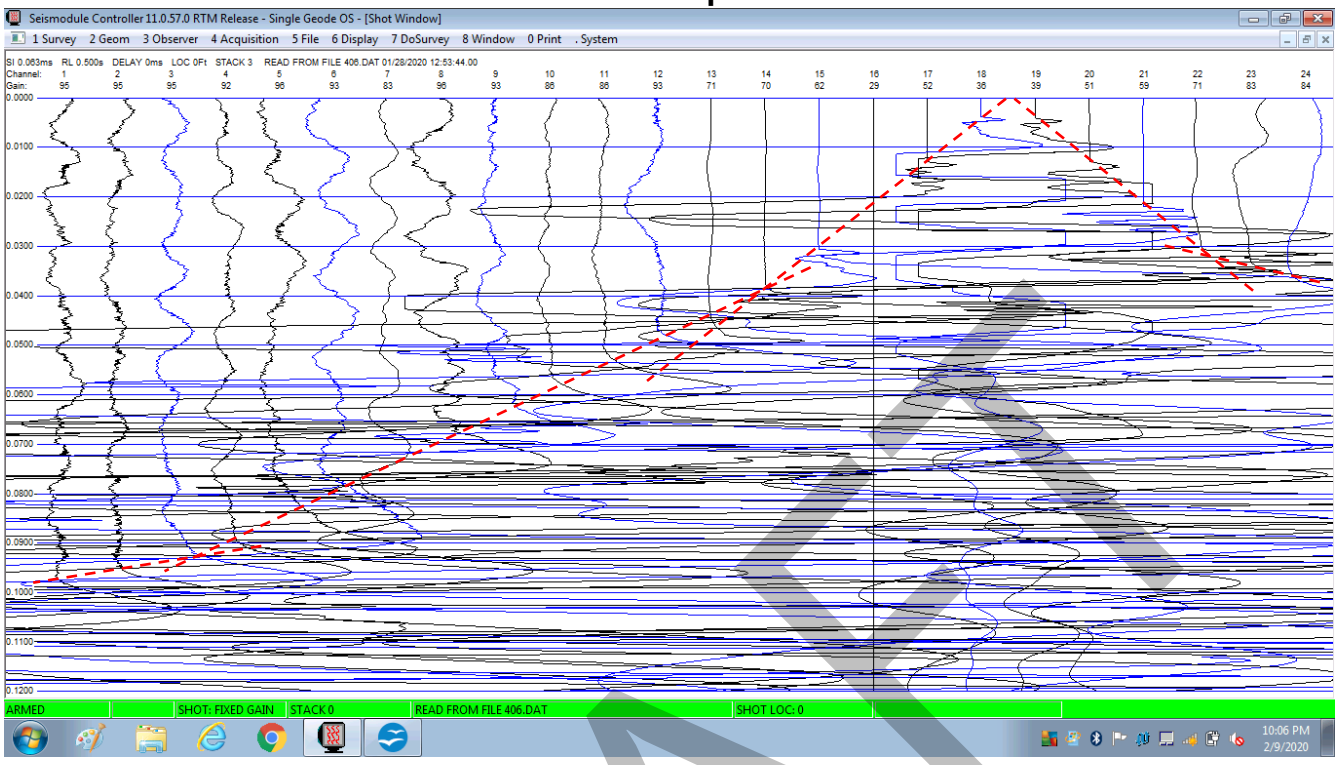

No anomaly apparent

Line 4 – shotpoint 8

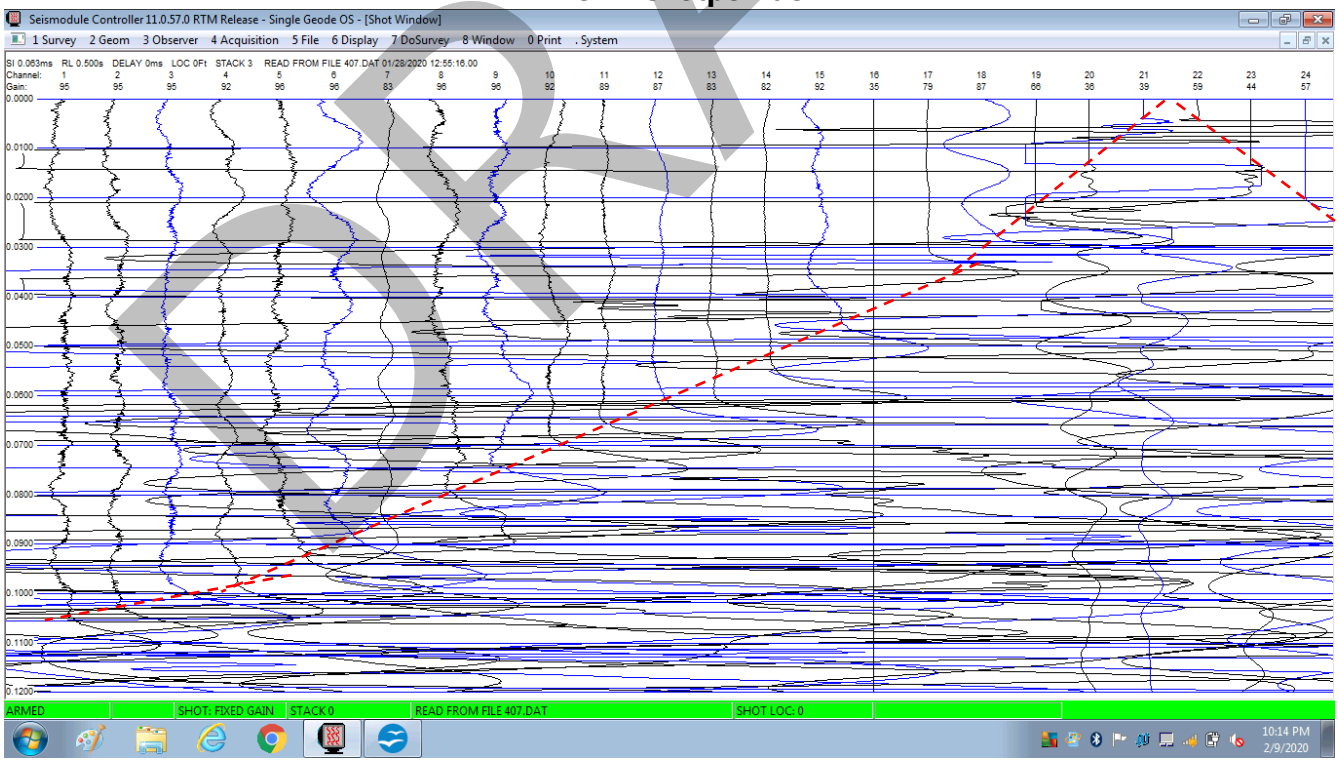

No anomaly apparent

Line 4 – shotpoint 9

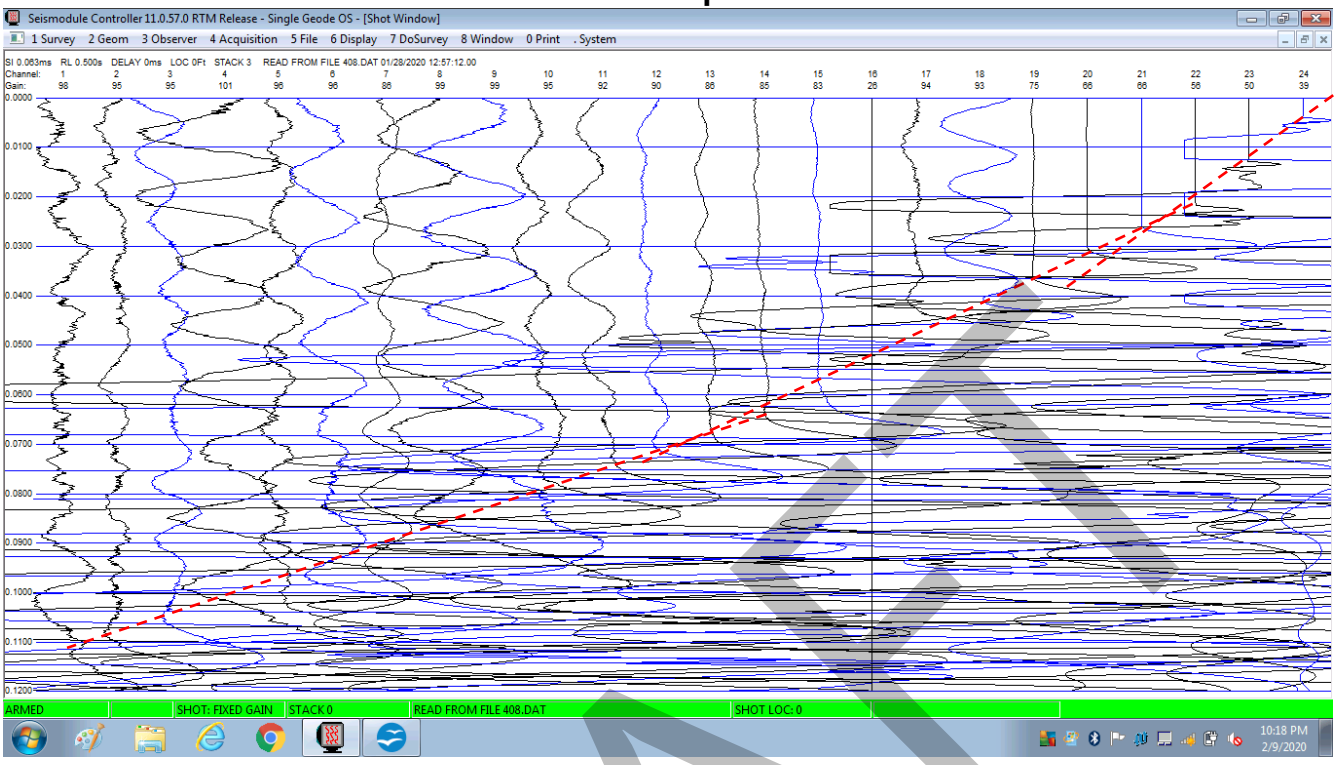

No anomaly apparent

APPENDIX C

DEEP RESISTIVITY SOUNDINGS

APPENDIX C
SURFACE RESISTIVITY

Surface resistivity measurements are normally used in civil engineering work to assist in determining parameters for electrical grounding conditions or the potential for corrosion of metal constructions, such as pipes or culverts, at a site. Under some conditions, surface resistivity measurements may be used for subsurface exploration, especially estimation of depth to groundwater and groundwater conductivity, or qualitative assessment of clay content in deep alluvium.

Resistivity is the inverse of conductivity and both parameters measure the same electrical property. Resistivity units of ohm-centimeters (ohm-cm) are typically used in civil engineering work. Fluids in the pore spaces provide the only electrical path in sands while clay particles also provide electrical paths in clays. Resistivities may be as low as several hundred ohm-cm in wet clays or as low as several thousand ohm-cm in wet sands. A reduction in moisture content typically results in an increase in resistivity. The difference in resistivity between a soil in a dry and saturated condition may be several orders of magnitude. Conductivity units of micromho-centimeters (umho-cm) are typically used in groundwater investigations and analysis, and water is typically considered to be brackish once the conductivity exceeds about 1,000 umho-cm. 1,000 ohm-cm is equal to 1,000 umho-cm, 3,333 ohm-cm is equal to 300 umho-cm, and 10,000 ohm-cm is equal to 100 umho-cm.

Since soil resistivity properties may vary greatly with soil moisture content and temperature changes, measured resistivity values should be considered to be approximate. In general, it can be anticipated that an increase in soil moisture results in a reduction in soil resistivity. Furthermore, resistivities of water and ion solutions may vary with the temperature of the solution. For example, a temperature increase from 50 to 100 degrees Fahrenheit nearly halves the resistivity of a water and NaCl solution (Schlumberger Log Interpretation Charts, 1972 Edition).

Equipment - Surface resistivity measurements are performed using a portable alternating current (AC) electrical energy source, AC voltage and current meters, and ground electrodes and associated cabling. For deep resistivity work, an AGI R-1 Stinger or L-and-R Ultra Minires resistivity meter is typically used. The four-point Wenner array method is normally used for field resistivity measurements. This method of measuring subsurface resistivity involves placing four electrodes in the ground in a line at equal distance spacings, applying a measured AC current to the outer two electrodes and measuring the AC voltage between the inner two electrodes. A measured resistance is calculated by dividing the measured voltage by the measured current. This resistance is then multiplied by a geometric factor which includes the spacing between each electrode to determine the apparent resistivity.

A subsurface resistivity profile is typically performed by making successive measurements at several electrode spacings at one location. Electrode spacings of 2.5, 5, 10, 20 and 30 feet are typically used. For deeper vertical soundings for alluvium characterization, electrode spacings of 5, 10, 20, 50, 100, 200, 333, 500, 750 and 1000 feet are typically used when conditions permit. Water is introduced to the electrode holes as they are driven into the ground to improve electrical contact. The depth of investigation is typically less than the maximum electrode spacing.

Interpretation - After resistivities from a Wenner array sounding have been calculated, further interpretation of the data may be warranted. When a large resistivity contrast is apparent, depth to groundwater or bedrock, or a change in soil electrical properties might be estimated from profiling data. Other properties which might be interpretable in non-clayey materials include porosity, groundwater conductivity and total dissolved solids. Calculating these various parameters serve as a check to verify that interpretations are consistent with known or anticipated subsurface conditions.

Interface Depth, 2-Layer System - The surface layer resistivity (R) is assumed from the closest array spacing readings. Curves of surface layer R to measured R ratios at increasing array spacing at various assumed interface depths are plotted against computed curves (Jakosky, 1950; Tagg, 1934)* until an assumed depth curve matches a computed curve. That assumed depth becomes the interpreted depth. A ratio of surface layer R to deep layer R is associated with the computed curve. This ratio may be used to estimate the deep layer R, which may be compared against the measured R at the greatest array spacing.

Interface Depth, Multi-Layer System – Interface depths and apparent resistivities are calculated in IPI2win Resistivity Sounding Interpretation software. Sounding resistivity readings are input into a data table where the software calculates apparent resistivity using to the aforementioned Wenner Array spacing. An interactive interpretation plot line matched to the field resistivity curve is used to select the interface depth and apparent resistivity for different layers. The interpreter may use several iterations of adding or removing interfaces, adjusting depths, and altering apparent resistivity to arrive at the correct interpretation.

Fluid Resistivity - Resistivities of non-clayey materials are controlled by the fluid resistivities in the pore spaces. Under saturated conditions, porosity and fluid resistivity may be analyzed using the concept of formation factor. The formation factor is the ratio of the resistivity of the saturated formation to the resistivity of the fluid in the pore spaces. The relationship between porosity and formation factor (Schlumberger, 1972, Chart Por-1) is shown below for various dry unit weights of non-clayey material assuming a specific gravity of 2.65.

Once a formation factor has been determined, the (no clay) formation resistivity is divided by the formation factor to obtain the fluid resistivity. Alternatively, the fluid resistivity is multiplied by the formation factor to determine the (no clay) formation resistivity. For example, given full saturation of a fresh groundwater fluid resistivity of 3,300 ohm-cm (300 umho-cm electrical conductivity), clean (no clay) formation resistivities will be about 59,400 ohm-cm, 36,300 ohm-cm, 22,100 ohm-cm, or 15,800 ohm-cm at formation factors of 18, 11, 6.7 and 4.8, respectively.

Dry Unit Wt (pcf)	Moisture Content at Saturation, %	Porosity %	Formation Factor
130	10	21	18
120	14	27	11
110	19	34	6.7
100	25	40	4.8

Clayey materials typically have considerably lower resistivities than can be accounted for by fresh water saturation of the pore spaces alone. Given a resistivity of 200 ohm-cm for a clay that completely fills the pore spaces in an otherwise granular material (replacing water at full saturation), formation resistivities will be about 3,600 ohm-cm, 2,200 ohm-cm, 1,340 ohm-cm or 960 ohm-cm at granular material porosities (that part of the formation not composed of clays) of 21%, 27%, 34% and 40%, respectively.

***References**

Jakosky, J.J., 1950, Exploration Geophysics, Trija Publishing Company, Los Angeles, California.
Schlumberger, 1972, Schlumberger Log Interpretation Charts, Schlumberger Limited, Houston, Texas.
Tagg, G.F., 1934, A.I.M.E. Geophysical Prospecting, Vol. 110, pp. 135-145.

Field Resistivity Measurements*

	R20-01			R20-02			R20-03		
Electrode Spacing 'a' feet	Readings 1st ohms	2nd ohms	Resistivity ohm-cm	Readings 1st ohms	2nd ohms	Resistivity ohm-cm	Readings 1st ohms	2nd ohms	Resistivity ohm-cm
5	26.0	26.0	24895	16.263	16.266	15573	20.5	20.5	19269
10	8.817	8.819	16886	8.413	8.413	16111	8.457	8.457	16195
20	3.603	3.603	13799	3.783	3.782	14487	2.893	2.893	11080
33	1.7380	1.7381	10983	1.8392	1.8391	11623	1.2559	1.2560	7937
50	0.9066	0.9067	8685	0.9560	0.9560	9154	0.5565	0.5565	5328
100	0.2782	0.2782	5328	0.2655	0.2655	5084	0.1914	0.1914	3665
200	0.0861	0.0861	3298	0.0899	0.0899	3443	0.0696	0.0696	2666
333	0.0385	0.0385	2455	0.0374	0.0374	2385	0.0314	0.0314	2002
500	0.0200	0.0201	1920	0.0178	0.0179	1709	0.0179	0.0179	1713
750	0.0134	0.0134	1920	0.0114	0.0115	1645	0.0128	0.0129	1846
1000	0.0108	0.0109	2078	0.0108	0.0109	2078	0.0114	0.0113	2174

*Measurements were completed using an L and R Ultraminires meter (Serial Number 290) operated in a four-point Wenner Array configuration.

Sounding R20-01

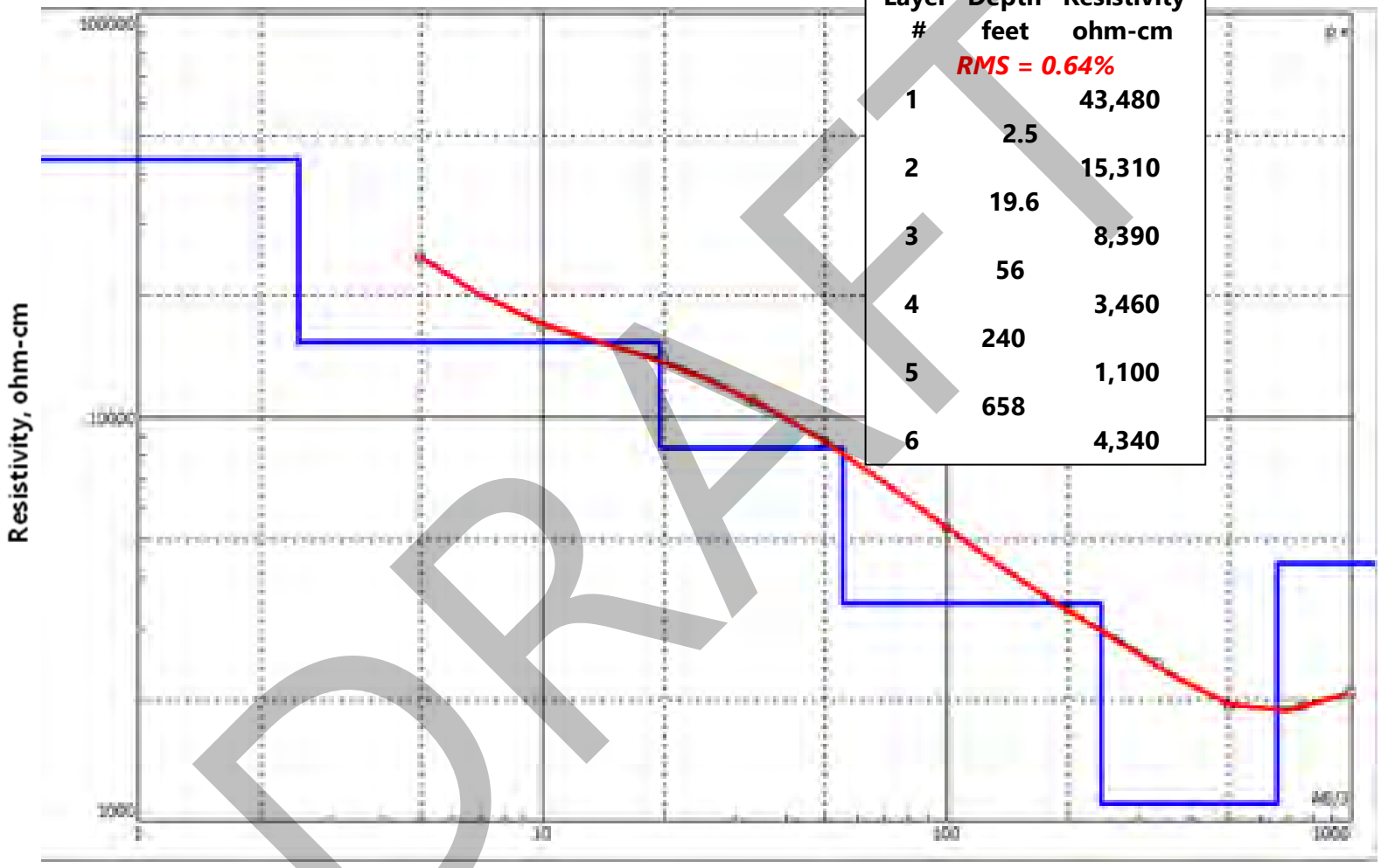

Layer #	Depth feet	Resistivity ohm-cm
	RMS = 0.64%	
1		43,480
	2.5	
2		15,310
	19.6	
3		8,390
	56	
4		3,460
	240	
5		1,100
	658	
6		4,340

Black trace and circles (behind red trace) are resistivity measurements plotted as a function of 'a'-spacing and resistivity (y-axis).
Blue trace is interpreted resistivity layers with resistivity (y-axis) for each layer as a function of depth (x-axis).
Red trace is the resulting resistivity curve as a function of depth that results from the layer depths and resistivities.

Sounding R20-02

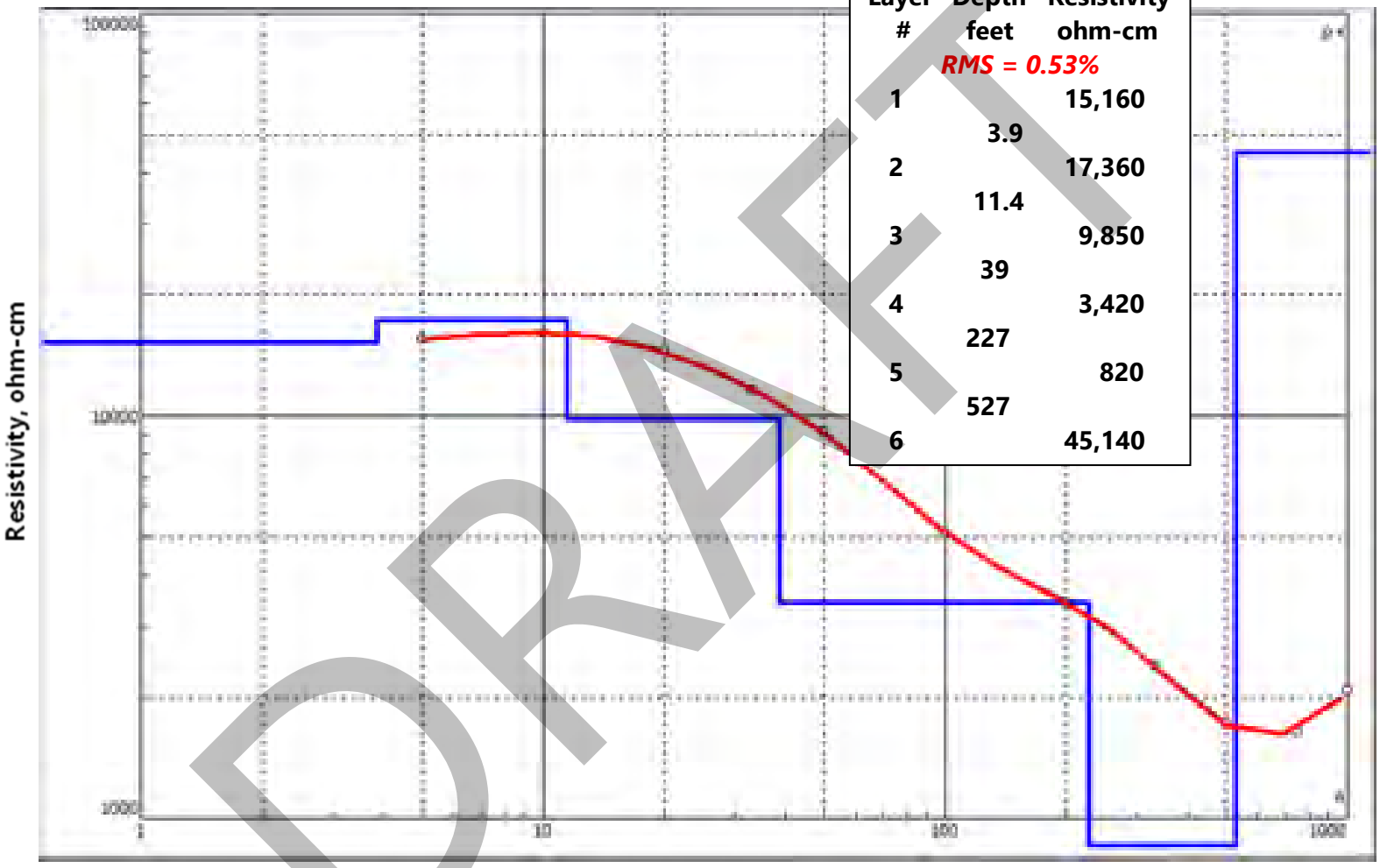

Layer #	Depth feet	Resistivity ohm-cm
	RMS = 0.53%	
1		15,160
	3.9	
2		17,360
	11.4	
3		9,850
	39	
4		3,420
	227	
5		820
	527	
6		45,140

Black trace and circles (behind red trace) are resistivity measurements plotted as a function of 'a'-spacing and resistivity (y-axis).
Blue trace is interpreted resistivity layers with resistivity (y-axis) for each layer as a function of depth (x-axis).
Red trace is the resulting resistivity curve as a function of depth that results from the layer depths and resistivities.

Sounding R20-03

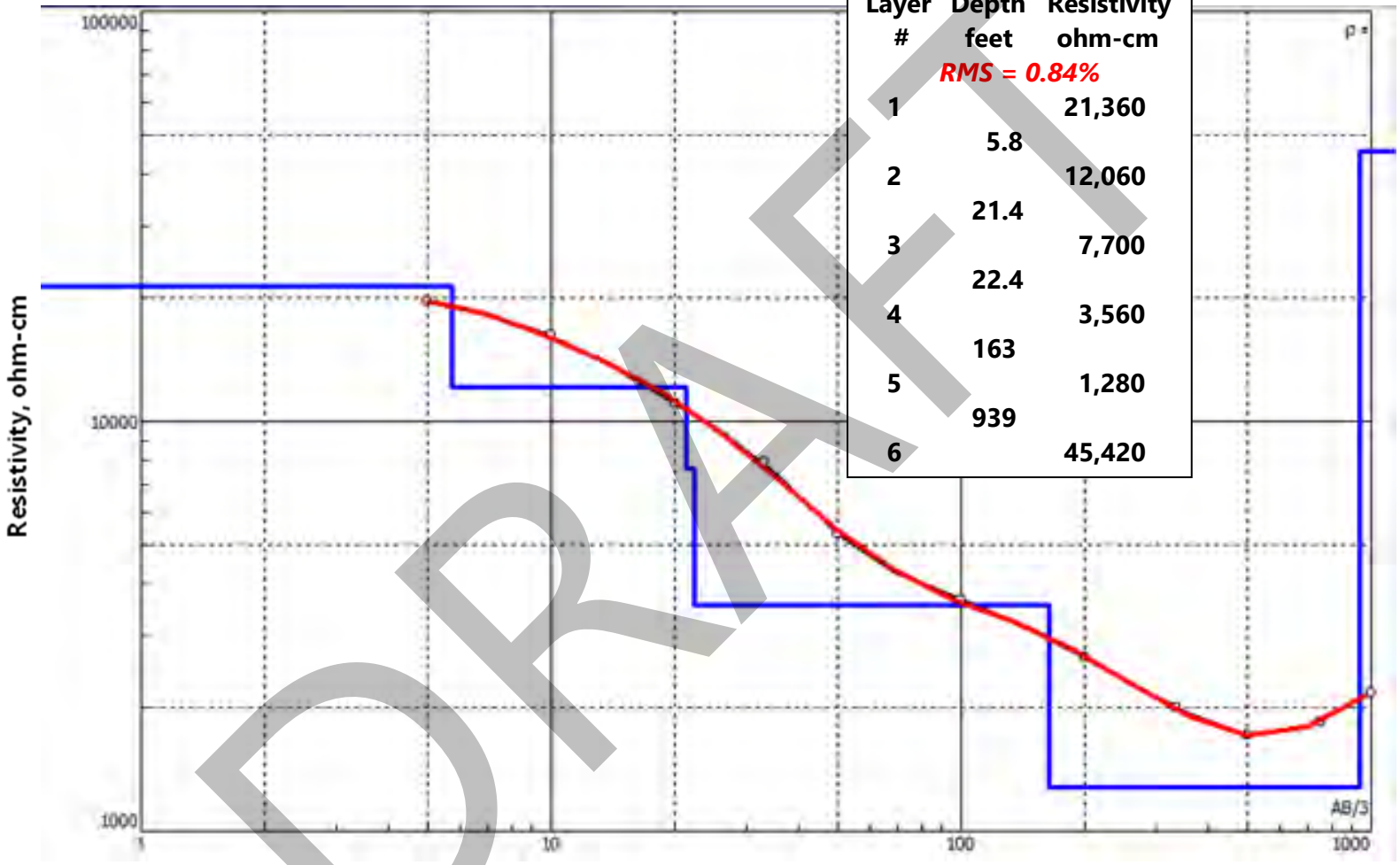

'a' spacing and interpretation depth, feet

Black trace and circles (behind red trace) are resistivity measurements plotted as a function of 'a'-spacing and resistivity (y-axis).
Blue trace is interpreted resistivity layers with resistivity (y-axis) for each layer as a function of depth (x-axis).
Red trace is the resulting resistivity curve as a function of depth that results from the layer depths and resistivities.